NUREG/CR-6783
SAND2002-1996P

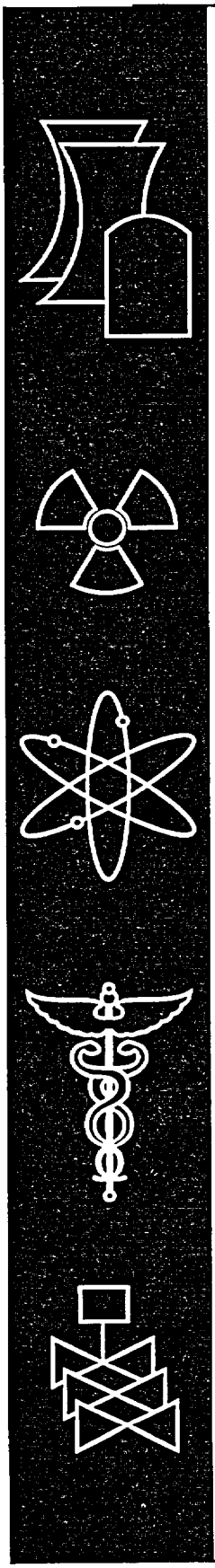

Structural Seismic Fragility Analysis of the Surry Containment

Sandia National Laboratories

U.S. Nuclear Regulatory Commission
Office of Nuclear Regulatory Research
Washington, DC 20555-0001

AVAILABILITY OF REFERENCE MATERIALS IN NRC PUBLICATIONS

NRC Reference Material

As of November 1999, you may electronically access NUREG-series publications and other NRC records at NRC's Public Electronic Reading Room at www.nrc.gov/NRC/ADAMS/index.html.
Publicly released records include, to name a few, NUREG-series publications; *Federal Register* notices; applicant, licensee, and vendor documents and correspondence; NRC correspondence and internal memoranda; bulletins and information notices; inspection and investigative reports; licensee event reports; and Commission papers and their attachments.

NRC publications in the NUREG series, NRC regulations, and *Title 10, Energy*, in the Code of *Federal Regulations* may also be purchased from one of these two sources.

1. The Superintendent of Documents
   U.S. Government Printing Office
   Mail Stop SSOP
   Washington, DC 20402–0001
   Internet: bookstore.gpo.gov
   Telephone: 202-512-1800
   Fax: 202-512-2250
2. The National Technical Information Service
   Springfield, VA 22161–0002
   www.ntis.gov
   1–800–553–6847 or, locally, 703–605–6000

A single copy of each NRC draft report for comment is available free, to the extent of supply, upon written request as follows:

Address: Office of the Chief Information Officer,
Reproduction and Distribution
Services Section
U.S. Nuclear Regulatory Commission
Washington, DC 20555-0001
E-mail: DISTRIBUTION@nrc gov
Facsimile: 301–415–2289

Some publications in the NUREG series that are posted at NRC's Web site address www.nrc.gov/NRC/NUREGS/indexnum.html are updated periodically and may differ from the last printed version. Although references to material found on a Web site bear the date the material was accessed, the material available on the date cited may subsequently be removed from the site.

Non-NRC Reference Material

Documents available from public and special technical libraries include all open literature items, such as books, journal articles, and transactions, *Federal Register* notices, Federal and State legislation, and congressional reports. Such documents as theses, dissertations, foreign reports and translations, and non-NRC conference proceedings may be purchased from their sponsoring organization.

Copies of industry codes and standards used in a substantive manner in the NRC regulatory process are maintained at—

The NRC Technical Library
Two White Flint North
11545 Rockville Pike
Rockville, MD 20852–2738

These standards are available in the library for reference use by the public. Codes and standards are usually copyrighted and may be purchased from the originating organization or, if they are American National Standards, from—

American National Standards Institute
11 West 42nd Street
New York, NY 10036–8002
www.ansi.org
212–642–4900

Legally binding regulatory requirements are stated only in laws; NRC regulations; licenses, including technical specifications; or orders, not in NUREG-series publications. The views expressed in contractor-prepared publications in this series are not necessarily those of the NRC.

The NUREG series comprises (1) technical and administrative reports and books prepared by the staff (NUREG–XXXX) or agency contractors (NUREG/CR–XXXX), (2) proceedings of conferences (NUREG/CP–XXXX), (3) reports resulting from international agreements (NUREG/IA–XXXX), (4) brochures (NUREG/BR–XXXX), and (5) compilations of legal decisions and orders of the Commission and Atomic and Safety Licensing Boards and of Directors' decisions under Section 2.206 of NRC's regulations (NUREG–0750).

NUREG/CR-6783
SAND2002-1996P

Structural Seismic Fragility Analysis of the Surry Containment

Manuscript Completed: June 2002
Date Published: October 2002

Prepared by
Eric W. Klamerus

Sandia National Laboratories
Albuquerque, NM 87185-0744

Prepared for
Division of Engineering Technology
Office of Nuclear Regulatory Research
U.S. Nuclear Regulatory Commission
Washington, DC 20555-0001
NRC Job Code W6251

Abstract

In a collaborative program between the United States Nuclear Regulatory Commission and the Nuclear Power Engineering Corporation (NUPEC) of Japan, the seismic behavior of a Reinforced Concrete Containment Vessel (RCCV) model was investigated. A 1:8 scale RCCV model was constructed by NUPEC and subjected to seismic simulation tests. Dynamic 3D finite element analyses were performed before and after the seismic tests.

Utilizing the same material models developed for the RCCV analysis, a detailed finite element model was developed for the Surry Nuclear Power plant containment structure and seismic analyses were performed. Material models that were validated by previous scaled model seismic tests and analyses were used. The Surry model was then subjected to 30 different earthquake time-history accelerations. In addition, Latin Hypercube Sampling was used to vary all the material and modeling parameters of the input to get a realistic distribution for this limited set of runs.

Fragilities were generated based on the limiting concrete shear strains. In general, the results show the Surry reinforced containment is highly resistant to seismic structural failure when it is modeled on a rigid rock foundation. The most significant variable in the response is the variability in the input earthquakes. Modeling on a rock site, rather than on a soil site, will produce higher concrete stresses and strains than for a less rigid site model, resulting in a conservative estimate of the structural capacity of a reinforced concrete containment. These predictions may be non-conservative for other failure modes (such as pipes breaking), however, because a containment on a soil site would probably see larger displacements than a containment attached to rock.

Contents

Appendices

Figures

Tables

Executive Summary

In a collaborative program between the United States Nuclear Regulatory Commission (NRC) and the Nuclear Power Engineering Corporation (NUPEC) of Japan, the seismic behavior of a Prestressed Concrete Containment Vessel (PCCV) model and a Reinforced Concrete Containment Vessel (RCCV) model were investigated. The work performed at NUPEC was under the sponsorship of the Ministry of International Trade and Industry (MITI), which became the Ministry of Economy, Trade and Industry (METI) in 2001 during a reorganization of the Japanese government, while the work performed in the U.S. has been sponsored by the NRC.

The NRC-sponsored program was separated into four parts. The first three parts have been completed. The first part analyzed and compared the predicted response of the 1:10 scale PCCV model to NUPEC's test results (James et al., 1999). The second part performed analyses of the 1:8 scale RCCV model (Cherry et al., 2001). The third part evaluated a typical U.S. prestressed containment based on what was learned from the PCCV test and analyses of the scaled models (Klamerus et al., 2001). The fourth, which is the subject of this report, was to evaluate a typical U.S. reinforced concrete containment based on what was learned from the tests and analyses of the scaled models. Sample fragility curves were developed for a typical U.S. reinforced concrete containment.

The NRC's objectives for the first two parts of the program were to evaluate the maturity of analysis methods for predicting the time-dependent behavior of concrete containments subjected to design-level and failure-level earthquakes, and to improve the analysis methods. The tests provided some valuable data on the behavior of concrete containment structures subjected to cyclic loading. This data was then used to calibrate the finite element models (i.e., select appropriate element size, select failure criteria, modify concrete constitutive models, etc). These calibrated models can then be used to predict the behavior of actual U.S. containment structures.

The NRC's objectives for the final two parts of the program were to use validated material models and methods to examine typical U.S. prestressed and reinforced concrete containments. Probabilistic methods were used because of significant uncertainty in various parameters, such as the input earthquake.

Sandia National Laboratories (SNL) was tasked with taking the information obtained from the RCCV model tests and analysis and performing a probabilistic structural analysis of an actual nuclear power plant reinforced concrete containment structure. Using the same level of detail as the analyses performed on the scaled test model, a detailed model was developed for the Surry Nuclear Power plant containment structure. Later, a coarse model was assembled that matched key features and structural parameters of the detailed model.

To determine a seismic fragility of a concrete structure, it is necessary to vary many material, modeling, and input parameters. For this study, dynamic analyses were performed by subjecting the coarse finite element model to 30 different earthquake time-history accelerations. In addition, Latin Hypercube Sampling (LHS), which provides a good distribution for a limited number of analyses, was used to vary all the material and modeling parameters of the input to get a realistic distribution.

For this study, two separate loading cases were analyzed. Both assumed the containment was rigidly attached to rock and that no soil-structure interaction or basemat uplift was permitted. The first case increased earthquake levels without any internal pressure. The second case increased earthquake levels while the containment vessel was loaded internally to the design pressure, or loss of coolant accident (LOCA).

After each analysis run, the modal frequencies were computed to observe the amount of damage for increasing earthquake inputs. For the case with no internal pressure, the frequencies dropped about 29% to 47%. When an internal LOCA pressure was applied, the frequencies dropped about 56% to 60%.

For each loading case, the peak average shear strains were calculated and saved for each analysis, as well as the peak concrete and rebar strains. In each case, the predicted failure was caused by concrete shear. The average failure level in multiplication factors (MFs) of various earthquakes scaled to envelope the Regulatory Guide 1.60 design response spectra was relatively high, more than 2.5 times MF both with and without LOCA pressure. The case with LOCA had a much lower mean (2.7 compared to 3.7).

When the failure levels were based on spectra anchored to peak ground acceleration (PGA), the average failure level in gs was lower than the results in terms of MFs. The means were still reasonably high both with and without LOCA pressure. The case with LOCA had a slightly lower mean (2.4g compared to 3.2g).

When the failure levels were based on spectra anchored to Spectral Accelerations (Sa) in the 2-5 Hz range, the average failure level in gs Sa were much lower than the results in terms of MFs or when spectra is anchored to PGA. The means were around 1.5 gs Sa for both with and without LOCA pressure. The case with LOCA had a lower mean (1.3g Sa compared to 1.8g Sa).

Although the mean failure prediction of structural failure is reasonably high, the large uncertainties yielded some probability of failure at only 1g when a LOCA pressure is applied (~5-25% probability of failure). This large uncertainty is the result of using so many different time history inputs. In some probabilistic safety analyses (PSAs), these large 'tailing' failure levels can have a significant effect on the overall plant risk when integrated with probabilistic seismic hazard curves.

The results show, in general, how robust the reinforced concrete containment structure is when it is modeled on a rigid rock foundation. The most significant variable in the response is the variability in the input earthquakes. Modeling on a rock site will produce higher concrete stresses and strains than for a less rigid site model, resulting in a conservative estimate of the structural capacity of a reinforced concrete containment. This should not be confused with, or inferred to be similar to, the containment's functional capacity. To determine the containment's functional capacity, all failure modes and types, on a plant specific case, must be examined, including basemat uplift, excessive distortion of piping, and effects of impact with other nearby structures. Modeling soil structure interaction (SSI) will significantly impact the frequencies, mode shapes of the structure, and the input earthquakes. Based on these results, response on a soil site will most likely be dominated by SSI and uplift, and the concrete will likely not be the failure mode, in other words, other things will probably fail before the reinforced concrete structure fails.

Abbreviations

2-D	two directions
3-D	three directions
3D	three dimensional
CCV	Concrete Containment Vessels
CDF	Cumulative Distribution Function
COV	Coefficient of Variation
FEM	finite element model
LHS	Latin Hypercube Sampling
LOCA	Loss of Coolant Accident
METI	Ministry of Economy, Trade and Industry
MITI	Ministry of International Trade and Industry
MF	Multiplication Factor
NRC	Nuclear Regulatory Commission
NUPEC	Nuclear Power Engineering Corporation
OBE	Operating Basis Earthquake
PCCV	Prestressed Concrete Containment Vessel
PSA	probabilistic safety analysis
RCCV	Reinforced Concrete Containment Vessel
P_d	design pressure
PGA	peak ground acceleration
PWR	Pressurized Water Reactor
PSA	probabilistic safety analysis
Sa	Spectral Acceleration
SD	Standard Deviation
SNL	Sandia National Laboratories
SRSS	square root of the sum of the squares
SSE	Safe Shutdown Earthquake
SSI	soil structure interaction

Acknowledgments

The analyses described in this report were funded by the Nuclear Regulatory Commission (NRC). The author gratefully acknowledges the efforts of Dr. Andrew Murphy, the NRC program manager, and Dr. Nilesh Chokshi, the initial NRC program manager, for the development and stewardship of the project and the valuable technical guidance provided throughout its stages.

In addition, Dr. Robert Kennedy, RPK Structural Mechanics Consulting, Inc., provided guidance and help in selecting critical parameters to include in the study and appropriate methods to perform the evaluation.

Sandia National Laboratories is operated for the United States Department of Energy under Contract DE-AC04-94AL85000. The results and conclusions described herein are based on analytical predictions performed at Sandia National Laboratories and do not necessarily reflect the opinions of the NRC.

1. Introduction

1.1 Objectives

The U.S. Nuclear Regulatory Commission (NRC) is moving towards a "risk informed, performance based" regulatory approach for U.S. nuclear power plants. Therefore, future evaluations of U.S. containment structures will need to incorporate probabilistic methods that can provide important risk insights.

Parameters such as damping and material properties are not exactly known, and the variability in the assumed values can significantly influence predicted results. For example, the concrete shear strength varies as a function of its measured compressive strength, confining pressures, and size and location of cracks, and is not well defined.

Much more important than modeling and material parameters that cause uncertainty in predicted behavior is that actual earthquake loadings are not known. For example, two earthquake records with the same peak acceleration but different frequency content could cause a structure to respond quite differently. Likewise, a design-level earthquake may occur while the vessel is under internal design pressure caused by a Loss of Coolant Accident (LOCA).

To gain risk insights into U.S. containment vessels, Sandia National Laboratories (SNL) was tasked with performing a probabilistic structural analysis of actual nuclear power plants' concrete containment structures, both reinforced and prestressed. A prestressed concrete containment (Zion) was analyzed and is reported in NUREG /CR-6740 (Klamerus et al., 2001). This report will analyze a reinforced concrete containment.

The sensitivity of a concrete structure to various uncertain parameters was studied by varying each separately in the analyses (e.g., damping, material properties, or seismic loading). In addition, each analysis incorporated a different earthquake time-history, scaled from an actual recorded earthquake. Although the absolute values of these parameters are uncertain, realistic distributions of possible values were defined, and sensitivity studies can show how these uncertainties affect the structural integrity and seismic margins of U.S. containments.

In order to perform these analyses, a validated concrete constitutive model and failure criterion were necessary. Section 1.2 describes the testing of an actual scaled reinforced concrete vessel and the analysis that validated a concrete constitutive model for predicting the actual behavior under cyclic loading, along with failure criteria. Using this concrete constitutive model and failure criterion, a typical full-sized U.S. containment structure was analyzed to determine the probabilistic failure capacity.

1.2 Verification of Analysis Capability

1.2.1 Testing of a Scale Model Reinforced Concrete Containment Vessel

In a collaborative program between the NRC and the Nuclear Power Engineering Corporation (NUPEC) of Japan, the seismic behavior of a Reinforced Concrete Containment Vessel (RCCV) model was investigated. NUPEC is operated under sponsorship of the Ministry of International Trade and Industry (MITI), which became the Ministry of Economy, Trade and Industry (METI) in 2001 during a reorganization of the Japanese government. The scaled model was constructed by NUPEC and subjected to seismic simulation tests using the high-performance shake table at the Tadotsu Engineering Laboratory (NUPEC Summary Report – 2001). A description of the test results and analytical predictions performed for the NRC is given in NUREG/CR-6707, Seismic Analysis of a Reinforced Concrete Containment Vessel Model (Cherry et al., 2001).

The primary objectives of the testing program were to demonstrate the capability of the RCCV to withstand the design-basis earthquake with a significant safety margin against major damage or failure, to verify the functional integrity and leak-tightness of the vessel, and to validate structural analysis computer codes.

The scaled model was representative of an actual containment structure while meeting the limitations of the test equipment and the necessary fabrication requirements. Acceleration time histories of the base motion were developed for typical design-level earthquakes at locations in Japan of reinforced concrete containment structures. These motions

were scaled so the fundamental frequency and the shear stresses in the wall near the basemat of the scaled model would be similar to those in an actual containment structure.

The scaled test model was first subjected to a series of low amplitude motions to determine fundamental frequencies and other characteristics of the test model and shake table. The response of the model to a design-basis earthquake was then evaluated by tests using individual horizontal and vertical components separately followed by tests using combined horizontal and vertical components.

A LOCA, in combination with an operating basis earthquake (OBE), was simulated by pressurizing the test model during a seismic simulation. Several sequential tests of design-level earthquakes were also conducted. The margin of safety for the scaled test model was determined by subjecting the model to seismic accelerations of larger and larger amplitudes until structural failure occurred. The test program also measured the fundamental frequencies of the test model after each test to determine the damage sustained by the model.

1.2.2 Seismic Test Results

During the test series, the RCCV model was subjected to gradually increasing excitation levels up to "design level" earthquakes. After each excitation, low-level random vibration tests measured the resonant frequency and damping ratio. The design-level earthquakes caused significant damage to accumulate. Fundamental frequencies were reduced by approximately 50% (from 13.7 Hz to 7 Hz) and the damping ratio approached 6%.

After the design-level tests were completed, the seismic failure level of the vessel was determined by gradually increasing the earthquake excitations until the model failed. Significant cracking accumulated during these "beyond-design-basis" earthquakes, and the stiffness of the model decreased.

During a two-times-design-level event, damage continued to accumulate, but the maximum shear stresses were still below the peak shear stresses that occurred during subsequent testing. This indicated that additional reserve strength still existed, even though considerable damage was accumulating.

The three-times-design-level and larger earthquakes all resulted in peak shear stresses of about the same magnitude, but the associated peak shear strains varied, depending on the simulated seismic event. This indicates that the structure had little reserve strength left. However, the structure was able to absorb the energy of subsequent simulated earthquakes through concrete cracking, concrete crushing, steel yielding, and other damage mechanisms. Of course, as damage accumulated, the effective damping level also increased, helping to offset the effects of the larger acceleration levels.

The vessel remained structurally intact and was able to resist additional earthquake loads during the beyond-design-basis tests. Although significant damage progressively accumulated in the model, catastrophic failure did not occur until it was subjected to a nine-times-design-level earthquake.

1.2.3 Comparison of Analyses to Test Results

As part of the collaborative program with NUPEC, and the NRC, through SNL, ANATECH Corp. researched the analytical modeling of the seismic behavior of RCCV structures (Cherry et al., 2001). The research evaluated the predictive capabilities of current analytical methods with the eventual goal of improving these capabilities for containment performance evaluation under seismic events.

The scope consisted of pretest predictions and post-test verification analyses of the NUPEC RCCV tests. These included a series of calculations under simulated design-level input motions, followed by calculations under amplified motions that eventually led to the failure of the test model.

At the conclusion of the test program, the records of test data, which included shake table input and response data, were used to perform post-test analyses of the test model. The post-test calculations were used to evaluate the effects of the assumptions used in the pretest calculations compared to the actual test conditions, such as the true loading delivered to the basemat in the tests. The analyses were conducted sequentially to simulate the sequence of the tests and to allow cumulative damage to develop. However, not all tests were analyzed, and only a subset of the actual tests was selected

for analytical evaluations. For pretest calculations, this subset was chosen a priori as that most likely to cause or extend damage. For the post-test calculations, the selected tests were those judged to be the most significant.

In the design-level tests that were analyzed, the measured input motions were similar to the target motions. However, for larger input motions, particularly horizontal-only motions where the vertical motion of the basemat was not controlled, the measured input motions were significantly different from the target motions. The pretest analyses of beyond-design-basis tests assumed that vertical accelerations were zero at the basemat control points, while in the actual tests, the model rocked and some of the vertical accelerations were almost as large as the horizontal accelerations. Therefore, it was necessary to perform the post-test analyses with both horizontal and vertical input accelerations, as measured by the accelerometers mounted on the basemat.

The software used to perform the analysis contained two options for shear resistance: a nominal resistance model based on material-property laboratory tests and a reduced-resistance model. The latter model is intended for structures with preexisting damage, a condition judged to exist in the test because of the progressively introduced damage in each test and because not every test was analyzed. Both models, however, underestimated the shear resistance of the structure at the higher load levels, with the latter (reduced-resistance) model showing significant under prediction. Using these findings, a modification of the standard shear model was introduced by adjusting the dependence of the shear modulus on the crack-opening strain. This modification affects the higher-level seismic motions more than lower-level motions because damage accumulates (i.e., more cracks develop) as the analyses proceed and because the test sequence proceeds from low-level seismic events to high-level events. Differences between target and actual accelerations had a greater effect on the results than the change in the concrete shear model.

Another significant finding from this program was the effect of damping on the response. Damping ratios observed during the test were about 1% for an undamaged structure, increased to about 5-6% during the design-level earthquakes, and were between 15-26% after major damage was sustained. Hysteretical damping represents much of the damping, particularly at the higher earthquake levels. The remaining damping is accounted for with a viscous damping ratio ranging from 1% to 4%. This damping factor was applied locally at the cracked integration points by invoking a crack-consistent damping model that represented damping as function of the crack status. When the analyses was run with this non-uniform damping applied, allowing the damping to increase during the analysis as cracks formed, the resulting agreement was much improved.

Finally, the testing program provided an opportunity to develop a shear-failure measure for concrete structures subjected to severe motions. Analytical interpretations of the test results indicate that impending shear failure of the structure would occur at a shear strain of about 0.5%, with a sizeable uncertainty band, averaged over the entire cross-section of the structure. Shear failure occurred in the RCCV test when the average shear strain was above 0.5%. The failure value of about 0.5% was applied because even though collapse did not occur at this shear strain level, a significant amount of damage was present, and it was presumed that the containment could no longer sustain internal pressure. This is proposed as a shear failure criterion. Since 0.5% shear strain is a structural measure rather than a material property measure, it can only be applied through post-processing the analysis results. Further work would be needed to incorporate a shear failure criterion into the concrete material model.

The agreement between the calculated time histories and the measured data records was generally good. Much better agreement occurred for global measures of response, rather than response that is directly affected by local concrete conditions. The higher resistance predicted by the analysis is in part because not all of the tests were analyzed, which resulted in lower damage accumulation in the analysis than actually occurred in the structure. The level of agreement between test and analysis achieved in this program indicates that, with the level of modeling sophistication used in the analysis, existing analysis capabilities can reliably predict the global behavior of reinforced concrete containment structures.

1.3 Fragility Analyses of a Typical U.S. Containment

The pre-test and post-test analyses were performed for a scaled reinforced concrete vessel model. The analysis results showed a good match to the test data. Therefore, the ability to analyze reinforced concrete vessels was validated.

Although the results of the scale model test performed at Tadotsu and follow-on analysis cannot be applied directly to U.S. containments, a significant amount of good information about the seismic behavior of reinforced concrete structures was gained. Differences between the scale model and U.S. containments include design differences, scaling issues associated with the test model and issues with the lumped mass lead weights in the model, etc. However, the tests provided some valuable data on the behavior of reinforced concrete containment structures subjected to cyclic loading. This data was then used to calibrate the finite element models. Using these calibrated models will allow SNL to predict the behavior of an actual U.S. containment structure.

Using the same level of detail as analyses performed on the scaled test model, a detailed model was built for the Surry Nuclear Power plant containment structure. Later, a coarse model was built that matched key features and structural parameters of the detailed model.

To determine the seismic fragility of a concrete structure, it is necessary to vary many material, modeling, and input parameters. For this study, dynamic analyses were performed by subjecting the coarse finite element model to earthquake time-history accelerations. This coarse model was necessary to keep the run time for each analysis to a minimum. In addition, Latin Hypercube Sampling (LHS), which provides a good distribution for a limited number of runs, was used to vary all the uncertain input parameters to get a realistic distribution. A different actual earthquake time-history was input for each analysis instead of using a single time-history and varying its parameters.

The analysis assumed the containment was rigidly attached to rock. No soil-structure interaction or basemat uplift was allowed. Fixing the model to rock is usually conservative, in that stresses and strains, particularly shear strains, will be higher, resulting in a conservative estimate of a containment's structural capacity. This simplification also allows the response of the concrete structure to be studied. However, the result should not be used directly in risk studies unless other containment functional capacities are also included, since some responses (such as displacement) are probably significantly under predicted. In order to determine the containments functional capacity, all failure modes and types, on a plant specific case, must be examined to include: soil structure interaction (SSI), basemat uplift, interaction with other nearby structures, penetrations and piping layout, structural failure, etc.

This report presents the results of a seismic failure analysis performed on the Surry containment vessel. The seismic level of excitation required to cause a structural failure and how likely it is to occur, both with and without an applied internal design pressure, is shown. In addition, the amount of damage for different levels of earthquakes applied to the analytical model is also presented.

2. Surry Containment Models

2.1 Actual Surry Containment

The RCCV post-test analysis of the 1:8 scale model tested at Tadotsu was able to predict the response of the vessel. Therefore, a three-dimensional (3D) model of a typical U.S. reinforced concrete containment is being modeled using the same material model and other modeling techniques for the scaled model test.

The containment chosen for this study was Surry. Surry is a reinforced concrete containment typical of many in the U.S. Several studies involving both seismic and pressure capacities have been performed on the Surry containment structure, allowing for some comparison.

The Surry Nuclear Power plant is a two unit, 781-megawatt per unit, Pressurized Water Reactor (PWR) located in Gravel Neck, Virginia. The plant is founded on a site characterized by a deep soil with alternating strata of clay and sands. The containment structure is in the shape of a cylinder with a hemispherical domed roof and a flat foundation slab. The foundation slab is conventionally reinforced with reinforcing steel. The entire containment structure is lined with a leak-tight 9.5mm (3/8-inch) welded steel plate in the cylinder and 12.7mm (.5-in.) welded steel plate in the dome. The entire liner is attached to the concrete by means of flat-headed anchors welded to the liner plate and embedded in the concrete.

Overall dimensions of the Surry containment are shown in Figure 2.1. The containment encloses the reactor pressure vessel, steam generators, reactor coolant pumps, and portions of the auxiliary and engineered safeguards system. Personnel and equipment access to the structure is provided by an equipment hatch. An emergency personnel air lock is also provided.

The Surry containment was designed to withstand an accident pressure of 0.310 MPa (45 psig). The OBE is 0.07g horizontal ground acceleration and 0.05g vertical ground acceleration acting simultaneously. The Safe Shutdown Earthquake (SSE) is 0.15g horizontal ground acceleration and 0.10g vertical ground acceleration acting simultaneously.

2.2 Detailed Surry Finite Element Model

The calculations in this report were performed with a concrete material model called ANACAP-U developed by ANATECH (James et al., 1997) coupled to the ABAQUS general purpose finite element program (Hibbit et al., 1997). A thorough description of the concrete constitutive model is given in the Appendix of James et al. (1999). To predict damage that may accumulate during a seismic event, the material model must account for the history dependence of cracking and the strength and stiffness degradation under cyclic loading. This requires time-marching, nonlinear dynamic analyses to be performed. Because of the large storage and run times required, care was taken to ensure that the number of degrees of freedom in the finite element model was small enough for efficient calculations while adequate to capture the critical response of the containment structure.

A detailed finite element model (FEM) was developed for the Surry containment structure, as shown in Figure 2.2. Approximately the same amount of detail that was used in the RCCV seismic model (Cherry et al., 2001) was incorporated into this full-sized model of Surry. In addition, the same concrete material model (described above) was used in both analyses. The concrete in the Surry containment was modeled with a total of 1476 solid elements (second order 20-node bricks). The liner was modeled using membrane elements. The rebars were smeared into the solid elements.

The equipment hatch and airlock were modeled as in the actual containment; however, all smaller penetrations were ignored. The model was assumed, for this analysis, to be rigidly attached to a rock site. Although the Surry containment is on a deep soil site of alternating layers of clay and sand, a rock foundation was modeled in this study for two reasons.

1) Fixing the model to rock is generally conservative, in that stresses and strains, particularly shear strains, will be higher. However, the displacements would probably be larger if SSI was included in the analysis and the base of the containment would be allowed to rotate. This can result in a higher likelihood of pipes attached to the containment wall to fail or structures adjacent to the containment to impact the containment during an earthquake. The main goal of this study was to determine the structural fragility of a reinforced concrete containment. Therefore, modeling on a rock site produces higher stress and strains in the containment, resulting in a conservative estimate of the structural capacity of a containment. This should not be confused with the

containment's functional capacity. To determine the containments functional capacity, all failure modes and types, on a plant-specific case, must be examined to include: SSI, piping, other nearby structures, uplift, etc.

2) By not modeling the soil and ignoring SSI, the model is much simpler, allowing for more analysis. Several different analyses must be performed with varied parameters to develop a fragility. If SSI was modeled, other structures on the site would also have to be included, particularly adjacent structures, since they could affect the input motion into the base of the containment structure. This would greatly increase the size and complexity of the analytical model and would result in much longer execution times.

The detailed Surry model was then analyzed in ABAQUS to determine the mass properties and modal frequencies and shapes. The results are shown in Table 2-1. Only the first 10 major modal frequencies are listed. The major modal frequencies were chosen by selecting modes with a large participation factor; the effective mass for these modes was significantly large compared to those neglected. The mode shapes for the first 10 major modal frequencies are shown in the next section, along with a comparison to the simpler coarse model.

A static pushover analysis was performed on the containment model by applying a gradually increasing gravity-type force horizontally and measuring the horizontal displacement at the top of the containment cylinder. The result of this static pushover is shown in Figure 2.3. A similar pushover was computed for the RCCV seismic model and is also shown in this plot. Dividing the displacements by the height of the structures normalized the curves. The normalized curves compare well at low g levels, even though the Surry containment is actual size, as opposed to the scale model RCCV, which had a lower height to diameter ratio and included a significant amount of weight attached to the top. The Surry curve matches well initially but then stiffens slightly above three times g.

2.3 Simple Surry FEM

After the Surry analysis was completed, it was deemed much too large to perform the multiple number of analyses necessary to determine a structural fragility. A much simpler model was necessary to run a suite of executions, with varying material properties and various earthquake time histories. This uncertainty analysis methodology and the chosen number of executions is discussed in Section 3.

Three things were required of this simple containment model. First, the principal response of the structure is in shear, so the element must handle shear well. Second, because of all the cracking and other damage that accumulates, the element must also track hysteresis effects as it cycles through its nonlinear phases. Third, the element needed to work with the ANACAP concrete material model, since that was the concrete constitutive model that was validated (James et al., 1999 and Cherry et al., 2001).

In a long beam (length/depth greater than 15), the primary result is bending, and shear is negligible. However, in short beams (i.e. containment structures represented by 10 beam elements would have a length/diameter ratio of about 0.2), shear cannot be neglected. The ABAQUS analysis software includes a Timoshinko beam element that accounts for shear in short beams. However, the component added to account for shear is linear elastic. If the element never exceeded its elastic limit, this element would do very well. If shear was only a small portion of the result and the non-shear portion of the result was nonlinear, the element would still do well. Since it is expected that the vessel response would be primarily shear and nonlinear (as demonstrated by the RCCV model test and analysis), the element wasn't adequate. The Timoshinko beam is nonlinear in bending, axial, etc., but the "deep beam" (i.e., shear) portion of the element configuration treats shear in a purely linear method. The element formulation does handle nonlinear behavior in all respects except for transverse shear, and transverse shear is the dominant load resisting part of a containment structure. This element would track hysteresis effects. It is possible to write a user element and define a Timoshinko beam that has nonlinear transverse shear; however, the time necessary and schedule to complete this program did not allow for code and development.

A lumped mass/spring model could be developed that would handle the transverse shear concerns discussed above. However, without writing a user-defined element, this model couldn't account for hysteresis effects. This approach would not require using the ANACAP concrete material model.

Each of the above two approaches had one fatal flaw. They could meet one of the two requirements (model nonlinear shear stiffness correctly or include hysteresis effects to account for accumulating damage), but not both. Using a coarse

grid of solid elements meets both of the requirements, with a slightly more complex model. This coarse model (detailed below) was still small enough, however, to run quickly for dynamic problems (the longest seismic analysis ran in about 10 hours; the shortest seismic events ran in about 1 hour).

A coarse finite element model was developed for the Surry containment structure, as shown in Figure 2.4. This model was made as coarse as possible, while still maintaining similar mass properties, stiffness properties, and modal frequencies to the original model. From this point, this model with fewer and larger elements will be referred to as the Coarse Model and the much heavier detailed model discussed previously will be referred to as the Original Model.

The same concrete material model (ANACAP-U) was used for both models. The concrete in the Coarse Model was modeled with a total of 92 solid elements (second order 20-node bricks). The liner was modeled using membrane elements. The rebars were smeared into the solid elements. All these element types were used in the original Surry containment model.

The equipment hatch and airlock fully incorporated into the Original Model were simply modeled by thinning certain sections of the Coarse Model, and all smaller penetrations were again ignored. The Coarse Model was also assumed to be rigidly attached to a rock site for the same reasons as the Original Model.

The Coarse model was then put through an analysis in ABAQUS to determine the mass properties and modal frequencies. The results are shown in Table 2-2, along with a comparison to the Original Model. The mode shape comparisons for the first 10 major modal frequencies are shown in Figures 2.5 through 2.14.

A static pushover analysis was performed on the Coarse Model by applying a gradually increasing gravity type force horizontally and measuring the horizontal displacement at the top of the containment cylinder. The result of this static pushover is shown in Figure 2.15. A similar pushover was computed for the Original Model and is also shown in this plot. The two sets of curves compare extremely well and are nearly identical.

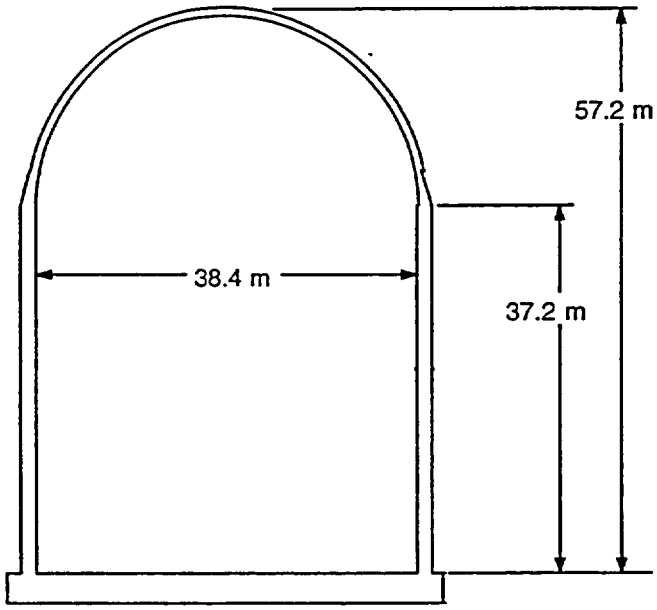

Figure 2.1 Overall Dimensions of the Surry Containment Structure

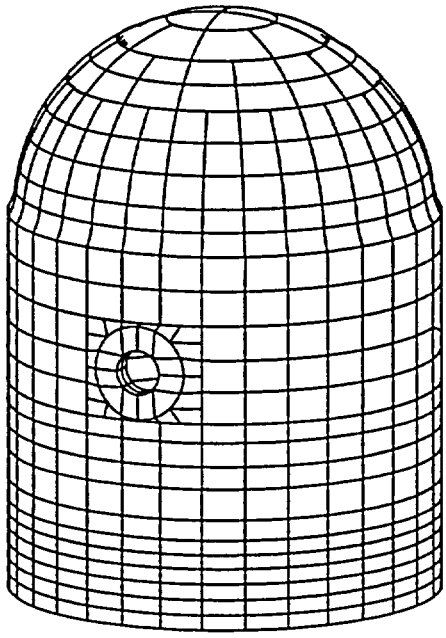

Figure 2.2 Surry Containment - Original Model

Table 2-1 Summary of Surry Model Output Parameters			
Total Mass	20,550,000 kg	45,300,000 lbm	
Center of Mass from origin (m)	X = 0.10	Y = -0.02	Z = 25.18
Moment of Inertia	I(XX) = 7.58e+10	I(YY) = 7.62e+10	I(ZZ) = 6.61e+10
Major Modal Frequencies	**Mode #**	**Frequency (Hz)**	**Direction**
1	1	6.433	Horizontal (X)
2	2	6.436	Horizontal (Y)
3	9	12.64	Vertical-Torsion
4	10	16.56	Horizontal (X)
5	16	17.35	Vertical-Axial
6	25	24.80	Horizontal (X)
7	26	24.88	Horizontal (Y)
8	33	25.98	Vertical
9	34	26.23	Horizontal (X)
10	35	26.26	Horizontal (Y)

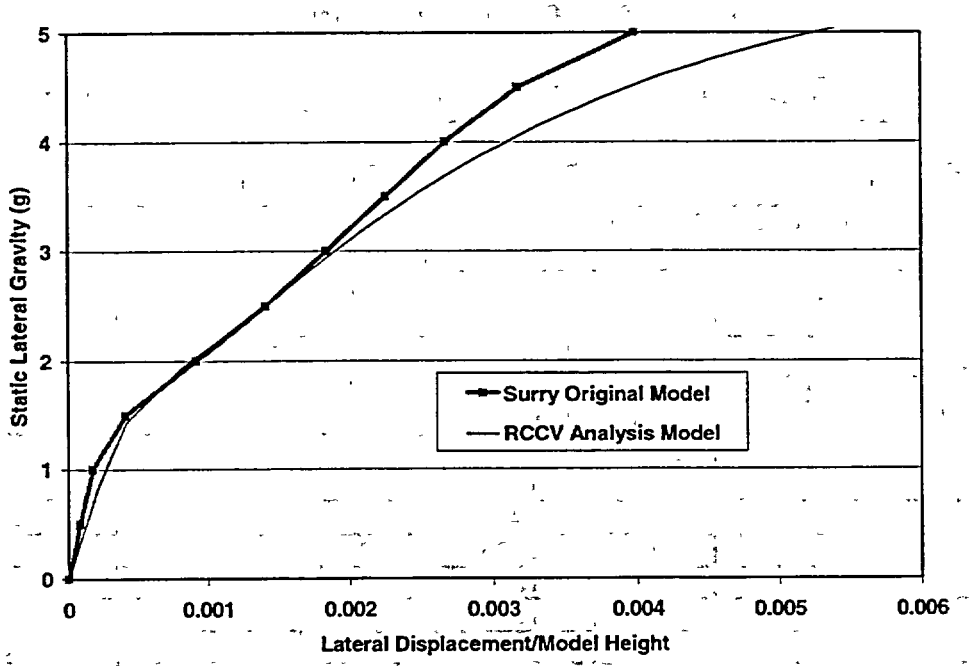

Figure 2.3 Static Pushover of Surry Containment Model Compared to RCCV Model

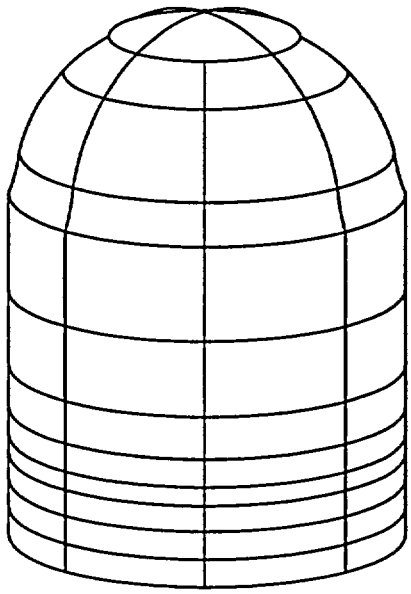

Figure 2.4 Surry Containment – Coarse Model

Table 2-2 Summary of Coarse Model and Comparison to Original Model Parameters					
Total Mass (Coarse)	20,650,000 kg		45,500,000 lbm		
Total Mass (Original)	20,550,000 kg		45,300,000 lbm		
Center of Mass from origin (m) (Coarse)	X = 0.20		Y = 0.02		Z = 25.20
Center of Mass from origin (m) (Original)	X = 0.10		Y = -0.02		Z = 25.18
Moment of Inertia (Coarse)	I(XX) = 7.59e+10		I(YY) = 7.64e+10		I(ZZ) = 6.65e+10
Moment of Inertia (Original)	I(XX) = 7.58e+10		I(YY) = 7.62e+10		I(ZZ) = 6.61e+10
Major Modal Frequencies	**Original Model**		**Coarse Model**		**Direction**
	Mode #	**Frequency (Hz)**	**Mode #**	**Frequency (Hz)**	
1	1	6.433	1	6.446	Horizontal (X)
2	2	6.436	2	6.466	Horizontal (Y)
3	9	12 64	7	12.65	Vertical-Torsion
4	10	16 56	10	16.73	Horizontal (X)
5	16	17 35	12	17.63	Vertical-Axial
6	25	24 80	20	25.14	Horizontal (X)
7	26	24 88	21	25.22	Horizontal (Y)
8	33	25 98	26	26.99	Vertical
9	34	26.23	23	26.45	Horizontal (X)
10	35	26 26	25	26.67	Horizontal (Y)

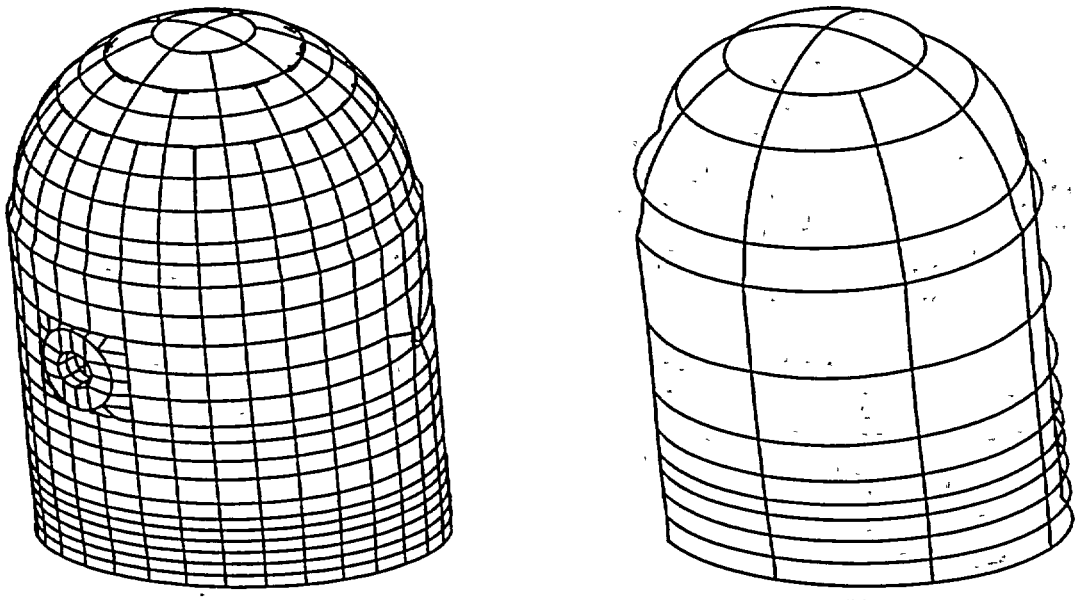

(a) (b)

Figure 2.5 First Major Modal Shape Comparison (a) Original (b) Coarse

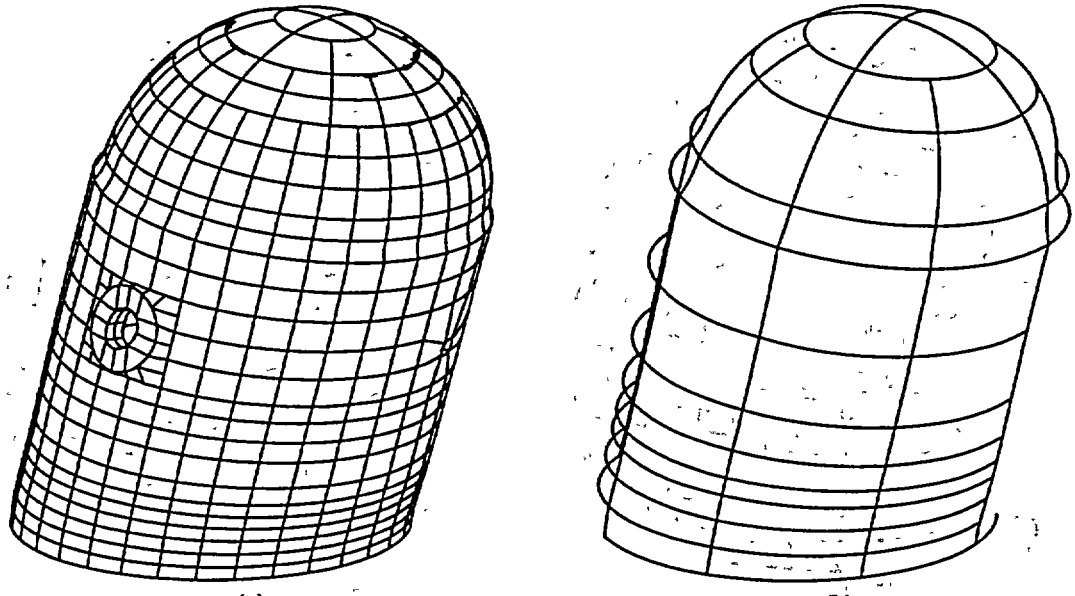

(a) (b)

Figure 2.6 Second Major Modal Shape Comparison (a) Original (b) Coarse

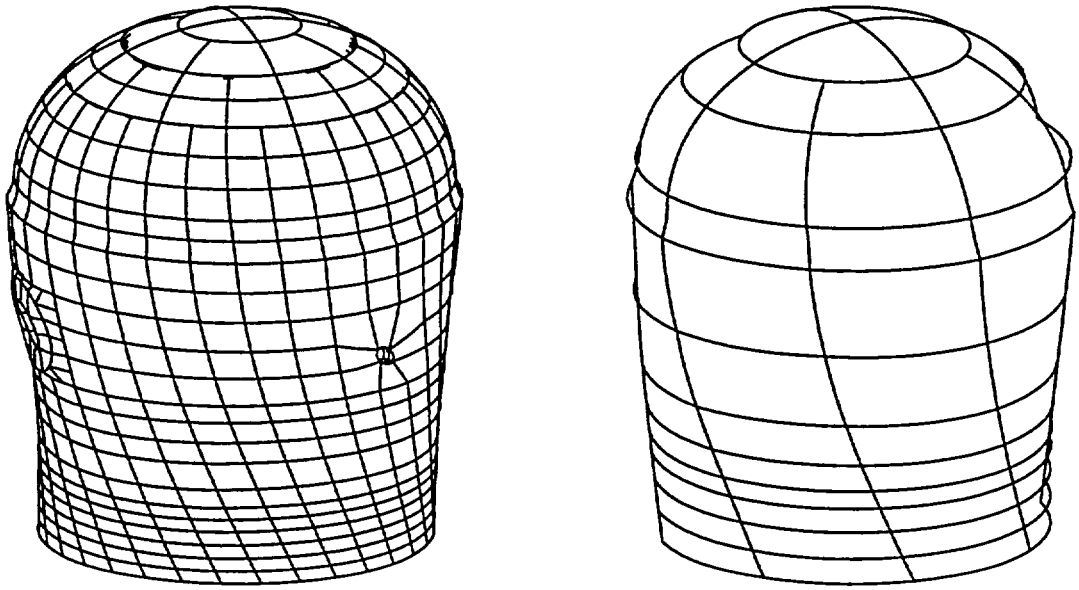

(a) (b)

Figure 2.7 Third Major Modal Shape Comparison (a) Original (b) Coarse

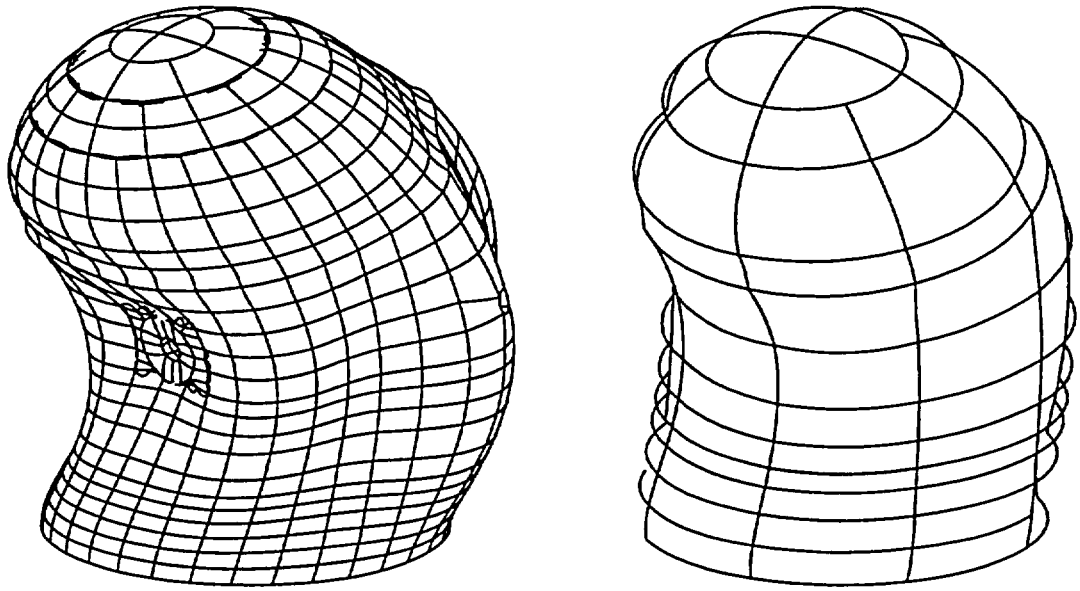

(a) (b)

Figure 2.8 Fourth Major Modal Shape Comparison (a) Original (b) Coarse

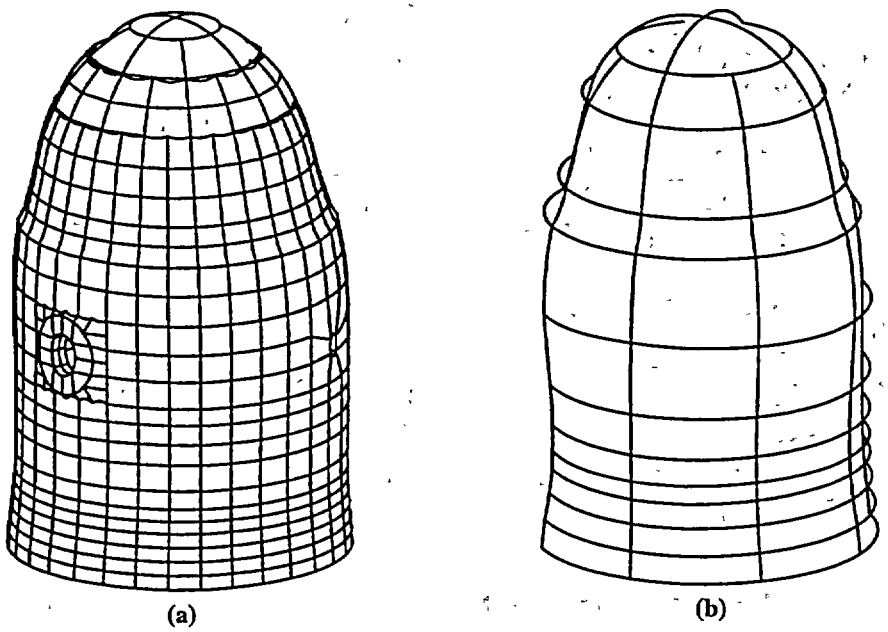

Figure 2.9 Fifth Major Modal Shape Comparison (a) Original (b) Coarse

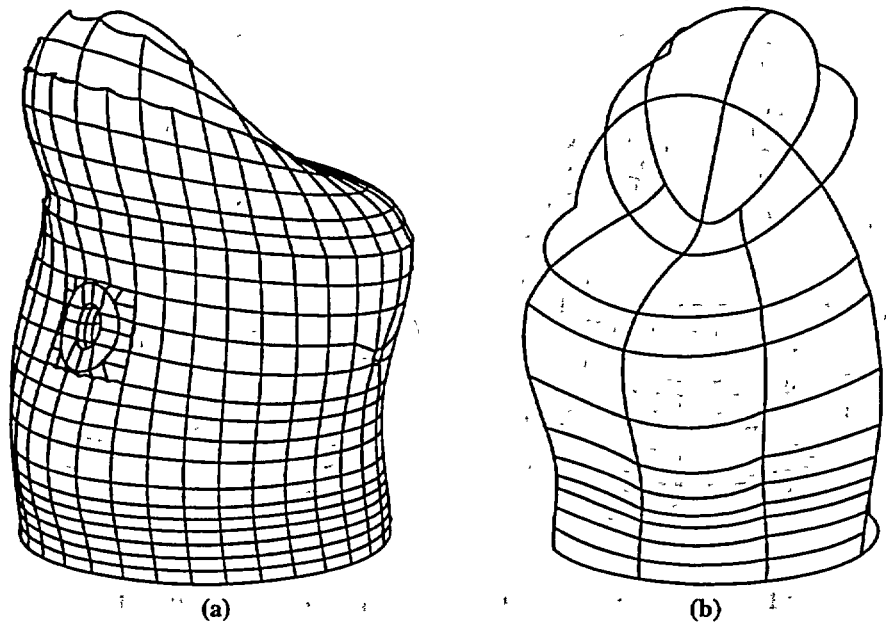

Figure 2.10 Sixth Major Modal Shape Comparison (a) Original (b) Coarse

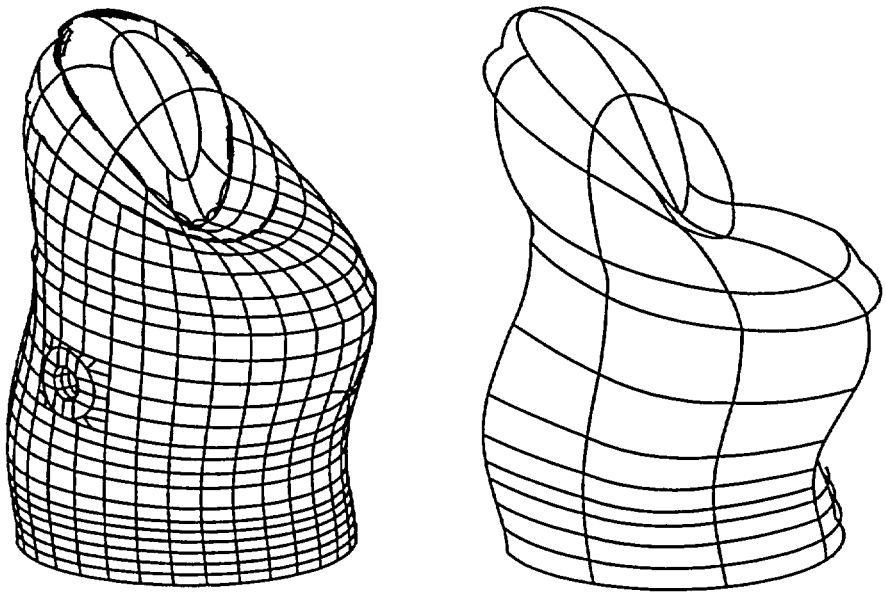

Figure 2.11 Seventh Major Modal Shape Comparison (a) Original (b) Coarse

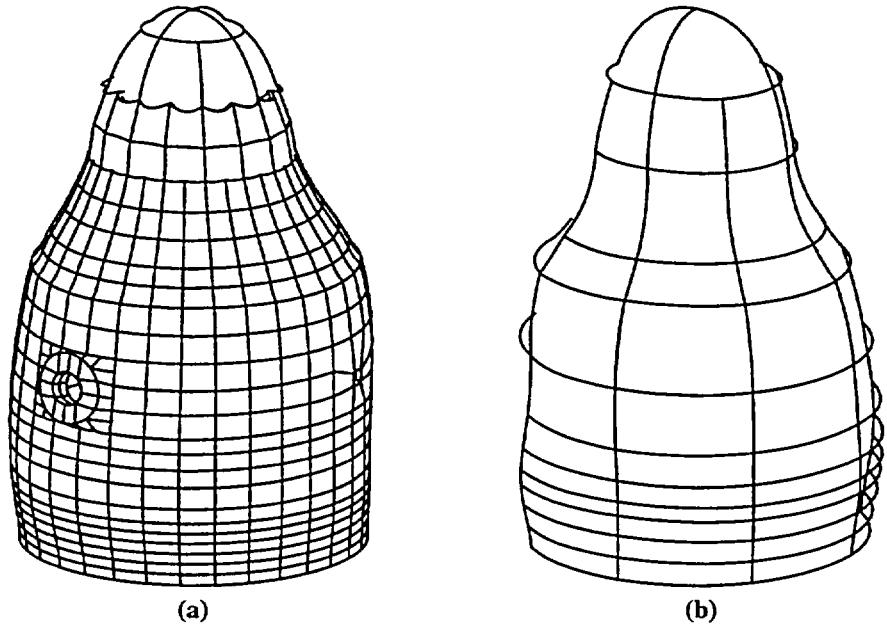

Figure 2.12 Eighth Major Modal Shape Comparison (a) Original (b) Coarse

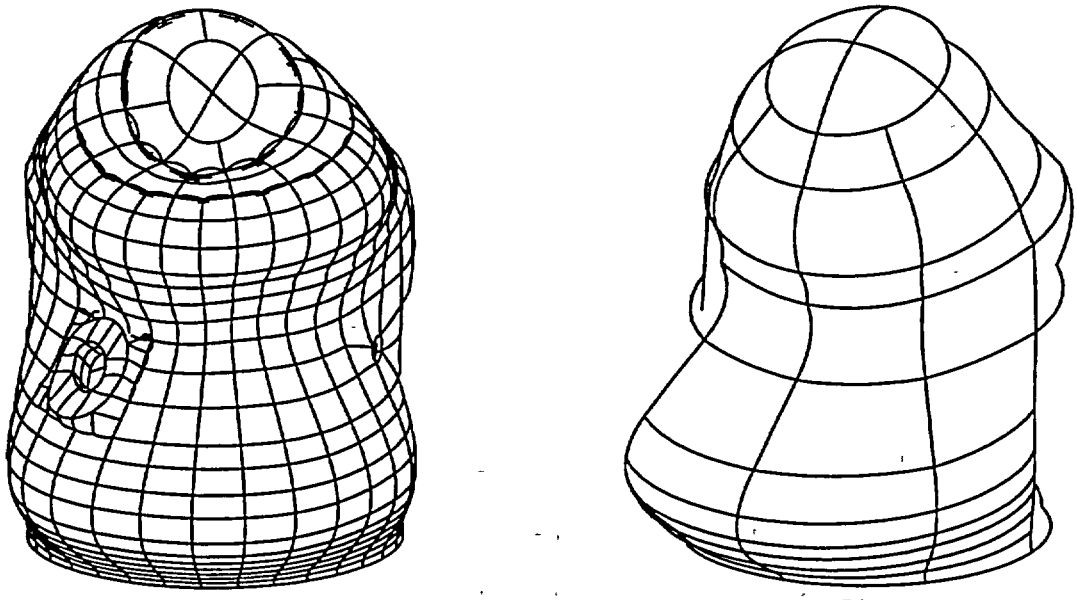

(a) (b)

Figure 2.13 Ninth Major Modal Shape Comparison (a) Original (b) Coarse

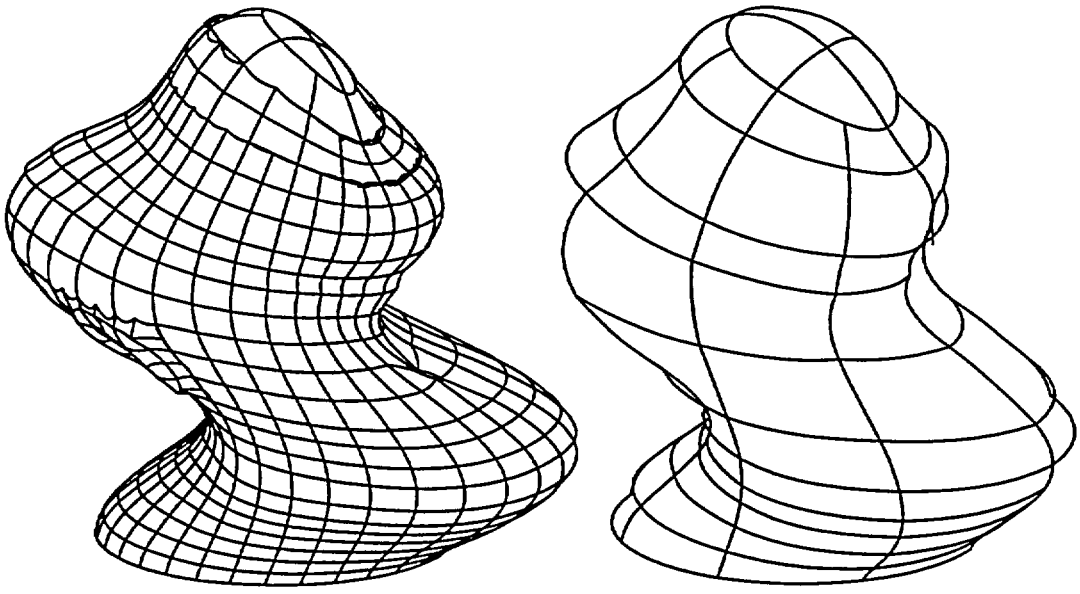

(a) (b)

Figure 2.14 Tenth Major Modal Shape Comparison (a) Original (b) Coarse

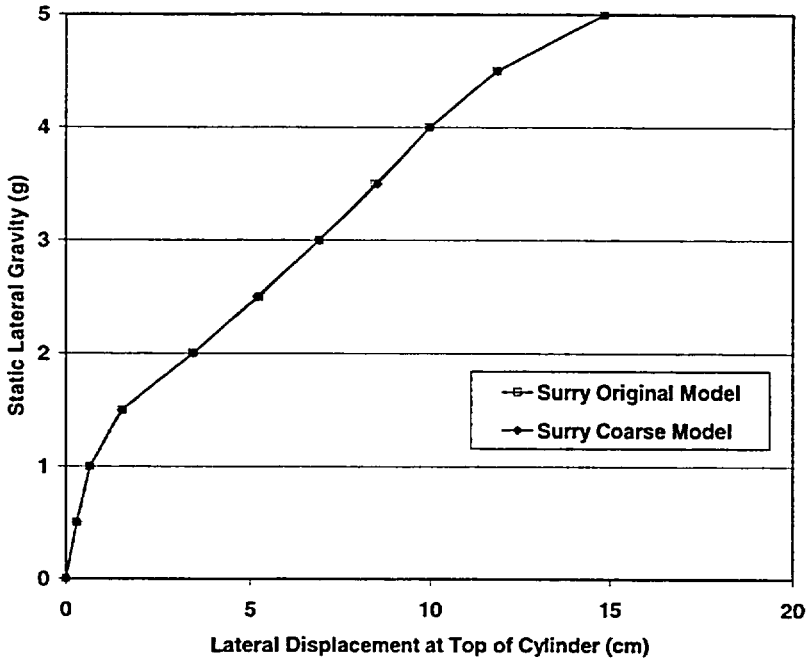

Figure 2.15 Static Pushover Results of Coarse and Original Models

3. Uncertainty Analysis Methodology

3.1 Latin Hypercube Method

In many uncertainty analyses, it is necessary to perform a suite of analyses by varying the input parameters. The variation in an output parameter (Y) is usually defined as a function of input variables $X_1, X_2, X_3, \ldots X_N$. This function can be simple, i.e., a uniform distribution, or complicated, such as a computer model. The question to be answered is: How does Y vary when the Xs vary according to some assumed joint probability distribution?

A conventional approach, developed in early computer models for performing uncertainty analysis, was the Monte Carlo method. This method involves repeatedly sampling from an assumed probability density function of X and evaluating Y for each sample. By sampling enough X variables, eventually the distribution of the resulting Y values will converge to the true distribution function. The problem with the Monte Carlo method is that it requires a significant number of sampling and calculations, depending on the number of different parameters being modeled and the relationship of the different parameters. It may take hundreds or thousands of samples to converge on the correct distribution.

An alternative approach, which can yield precise estimates with fewer samples, is to use a constrained sampling scheme. The scheme applied in this study, developed by McKay, Conover, and Beckman (Mckay et al., 1979), is Latin Hypercube Sampling (LHS). LHS selects J different values from each of N variables $X_1, X_2, X_3, \ldots X_N$ in the following manner. The range of each variable is divided into J non-overlapping intervals on the basis of equal probability. One value from each interval is selected at random with respect to the probability density in the interval. The J values thus obtained for X_1 are paired in a random manner (equally likely) with the J values of X_2. These J pairs are combined in a random manner with the J values of X_3 to form J triplets, and so on, until J N-tuplets are formed. This is the basis of the LHS.

To determine a seismic fragility of a concrete structure, it is necessary to vary many material, modeling, and input parameters. For this study, dynamic analyses were performed by subjecting a containment model to complete earthquake time-history accelerations. When using the Coarse Model discussed in the previous section, each analysis run took from 1 to 10 hours to complete, depending on the length of the earthquake record. The

refore, it was necessary to vary as many parameters as possible using LHS to get a realistic distribution of failures. These material and modeling parameters are shown in Section 3.2. A different actual earthquake time-history was input for each analysis instead of using a single earthquake and varying its parameters using LHS. This is discussed later in Section 3.3.

3.2 Uncertainties in Reinforced Concrete Containment Analysis

For the analysis of the Surry containment, certain parameters were varied according to the LHS method described above to gain insight into how these parameters affect the structural response and margin of the vessel. Several parameters were varied in this study. In order to vary these parameters, one must determine the uncertainties involved.

There are basically two types of uncertainties: random uncertainties and systematic uncertainties. Random uncertainties are typically inherent in the model or materials, such as material properties, failure limits, damping, etc. The random uncertainties included in this study are:

1) Material Properties (Modulus, Compressive or Yield Strength)
   a) Concrete
   b) Rebar
   c) Liner
2) Analytical Failure Limits (Maximum Strain)
   a) Concrete
   b) Rebar
   c) Liner
3) Damping
4) Earthquake Input.

Systematic uncertainties are typically analytically induced. These can include modeling accuracy (i.e., using a coarse mesh, symmetry assumptions, missing details in the FEM, time steps used in the analysis, etc.). They might also include the accuracy of the finite element methodology (i.e., concrete constitutive model accuracy, flow rules in steel plasticity, etc.).

For this study, an overall systematic uncertainty was used to include all these uncertainties with a single analytical model factor applied in the final stages of the uncertainty analysis.

In some cases, the specified uncertainties are both random and systematic. For example, the concrete shear strain limit has a random range of uncertainty, but part of the distribution selected accounts for the uncertainty of the failure limit. Similarly, the damping ratio uncertainty is part random and part systematic.

The material properties used in this study are shown in Table 3-1. The material properties were taken from several reports on the structural properties of the Surry containment (Pananos et al., 1984 and NUREG-1150, 1990). The concrete shear strain limit was taken from the analysis report on the PCCV and RCCV model (James et al., 1999 and Cherry et al., 2001). Although collapse did not occur in the RCCV model until shear strains exceeded 0.5%, the amount of damage was significant enough to justify using the same failure strain determined from the PCCV tests.

Distributions were assumed to be either normal or lognormal based on previous work and experienced judgment. Similarly, the uncertainties, coefficient of variation (COV) for normal distributions, and logarithmic standard deviation (β) for lognormal distributions were based on previous work and experienced judgment.

Other modeling properties used in this study are shown in Table 3-2. These include the level of viscous damping and the overall analytical model factor. The amount of viscous damping used in this study incorporates the crack-consistent damping model developed during the RCCV model analysis and described in Section 1. In the RCCV analysis (Cherry et al., 2001), the structural viscous damping was varied from 1% to 4% depending on the amount of cracking at each integration point, and produced very comparable results. Concrete elements with no cracks had a viscous damping of 1%, and as cracks developed at integration points, the damping increased up to a maximum of 4%. For the Surry analyses discussed in this report, the viscous damping initially varied about a mean of 1%. When cracking occured, the amount of damping at that integration point would vary about an increased mean up to 4%, as shown in Table 3-2. (Note that concrete cracking, rebar plastically straining, liner plastically straining, and other non-viscous damping mechanisms are accounted for in the analysis, but are not included in the viscous damping values shown in Table 3-2.)

As stated previously, all the modeling uncertainty in this study was included in one analytical modeling factor with a mean of 1.0. The associated uncertainty considers using a coarse mesh, missing details (penetrations), time step, concrete constitutive model accuracy, etc. This factor, uncertainty, and distribution type are shown in Table 3-2.

All the parameters shown in Tables 3-1 and 3-2 were varied according to LHS. A series of 30 different cases of random properties were generated for input into the ABAQUS model. Thirty cases were chosen because probabilistic studies using LHS show that a minimum of 15 different analyses are usually necessary to achieve a reasonable distribution. For this study, this number was doubled to 30. Since each seismic analysis took between 1 and 10 hours (depending on the different earthquake inputs), and each earthquake input was analyzed at three to five different amplitude levels, over 100 runs could be performed in a reasonable amount of time. The only parameter remaining to be varied was the earthquake time-histories input for each of the 30 analysis cases.

3.3 Earthquake Inputs

As mentioned above, 30 different analysis runs were necessary to capture the variation in the failure of the Surry containment structure. Thirty different actual recorded time histories, from as many different earthquakes were necessary to capture the random behavior and variability of earthquakes.

3.3.1 Selection of 30 Earthquake Records

Acceleration records for 1074 different locations and from 140 different large earthquakes were obtained. These earthquakes were recorded worldwide.

This list of acceleration records was filtered to select those that:

1. Had a magnitude of 5.7 or greater,
2. Were recorded at a rock site (defined as rock or less than 5 meters of soil over rock), and
3. Were 50 km or closer to the fault.

If the site (rock, soil, etc.) or the distance to the fault wasn't known, which is the case for many of the earthquakes recorded outside of North America, the earthquake was removed from the list. This subset of records was examined and a few records that didn't have all three components of motion available were removed. In addition, a few recordings made on upper dam abutments were significantly different than nearby ground measurements, and were also removed from the list. Out of the original 1074 earthquake records, 71 passed this filter and were considered in the following step.

The 71 acceleration records were recorded at various locations during 23 separate earthquakes. The final selection of 30 strong motion earthquakes (Table 3-3) was made from this group of 71 earthquakes by following two procedures.

1. All earthquakes that were recorded at less than 10 km were included in Table 3-3. These records all came from separate earthquakes.

2. For records between 10 km and 50 km from the fault, there were between 0 and 13 acceleration records for each earthquake (one to five records was most common). One acceleration record was randomly chosen from each of these subgroups. This record was included in the list of 30 chosen earthquake inputs.

3.3.2 Selecting the Critical Portion of Earthquake Record and Time Increment

Each record (30 earthquake events, each with three components of acceleration) was examined, and the "strong motion" portion of each record was selected. These digitized earthquakes had intervals of 0.005 seconds, 0.01 seconds, or 0.02 seconds. The following method was used to shorten each earthquake record as much as practical.

1. Strong motion estimates were made purely by visually observing each set (i.e., all three components) of acceleration time-history data. For example, assume a record contained 40 seconds of data. A visual observation of the X and Y components of motion showed the largest motions occurred between 5 and 15 seconds, while a visual observation of the Z component showed the largest motions between 0 and 15 seconds. For this record, the strong motion estimate would have been between 0 and 15 seconds, and only the portion of each record between 0 and 15 seconds would be used in finite element analyses. Shock response spectra the components of each earthquake were used to verify that the "shortened" earthquake was comparable to the "original" version, as discussed in item 3.

2. For the earthquakes that were digitized at intervals of 0.005 seconds, every other digitized point was used in the subsequent analysis, so that the interval between points became 0.01 seconds. Records that were digitized at intervals of 0.01 seconds were not adjusted, nor were records that were originally at 0.02 second intervals. Therefore, all records used in the finite element analyses had time intervals of 0.01 or 0.02 seconds. In item 1, an earthquake was reduced from 40 seconds to 15 seconds. If the time interval of this earthquake was 0.005 seconds, the size of the earthquake would be further reduced by only using every other point in the record. This reduces the analysis time by a factor of about 5 $1/\{(15/40)*(1/2)\}$. Note that during the actual finite element analyses, a calculation time step of 0.01 seconds was used, even for earthquake records with time intervals of 0.02 seconds. (All of the records with 0.02 second intervals had little high frequency response, which is the reason for the longer time interval in the first place.) It was important to use the same time-step in the analysis so that differences weren't introduced in the results because of different sized time steps.

3. For each record, the acceleration response spectra were calculated at 5% damping for the original, unabridged records, and also for the shorter-duration, modified time-step records. In all cases, the two spectral curves were almost the same (within a few percent) for frequencies below the lowest resonant frequency of 6.4 Hz for the Surry model. The two spectral curves still compared very favorably up to about 10 Hz. Above 10 Hz, about one-quarter of the records showed up to 20% difference in the response between the original record and the modified record. The remaining three-quarters of the records matched very well even above 10 Hz. The primary reason for differences

above 10 Hz was the change in the time-step for records with considerable high-frequency content that were originally digitized at 0.005 seconds, not the shorter duration of the modified record.

The resulting time histories for each of the 30 earthquake events with three components of acceleration are shown in Appendix A.

3.3.3 Determining a Scale Factor for Each Earthquake Record

The last step was to "normalize" the magnitude of the 30 earthquakes, since they all came from different magnitude earthquakes and different distances from the earthquake epicenter. The earthquakes were normalized with a scaling factor to make all about the same magnitude. The method used to select a scaling factor for each of the 30 earthquakes is described below.

1. Start with three components of the acceleration record. Two orthogonal horizontal components are acceleration in the x direction x(t), acceleration in the y direction y(t), and the vertical component is acceleration in the z direction z(t).

2. Using the two horizontal accelerations, x(t) and y(t), calculate acceleration response spectra for the combined motion at 5% damping. This gives spectral response acceleration in the horizontal direction H(f) by calculating the response of a single degree of freedom system at a selected frequency, first for the x(t) input and then for the y(t) input. Since both systems and their responses are linear by definition, the magnitude of the resulting horizontal response can be obtained by calculating the square root of the sum of the squares (SRSS) and the peak horizontal response for that frequency. This was repeated at the next selected frequency, and so forth. The response spectrum calculated the peak response in any horizontal direction. Because of the way the two horizontal components are combined, the resultant direction of the peak acceleration varies as a function of frequency.

3. In calculating the response spectra, the frequency intervals were equally spaced on a log scale. Therefore, on a linear scale, the points were closer together at low frequencies and were farther apart at high frequencies.

4. The average spectral acceleration H(f) was calculated for many small segments of the curve. Each average was calculated for a segment that was 10% of the total curve. Response spectra were calculated at 201 frequency points, and each "averaged" segment of the curve consisted of 21 points. For example, an average was calculated for the responses from the 1st to the 21st frequency, another average was obtained from the 2nd to the 22nd frequency, another from the 3rd to the 23rd frequency, and so forth, until the last average was obtained from the 181st to the 201st frequency. Each of these averages was compared to the corresponding median point from the Regulatory Guide 1.60 design response spectra shape for the horizontal direction for a Multiplication Factor (MF) = 1.0 input earthquake and 5% damping, shown in Figure 3.1. That is, the frequency of the 11th response spectra point was the median frequency average of the 1st to 21st points, and the average was compared to the value of the Regulatory Guide 1.60 design curve at this median frequency. A scaling factor was selected (i e., by multipling every acceleration in the time history record by the constant scaling factor) so that the average response was equal to Regulatory Guide 1.60 design value. Scaling factors were calculated for each of the 181 segments considered (i.e., the 11th median frequency to the 191st median frequency), and the smallest of the 181 scale factors was selected. This scaling factor was then multiplied by each acceleration in the two horizontal and one vertical time history records for that earthquake. The net effect is that each earthquake is "normalized" so that it equals (and even slightly exceeds at a few points) the Regulatory Guide 1.60 design values for some frequencies but is smaller at most other frequencies.

   (Initially, the scaling factor was based on the average between 0.4 times the resonant frequency of the containment vessel and 1.2 times the resonant frequency (i.e., between 1.76 Hz and 5.28 Hz). This produced very unrealistic earthquakes for a few of the 30 cases. For example, although the input accelerations were scaled to about MF=1.0 in the 1.76 to 5.28 Hz range, some of the scaled earthquakes had up to 6 g input accelerations in the 10 to 15 Hz range, which is not realistic. The second attempt selected the scale using two averages, one between 1.76 and 5.28 Hz and the other between 5.28 and 15 Hz. This produced better results, but a few earthquakes with large input energies near 5.28 Hz weren't handled well because the portion of the earthquake

with high-energy content got divided between the two different averages. Finally, it was concluded that the best way to handle this was by calculating the average of many overlapping segments, as previously described.)

5. This process is repeated for each earthquake. Select a constant C, different for each earthquake, that will be multiplied by every acceleration in the x(t), y(t), and z(t) record. All 30 earthquakes will be near the Regulatory Guide 1.60 response spectra design earthquake level for 5% damping over some frequency range.

6. For each scaled earthquake, calculate the response spectra, X(f), Y(f), and Z(f) from x(t), y(t), and z(t). Calculate the mean response spectra shape by averaging all 60 horizontal X(f) and Y(f) records. For example, [X1(f) + Y1(f) + X2(f) + Y2(f) + . . . + X30(f) + Y30(f)] / 60. Repeat for the vertical components. Calculate the response spectra shape at +/- 1 standard deviations.

This scaling makes each earthquake reach some "design level" earthquake and normalizes them to account for different magnitude earthquakes and different distances from the fault. The principal difficulty in scaling the earthquakes is the difference in frequency content. Many of the earthquakes have most of the energy focused in the low-frequency ranges, but some events have most of the energy focused in the high-frequency range. Although both types of earthquake motion have occurred, it is difficult to compare the two. However, it is critical that differences in frequency content and phasing are included in this study to assess the effect of these differences. Therefore, every attempt was made to include as many different earthquakes, distances from fault, and rock types as possible.

The 30 earthquakes selected for these analyses and the scale factor applied to modify the earthquake level are described in Table 3-3. The critical portion of the earthquake record and the time increments selected for each earthquake are shown in Table 3-4.

The response spectra for each of the 30 scaled earthquakes are shown in Appendix B. The average (or mean) of all 30 horizontal response accelerations in both directions, as described in #6, is shown in Figure 3.2. The peak horizontal response acceleration at each frequency is also shown. The mean curve is low because it represents the average of all 60 earthquake inputs. The mean coupled earthquake response (also shown on the plot) is the average of all 30 coupled earthquake responses. The coupled responses represent a peak response input on the analytical model in constantly shifting directions. The peak response curve represents an envelope of the maximum responses input to the finite element model. This is probably more relevant because containment failure is usually governed by the maximum strains that occur during the earthquake time-history, not the average strains during the entire earthquake.

The variations of scaled earthquake time histories are shown in Figure 3.3. The mean curve from Figure 3.2 is plotted along with the mean plus one standard deviation (SD) along with the mean minus one SD. The variation or uncertainty in earthquake input is large due to the nature of the scaling process and the variation in peak frequency response among the 30 time histories.

Table 3-1 Material Properties, Uncertainties and Distributions				
Material	**Property**	**Mean**	**Uncertainty [1&2]**	**Distribution**
Concrete	Elastic Modulus Factor[3]	1.00	COV = 0.15	Normal
	Compressive Strength (f'_c)	360 kg/cm^2 (5160 psi)	β = 0.14	Lognormal
	Tensile Strain Limit	9.0e-5	COV = 0.20	Normal
	Shear Strain Limit	0.005	COV = 0.20	Normal
Rebar	Elastic Modulus	2.0E6 kg/cm^2 (29,000 ksi)	COV = 0.06	Normal
#14 & #18	Yield Strength	4,200 kg/cm^2 (60 ksi)	β = 0.11	Lognormal
	Tensile Strain Limit	0.05	COV = 0.20	Normal
Rebar	Elastic Modulus	2.0E6 kg/cm^2 (29,000 ksi)	COV = 0.06	Normal
#7 & #11	Yield Strength	3,400 kg/cm^2 (48 ksi)	β = 0.11	Lognormal
	Tensile Strain Limit	0.05	COV = 0.20	Normal
Liner	Elastic Modulus	2.0E6 kg/cm^2 (29,000 ksi)	COV = 0.06	Normal
	Yield Strength	3,300 kg/cm^2 (47 ksi)	β = 0.10	Lognormal
	Tensile Strain Limit	0.05	COV = 0.20	Normal

[1] COV = Standard Deviation / Mean

[2] β = Logarithmic Standard Deviation » COV when b < 0.30

[3] Concrete Elastic Modulus = Factor*57,600*$(f'_c)^{1/2}$, f'_c in psi

Table 3-2 Modeling Properties, Uncertainties and Distributions			
Property	**Mean**	**Uncertainty [1]**	**Distribution**
Viscous damping (variable at each integration point)	(1% to 4%) 0 cracks = 1 00% 1 crack = 2.00% 2 cracks = 3.00% 3 cracks = 4.00%	COV = 0.25	Normal
Analytical Model Factor	1.00	COV = 0.15	Normal

[1] COV = Standard Deviation / Mean

Table 3-3 Earthquake Description						
#	Earthquake	Mag	Dist (km)	Rock Type	PGA (gs) vert/hor/hor	Scale Factor Used to Modify EQ
1	Cape Mendocino – 1992	7.1	8	Franciscan Formation	0.75 / 1.50 / 1.04	0.600
2	Chalfant Valley, 1986	6.2	41	Volcanic	0.02 / 0.04 / 0.04	15.3
3	Coalinga – 1983	5.8	11	Pliocene Tertiary	0.14 / 0.22 / 0.19	4.19
4	Coalinga – 1983	6.4	34	Miocene Tertiary	0.03 / 0.06 / 0.10	10.3
5	Coyote Lake – 1979	5.7	3	Franciscan Formation	0.12 / 0.16 / 0.28	3.92
6	Friuli, Italy – 1976	6.1	13	rock type not specified	0.06 / 0.06 / 0.13	7.10
7	Gazli, USSR – 1976	6.8	3	rock type not specified	1.26 / 0.61 / 0.72	0.859
8	Helena - 1935	6.2	8	Permian	0.10 / 0.15 / 0.17	4.78
9	Imperial Valley - 1979	6.5	26	Volcanic	0.21 / 0.17 / 0.16	4.18
10	Kobe, Japan – 1995	6.9	0.2	rock type not specified	0.38 / 0.29 / 0.31	1.63
11			49	rock type not specified	0.08 / 0.09 / 0.11	7.80
12	Landers – 1992	7.3	1.1	rock type not specified	0.82 / 0.73 / 0.79	0.721
13			42	Granite	0.04 / 0.08 / 0.06	12.8
14	Loma Prieta – 1989	6.9	6	rock type not specified	0.89 / 0.56 / 0.61	0.948
15			21	Pleistocene Quaternary	0.05 / 0.06 / 0.08	5.97
16	Mammoth Lakes – 1980	6.0	20	Volcanic	0.08 / 0.11 / 0.07	9.58
17	Morgan Hill – 1984	6.2	0.1	Franciscan Formation	0.39 / 0.71 / 1.29	0.941
18			16	Franciscan Formation	0.09 / 0.07 / 0.10	6.66
19	Nahanni, Canada - 1985	6.8	6	Permian or older	2.09 / 0.98 / 1.10	0.753
20			16	Permian or older	0.14 / 0.15 / 0.14	2.88
21	Northridge – 1994	6.7	8	rock type not specified	1.23 / 1.59 / 1.29	0.734
22			42	rock type not specified	0.07 / 0.14 / 0.26	3.77
23	N. Palm Springs – 1986	6.0	26	Granite	0.10 / 0.14 / 0.11	4.52
24	Parkfield – 1966	6.1	10	Jurassic	0.14 / 0.36 / 0.27	2.94
25	Santa Barbara – 1978	6.0	37	rock type not specified	0.03 / 0.07 / 0.03	13.4
26	San Fernando – 1971	6.6	20	Granite	0.09 / 0.09 / 0.20	4.96
27	Spitak, Armenia – 1988	6.8	30	rock type not specified	0.12 / 0.20 / 0.18	4.04
28	Victoria, Mexico - 1980	6.1	35	Volcanic	0.30 / 0.62 / 0.59	1.29
29	Whittier Narrows – 1987	6.0	9	rock type not specified	0.23 / 0.30 / 0.20	2.50
30			21	Granite	0.12 / 0.12 / 0.19	3.55

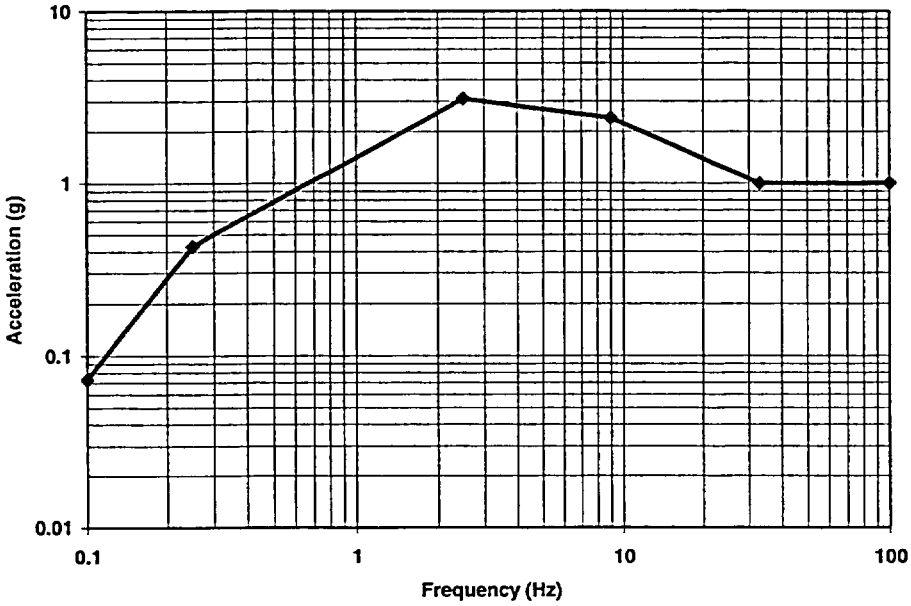

Figure 3.1 Regulatory Guide 1.60 Design Response Spectra – 5% Damping

Table 3-4 Earthquake Records to be used in Finite Element Analyses						
#	Earthquake	Original Duration (sec)	Reduced Duration Earthquake (sec)		Time Increment	
			Start Time	End Time	Original EQ	Reduced EQ
1	Cape Mendocino – 1992	29.98	0.0	8.5	0.02	0.02
2	Chalfant Valley, 1986	39.98	0.0	20.0	0.005	0.01
3	Coalinga – 1983	17.22	0.0	10.0	0.005	0.01
4	Coalinga – 1983	39.99	1.5	20.0	0.01	0.01
5	Coyote Lake – 1979	28.82	1.25	10.0	0.005	0.01
6	Friuli, Italy – 1976	16.45	0.0	7.5	0.005	0.01
7	Gazli, USSR – 1976	16.26	3.0	13.0	0.005	0.01
8	Helena - 1935	39.99	0.0	5.0	0.01	0.01
9	Imperial Valley - 1979	63.73	0.0	40.0	0.01	0.01
10	Kobe, Japan – 1995	31.99	3.0	13.0	0.01	0.01
11		53.99	10.0	25.0	0.01	0.01
12	Landers – 1992	48.12	5.0	25.0	0.005	0.01
13		49.98	0.0	40.0	0.02	0.02
14	Loma Prieta – 1989	24.96	5.0	15.0	0.005	0.01
15		38.98	0.0	20.0	0.005	0.01
16	Mammoth Lakes – 1980	39.99	0.0	10.0	0.005	0.01
17	Morgan Hill – 1984	29.95	0.0	7.0	0.005	0.01
18		29.97	1.0	10.0	0.005	0.01
19	Nahanni, Canada - 1985	20.56	1.0	11.0	0.005	0.01
20		19.09	2.5	12.5	0.005	0.01
21	Northridge – 1994	39.98	3.0	10 0	0.02	0.02
22		34.98	5.0	20.0	0.01	0.01
23	N. Palm Springs – 1986	24.00	2.5	5.0	0.005	0.01
24	Parkfield – 1966	30.32	2.0	6.5	0.01	0.01
25	Santa Barbara – 1978	11.56	2.0	10.0	0.01	0.01
26	San Fernando - 1971	29.99	0.0	10.0	0.01	0.01
27	Spitak, Armenia – 1988	19.89	7.5	15.0	0.01	0.01
28	Victoria, Mexico - 1980	24.44	3.0	13.0	0.01	0.01
29	Whittier Narrows – 1987	29.92	0.0	10 0	0.02	0.02
30		39.99	0.0	10.0	0.005	0.01

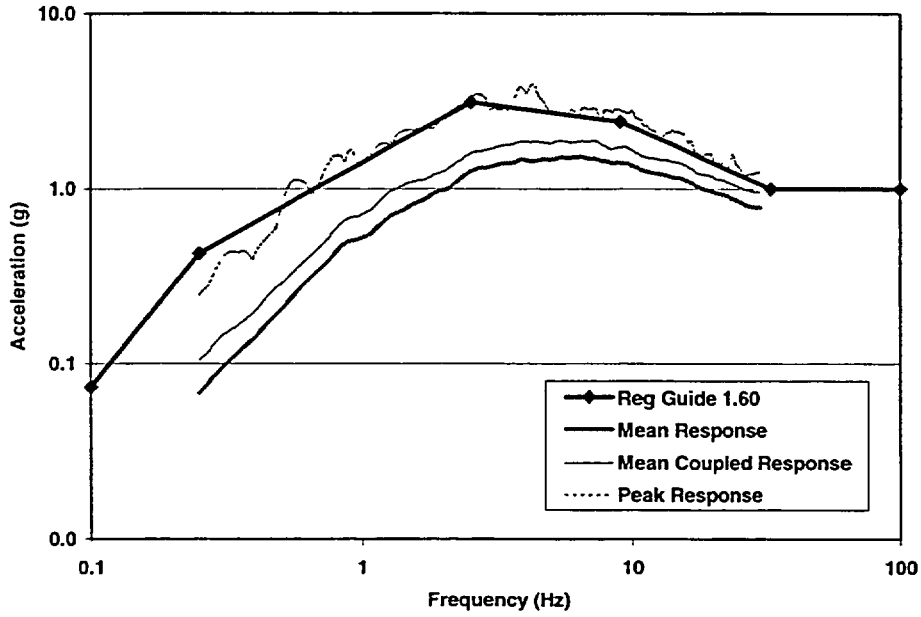

Figure 3.2 Comparison of Average, Coupled, and Peak Horizontal Response Spectra

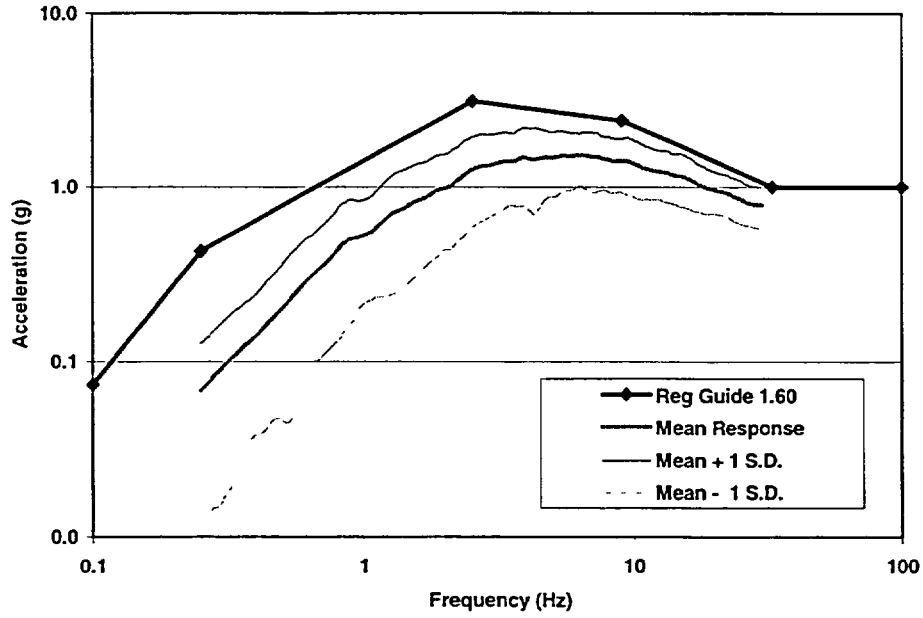

Figure 3.3 Comparison of Mean with Standard Deviation Variation

4. Analysis Results

4.1 Procedure

The 30 seismic analyses (at various seismic levels) were done to predict the magnitude of the failure earthquake for the Surry Coarse Model under the various parameters specified by the LHS technique. Each run was performed under input earthquakes scaled to be MF=1.0 times to envelope the Regulatory Guide 1.60 response spectra, 2.0 times, 3.0 times, 4.0 times, and 5.0 times the response spectra. The peak average shear strains were calculated and saved for each analysis, as well as the peak concrete and rebar strains. In each case, the predicted failure was caused by concrete shear. Other failure criteria, such as rebar or liner strains, did not control the failure. In addition, the accelerations at the top of the containment and relative displacements between the top and the basemat were saved.

Two separate loading cases were analyzed. The first case subjected the structure to increasing earthquake levels (MFs) without any internal pressure. The second case subjected the structure to increasing earthquake levels (MFs) while the containment vessel was loaded internally with the design pressure. It was hoped that a simplified method of predicting the seismic margin could be developed after a thorough evaluation of the analysis results.

4.2 Earthquake Only Loading

The first set of analyses was run on the Surry Coarse Model described in Section 2 with the earthquake histories described in Section 3. A total of 30 cases were analyzed using different scaled earthquake time-history inputs. The material properties were also varied in all 30 cases according to an LHS plan. Initially, the input motions were scaled to the MF=1.0 level. This MF=1.0 level corresponds to an earthquake enveloped by the Regulatory Guide 1.60 design response spectra. After the analysis was completed for all 30 cases, a second group of runs were executed with double the input motions and corresponds to a MF=2.0 level input. Similarly a level MF=3.0 was followed by a MF=4.0 and finally a MF=5.0 level input was run.

After each analysis run, the modal frequencies were computed for the damaged containment model. For comparison, the first modal frequency results for the original model and for each MF input are shown in Table 4-1 for all 30 cases. The frequency reduction percentages are shown on the right side. At the bottom of the table, the mean of all 30 runs for each MF is shown along with the COV. As expected, at higher level input earthquakes, the fundamental frequency decreases. The average dropped about 29% after the MF=1.0 input, approximately 40% after the MF=2.0 input, and 47% after the MF=3.0 input. At MF=4.0 and 5.0, some of the analysis cases were not run because the model had already failed, and thus further analysis at higher MFs was not necessary.

In order to determine when failure would occur in each case, additional data, including the concrete shear strains and rebar strains, were saved after each analysis run. Comparing them to the strain limits shown in Table 3-1, which were also varied according to LHS, a failure level could be determined. The maximum rebar strains never governed the failure. In each case, it was the concrete shear strain that resulted in failure.

The average concrete shear strain was computed across the entire cross-section of the model at a particular integration point elevation. Since the two sides perpendicular to the direction of acceleration carry nearly all the shear load, only the elements within a 90° section on both sides of the containment wall provided the shear resistance. Because the direction of peak acceleration is not known, the average shear strain was computed in eight different azimuthal directions between 0° and 180°. For each direction, only those shear strains at integration points within a 90° section of each side were included in the average. Including the other two 90° sections, which carry very little shear load and typically have lower shear strains, would lower the overall average shear strain.

The peak average concrete shear strain from the eight different directions and elevations were saved and are shown in Table 4-2. At the MF=1.0 input, the average shear strain was 0.0010, as shown at the bottom of the table. At the MF=2.0 input, the average shear strain was 0.0023 and at MF=3.0, the average was 0.0047. Each case was run for the MF=1.0, 2.0, and 3.0 input. For each case, the peak average concrete shear strain was compared to the LHS value of the concrete shear strain limit, shown on the right side of the table. The analysis continued with a MF=4.0 and 5.0 analysis, until the maximum average shear strain exceeded the strain limit or MF=5.0 was reached.

4.3 Earthquake with Internal LOCA

The second set of analysis runs were the same as shown previously, but for this set of cases, a uniform constant pressure was applied to the inside of the containment model. The amount of pressure corresponded to an internal LOCA. This LOCA pressure is the design pressure (Pd) of the actual Surry containment, which is 0.310 MPa (45 psig). A total of 30 cases were again analyzed using different scaled earthquake time-history input. The material properties were also varied in all 30 cases according to an LHS plan. Initially, the input motions were scaled to the MF=1.0 level and increased up to MF=5.0.

After each analysis run, the modal frequencies were computed for the damaged containment model. For comparison, the first modal frequency results for the Original Model and for each MF input, for all 30 cases, are shown in Table 4-3. The percent reductions are shown to the right. At the bottom of the table, the mean of all 30 runs for each level is shown along with the COV. As expected, at higher level input earthquakes, the fundamental frequency decreases. The LOCA pressure alone lowered the average fundamental frequencies about 40%. After the MF=1.0 level earthquake, the averages dropped to 56%. They dropped to 58% after the MF=2 0 input and 60% after the MF=3.0, compare these to 29%, 40%, and 48% for the "No LOCA" case. The LOCA pressure had a significant effect on the frequency reductions. In a reinforced concrete containment analysis, the LOCA pressure will cause significant cracking, resulting in significantly reduced frequencies.

Again, data including the concrete shear strains and rebar strains were saved after each analysis run. By comparing them to the strain limits shown in Table 3-1, which were also varied according to LHS, a failure level was determined. Again, it was always the concrete shear strain that resulted in failure first.

The average concrete shear strain was computed across the entire cross-section of the model at a particular integration point elevation as described for the previous case. The maximum average shear strains are shown in Table 4-4. At the MF=1.0 input, the average shear strain was 0.0018, as shown at the bottom of the table. At the MF=2.0 input, the average shear strain was 0.0041 and at MF=3.0, the average shear strain was 0.0078. These were compared to the No LOCA results of 0 0010, 0.0023, and 0.0047, respectively. As shown, each case was run for the MF=1.0, 2.0, and 3.0 inputs. For each case, it was determined if the maximum shear strain exceeded the LHS value of the concrete shear strain limit for that case, shown on the right side of the table. The analysis continued with a MF=4.0 and 5.0 input analysis until the maximum average shear strain exceeded the strain limit or MF=5.0 was reached.

4.4 Probability of Failure

Using the data in Table 4-2 and Table 4-4, estimates of containment failure can be determined. First, the failure level was determined for each of the 30 cases analyzed. The level was determined by interpolating between the MFs, which yielded strains on both sides of the concrete shear strain limit for that particular case. When failure was not reached by the MF=5.0 input, extrapolation using the MF=4.0 and 5.0 strains were used with a maximum limit of MF=6.0. After all 30 cases were completed, the analytical modeling uncertainty factor (discussed in Section 3) was applied. The same process was again performed for the case with an internal LOCA pressure applied. The resulting failure levels for both cases were averaged and are shown in Table 4-5.

The average failure level in MFs, was relatively high; about 3.7 times MF without a LOCA pressure and about 2.7 times MF with a LOCA pressure. The COV is much higher for the case with LOCA; 0.56, compared to 0 41 without LOCA. These uncertainties are significantly higher than any of the material modeling variations. Therefore, the uncertainty in these estimates of the Surry containment structural failure are primarily driven by the variation in different earthquake time histories.

Next, each of the 30 failure points were sorted by failure level and assigned an equal probability of occurrence. This data was then plotted as a function of the probability of failure or Cumulative Distribution Function (CDF), as shown in Figure 4.1. From this plot the 5%, 10%, or median (50%) probability of failure can be inferred. For example, the 5% probability of failure is only MF=1.7 for the No LOCA case and MF=0.9 for the case with internal LOCA pressure. Lognormal curves were then fitted using the means and COVs, shown in Table 4-5, and plotted in Figure 4.2 for both cases.

Most often, probabilities of failure are given in terms of g or peak ground acceleration (PGA). It should be clarified that the failure levels shown so far are all in terms of earthquake multiples enveloping the Reg. Guide 1.60 response Spectra.

As discussed in Section 3, the earthquake inputs were all scaled to envelope the response spectra, and not scaled by PGA or to a particular range of response frequencies. Assuming the MF is comparable to PGA or spectral accelerations (Sa) would be non-conservative, since most of the scaled earthquake inputs have a PGA less than 1.0 g and the Sa between 2-5 Hz is about one-half that of the Reg Guide 1.60 Spectra in the 2-5 Hz range.

In order to estimate the Surry containment fragility in terms of PGA, the following modifications were made to the failure calculation. First, a PGA was determined for each of the 30 earthquake input histories. Table 4-6 summarizes some of the earthquake information, including the vertical PGA, both horizontal PGAs, and the scale factor applied to each time history. Simply multiplying the horizontal PGAs by the scale factor only shows the maximum PGA in either the X or Y direction. In order to find the maximum PGA that the containment model experiences, the maximum coupled PGA from both horizontal time histories is determined (see Table 4-6). The average of these coupled PGAs is also shown as 0.89 g, which is less than 1.0 g but much higher than the average of all 60 horizontal PGAs (0.71g).

This peak coupled horizontal acceleration is then replaced by the MF=1.0 for each of the 30 cases. The value for MF=2.0 is twice the maximum coupled PGA, and so forth. The resulting failure levels (in terms of PGA) both with and without LOCA are shown in Table 4-5.

The average failure level in g or PGA is lower than the results in multiples of the response spectra (MFs), but still reasonably high at around 3.2g without LOCA pressure and 2.4g with LOCA pressure. The uncertainty or COV is again higher for the LOCA case at 0.55, compared to 0.36 for the No LOCA case.

Next, each of the 30 failure points were sorted by failure level and assigned an equal probability of occurrence. This data was then plotted as a function of the probability of failure or CDF, as shown in Figure 4.3. From this plot, the 5%, 10%, or median (50%) probability of failure can be inferred. For example, the 5% probability of failure is 1.6g for the No LOCA case and only 0.7g for the case with internal LOCA pressure. A lognormal curve was then fitted using the means and COV, shown in Table 4-5, and is plotted in Figure 4.4 for both cases.

Another fragility curve was developed and keyed to Sa in the 2-5 Hz range. This range was selected because the undamaged fundamental frequency of the Surry model was about 6 Hz and the damaged frequencies were between 2-4.5 Hz, as shown in Table 4-1 and 4-3. Table 4-7 shows the scaled Sa at 2, 3, 4, 5, and 2-5 Hz for each of the 30 cases. The ratio of the Sa in the 2-5 Hz range to the Reg. Guide 1.60 Spectra in the same range is shown in the last column of Table 4-7. The MFs were then divided by these ratios for each of the 30 cases and fragilities were determined, as shown in Table 4-5.

The average failure level in gs Sa, or responses keyed to Sa in the 2-5 Hz range, is much lower than the results in multiples of the response spectra (MFs) and results keyed to PGA; about 1.8 gs Sa without LOCA pressure and about 1.3 gs Sa with LOCA pressure. The COV is also much lower, about 0.27 for No LOCA and 0.37 with LOCA. This is a result of keying all the earthquake responses to the frequencies dominating the modal behavior of the structure (2-5Hz).

Next, each of the 30 failure points were sorted by failure level and assigned an equal probability of occurrence. This data was then plotted as a function of the probability of failure or CDF, as shown in Figure 4.5. From this plot, the 5%, 10%, or median (50%) probability of failure can be inferred. For example, the 5% probability of failure is 1.0g Sa for the No LOCA case and only 0.6g Sa for the case with internal LOCA pressure. A lognormal curve was then fitted using the means and COV, shown in Table 4-5, and is plotted in Figure 4.6 for both cases.

Although the mean prediction of structural failure is reasonably high when keyed to PGA or MF of Regulatory Guide Spectra (2.4 – 3.7 times), the large uncertainly yields some probability of failure at only 1.0 (~ 5%-10% probability of failure with LOCA pressure). The mean prediction of structural failure is somewhat lower when keyed to Sa in the 2-5 Hz range (1.3 - 1.8 times); the smaller uncertainly yields some probability of failure at only 0.7g Sa (~ 10% probability of failure with LOCA pressure). This uncertainty is the result of using so many different time history inputs and is much higher when an MF is used or earthquakes are scaled to PGA.

In some probabilistic safety analyses (PSAs), these large 'tailing' failure levels significantly affect the overall plant risk when integrated with seismic hazard curves.

4.5 Comparison of Reinforced and Prestressed Concrete Containment Seismic Analyses

Results from the seismic fragility analysis of a Prestressed Concrete Containment were reported previously in NUREG/CR-6740 (Klamerus et al., 2001). Zion was the prestressed containment analyzed in that report. Whenever possible, the analysis procedures and methodology were identical to the seismic analysis of the reinforced concrete containment (Surry) in this report.

Both analyses included: the development of a fine and coarse finite element mesh model; coarse models with similar element sizes and identical number of elements; pushover analyses performed on both sets of models; and modal frequencies between coarse and fine meshes that compared well. The seismic analysis of the Coarse Model included the following similarities:

1) ANACAP-U concrete model in the finite element code ABAQUS,
2) Concrete shear strain limit (0.005, COV= 0.20),
3) Analytical model factor identical (COV = 0.15) ,
4) Used LHS to vary material properties,
5) Separate analyses performed with and without internal LOCA pressure,
6) Five earthquake levels (1 MF, 2 MF...5 MF),
7) Thirty different analyses at each earthquake level, and
8) The same 30 earthquake time histories, scaled to the Regulatory Guide 1.60 spectra, duration, and time increments.

The following were calculated and tabulated for both sets of analysis:

1) First modal frequency reductions,
2) Maximum average concrete shear strains,
3) Failure levels in terms of MF, PGA, and Sa in the 2-5 Hz range, and
4) Means, COV, and curves fitted for each term.

Some significant differences existed between the reinforced and prestressed concrete containments and analyses.

1) Key differences in Containment Geometry:
   a) Zion 50% larger (free volume - 86,000 m^3 for Zion, 57,000 m^3 for Surry).
   b) Surry 30% thicker cylinder walls
2) No tendons and no prestressing were modeled in reinforced concrete containment (Surry).
3) LOCA Pressure was
   a) 0.324 MPa (47 psig) for Zion, and
   b) 0.310 MPa (45 psig) for Surry.

One difference in the analysis was that the crack consistent viscous damping factor was 1% to 5% for the prestressed containment (Zion) and 1% to 4% for reinforced containment (Surry), depending on the number of cracks at each integration point. In addition, the simple half-model excited in only two directions (2-D) was not performed for the reinforced concrete containment (Surry). Simplifying the analysis to 2-D is primarily affected by how the two horizontal earthquake components are combined into one. Therefore, the results of a 2-D earthquake analysis of Surry would have yielded no additional information, but only verified the results found in the Zion 2-D analysis.

The first comparison between the prestressed and reinforced concrete containments is the results of the simple static pushover analysis. The lateral displacement at the top of the containment was normalized to the model height for both containments and plotted versus an increasing static lateral gravity load, as shown in Figure 4.7. As shown in this plot, the initial stiffness of the reinforced containment is higher. This is primarily due to the shorter and thicker cylinder walls in the reinforced containment. However, the reinforced containment starts to yield earlier and is actually softer at 2 gs, because the steel bars in the reinforced containment yield well before the tendons in the prestressed containment. Conversely, once the tendons start to yield significantly, the prestressed containment deflects significantly more above 2.5 gs, also shown in Figure 4.7, because the prestressed containment has less steel area resisting these lateral deflections.

The next comparison was between the modal frequency reductions following each earthquake input motion. The overall mean values and COVs from the 30 separate runs are shown in Table 4-8. The initial fundamental frequencies are shown prior to any earthquake input and differ; 4.42 Hz for the prestressed containment (Zion) and 6.31 Hz for the reinforced containment (Surry). Again, this reflects the shorter and thicker walls at Surry, resulting in a higher initial stiffness.

The reduced fundamental frequencies are shown after the 1 MF, 2 MF, and 3 MF level earthquake inputs. Reduced frequencies at higher earthquake inputs are not shown because not all 30 earthquake analysis were run for the 4 MF and 5 MF level inputs. The frequency reduction percentage after each earthquake input is also shown in the last three columns, which allows for direct comparison between the Zion and Surry results. As shown, frequency reductions were much more significant for the reinforced concrete containment (Surry) after only 1 MF. The reduction in the fundamental frequency was almost double for the reinforced containment at this level, both with and without the LOCA pressure applied. At higher earthquake inputs (3 MF), the reinforced containment frequencies reduced more than the prestressed frequencies, but the difference was much lower because at this point the prestressed containment was experiencing significant damage as well.

In addition, after the internal LOCA pressure was applied to the reinforced concrete containment, the initial fundamental frequency dropped about 40%. Application of the internal LOCA pressure causes significant concrete cracking to occur, resulting in reduced stiffnesses and frequencies. Conversely, the prestressed containment, which is typically designed with enough prestressing to maintain compression in the concrete at the LOCA pressure, experienced zero loss in frequency after the LOCA pressure was applied.

The maximum average concrete shear strains were also compared and are shown in Table 4-9. For low-level earthquakes (1 MF), the shear strains are comparable between the reinforced and prestressed concrete containments. However, at higher earthquake inputs (3 MF), the prestressed containment (Zion) showed much higher strains; 0.0140 compared to 0.0047 for the reinforced containment (Surry), for the case with no LOCA. When an internal LOCA pressure was applied, the difference was less significant; 0.0118 compared to 0.0078 for the prestressed and reinforced containments, respectively.

The average failure levels were also compared for both types of containments and are shown in Table 4-10. The maximum average concrete shear strain in both the prestressed and reinforced concrete containments governed failure. Analysis of the reinforced concrete containment (Surry) resulted in a higher mean failure level for all cases, both with and without LOCA pressure and for all three categories of normalized earthquake inputs. Without an internal LOCA pressure applied, the mean failure levels were 30-40% higher for the reinforced containment (Surry) compared to the prestressed containment (Zion). With an internal LOCA pressure applied, the reinforced containment was only 6-12% higher than the prestressed containment. An example of this comparison between reinforced and prestressed concrete containment fragility curves is shown for one of the cases (no LOCA, earthquake normalized to PGA) in Figure 4.8.

This comparison between the analysis results of a prestressed concrete containment (Zion) and reinforced concrete containment (Surry) shows that, for these two specific containments, the reinforced containment is more robust, based on the average failure levels of both containments. The seismic design requirements were very similar at both sites; Zion was slightly higher, with a specified horizontal SSE of 0.17g, whereas Surry's horizontal SSE was 0.15g.

The robustness of this reinforced concrete containment is primarily because of the much thicker cylinder walls and because a reinforced containment without prestressing contains significantly more reinforcing steel than the prestressed containment. On the other hand, the reinforced containment will probably experience more concrete damage than the prestressed containment, particularly with an internal LOCA pressure applied. The results herein showed frequency reductions at increasing earthquake inputs were more significant in the reinforced concrete containment as a result of significant concrete cracking. This additional concrete cracking can be attributed to the lack of prestressing steel tendons, which yield at a much higher level, typically 3-4 times that of reinforcing bars.

Table 4-1. First Modal Frequency Reduction (No LOCA)											
Case	Initial	Final - 1st Bending Frequency					Reduction Percentage				
#	Freq.	1 MF	2 MF	3 MF	4 MF	5 MF	1 MF	2 MF	3 MF	4 MF	5 MF
1	7.30	5.53	4.27	4.43	2.91		24%	41%	39%	60%	
2	6.06	4.13	3.49	3.39	2.38		32%	42%	44%	61%	
3	6.80	4.77	4.33	4.18	3.39		30%	36%	39%	50%	
4	5.77	4.90	3.53	2.32			15%	39%	60%		
5	6.19	4.17	3.43	2.57			33%	45%	58%		
6	6.59	4.14	3.36	3.01	2.85		37%	49%	54%	57%	
7	6.21	4.94	4.78	3.75	3.29	2.54	20%	23%	40%	47%	59%
8	6.32	4.37	4.47	3.29	2.92	2.69	31%	29%	48%	54%	57%
9	7.03	4.62	4.09	3.08			34%	42%	56%		
10	5.45	5.15	3.34	3.44	2.72		5%	39%	37%	50%	
11	6.57	3.36	3.02	2.59			49%	54%	61%		
12	6.93	4.70	3.99	3.88	3.55	3.13	32%	42%	44%	49%	55%
13	6.11	4.28	3.94	3.38	3.25	2.73	30%	36%	45%	47%	55%
14	6.35	4.11	3.91	3.57	2.84	2.31	35%	38%	44%	55%	64%
15	6.21	4.18	3.67	3.77	3.51	2.98	33%	41%	39%	44%	52%
16	5.89	3.44	2.67	2.63			42%	55%	55%		
17	5.91	3.53	3.04	2.91			40%	49%	51%		
18	6.27	4.97	4.27	4.76	4.43	3.62	21%	32%	24%	29%	42%
19	6.27	4.78	4.37	3.83	3.09	2.76	24%	30%	39%	51%	56%
20	5.80	4.02	3.59	3.62	3.65	3.42	31%	38%	38%	37%	41%
21	6.65	4.98	3.66	2.99	2.54		25%	45%	55%	62%	
22	5.83	3.23	2.95	2.38			45%	49%	59%		
23	6.41	5.76	5.00	4.49	4.08	3.80	10%	22%	30%	36%	41%
24	6.53	5.30	3.70	2.95			19%	43%	55%		
25	6.80	5.95	4.05	3.12			12%	40%	54%		
26	6.99	3.71	3.23	2.84			47%	54%	59%		
27	6.03	5.07	4.50	2.71			16%	25%	55%		
28	5.91	4.56	4.46	4.45	4.22	3.42	23%	25%	25%	29%	42%
29	6.07	3.93	3.07	2.69			35%	49%	56%		
30	6.08	3.86	3.69	3.66	3.52	3.74	36%	39%	40%	42%	39%
Mean =	6.31	4.48	3.79	3.36			28.9%	39.8%	46.7%		
COV =	0.07	0.16	0.15	0.20			0.38	0.23	0 23		

Table 4-2. Maximum Average Shear Strains (No LOCA)						
Case #	Maximum Average Concrete Shear Strains					Strain Limit
	1 MF	2 MF	3 MF	4 MF	5 MF	
1	0.0005	0.0012	0.0020	**0.0045**		0.0029
2	0.0009	0.0018	0.0028	**0.0105**		0.0033
3	0.0013	0.0026	0.0031	**0.0077**		0.0047
4	0.0007	0.0025	**0.0100**			0.0051
5	0.0007	0.0024	**0.0084**			0.0049
6	0.0012	0.0028	0.0050	**0.0069**		0.0052
7	0.0006	0.0012	0.0038	0.0032	0.0064	0.0069
8	0.0007	0.0023	0.0031	0.0048	**0.0077**	0.0052
9	0.0012	0.0021	**0.0056**			0.0038
10	0.0003	0.0020	0.0028	**0.0066**		0.0046
11	0.0016	**0.0062**	**0.0092**			0.0045
12	0.0009	0.0018	0.0022	0.0026	0.0038	0.0056
13	0.0010	0.0024	0.0030	0.0044	0.0052	0.0057
14	0.0006	0.0014	0.0026	0.0040	**0.0106**	0.0064
15	0.0006	0.0011	0.0021	0.0026	**0.0063**	0.0049
16	0.0033	**0.0060**	**0.0139**			0.0040
17	0.0011	0.0040	**0.0071**			0.0059
18	0.0007	0.0012	0.0017	0.0024	0.0032	0.0042
19	0.0008	0.0013	0.0025	0.0046	0.0053	0.0055
20	0.0005	0.0008	0.0018	0.0020	0.0037	0.0067
21	0.0008	0.0025	0.0054	**0.0107**		0.0062
22	0.0021	**0.0048**	**0.0096**			0.0046
23	0.0005	0.0006	0.0020	0.0026	0.0035	0.0048
24	0.0008	0.0026	**0.0057**			0.0036
25	0.0006	0.0022	**0.0048**			0.0043
26	0.0022	0.0031	**0.0046**			0.0041
27	0.0006	0.0017	**0.0054**			0.0053
28	0.0006	0.0011	0.0018	0.0024	0.0035	0.0054
29	0.0007	0.0029	**0.0073**			0.0061
30	0.0010	0.0013	0.0022	0.0020	0.0030	0.0058
Mean =	0.0010	0.0023	0.0047			0.0050
COV =	0.63	0.59	0.65			0.20

Table 4-3 First Modal Frequency Reduction (With Internal LOCA)													
Case	Initial	Final - 1st Bending Frequency						Reduction Percentage					
#	Freq.	LOCA	1 MF	2 MF	3 MF	4 MF	5 MF	LOCA	1 MF	2 MF	3 MF	4 MF	5 MF
1	7.30	7.30	2.92	2.89	2.74			0%	60%	60%	62%		
2	6.06	3.40	2.65	2.48	2.39			44%	56%	59%	61%		
3	6.80	6.45	2.87	2 81	2.67	2.54		5%	58%	59%	61%	63%	
4	5.77	3.27	2.71	2.44	2.29			43%	53%	58%	60%		
5	6.19	3.47	2.79	2.71	2.54			44%	55%	56%	59%		
6	6.59	3.50	2.75	2.70	2.60			47%	58%	59%	61%		
7	6.21	3.50	2.79	2 61	2.50			44%	55%	58%	60%		
8	6.32	3.11	2.65	2.52	2.42			51%	58%	60%	62%		
9	7.03	7.03	2.93	2 65	2.39			0%	58%	62%	66%		
10	5.45	2.84	2.53	2.39	2.36			48%	54%	56%	57%		
11	6.57	3.60	2.66	2.50	2.38			45%	60%	62%	64%		
12	6.93	3.74	3.11	2.87	2.79	2.70	2.66	46%	55%	59%	60%	61%	62%
13	6.11	3.34	2.72	2.65	2.51			45%	56%	57%	59%		
14	6.35	3.56	2.85	2.84	2.56	2.45		44%	55%	55%	60%	61%	
15	6.21	3.36	2.72	2.67	2.52	2.46		46%	56%	57%	59%	60%	
16	5.89	3.04	2.52	2.40	2.32			48%	57%	59%	61%		
17	5.91	3.14	2.64	2.48	2.42			47%	55%	58%	59%		
18	6.27	3.68	3.04	2.87	2.82	2.70	2.64	41%	52%	54%	55%	57%	58%
19	6.27	3.52	2.78	2.75	2.64	2.54	2.49	44%	56%	56%	58%	60%	60%
20	5.80	3.06	2.66	2.65	2.65	2.63	2.63	47%	54%	54%	54%	55%	55%
21	6.65	3.69	2.75	2.59	2 48	2 41		44%	59%	61%	63%	64%	
22	5.83	3.08	2.56	2.36	2 27			47%	56%	60%	61%		
23	6.41	3.54	3.08	2.76	2.75	2.71	2.66	45%	52%	57%	57%	58%	58%
24	6.53	3.69	2.80	2.58	2 46			44%	57%	60%	62%		
25	6.80	6.80	2.91	2.78	2.70			0%	57%	59%	60%		
26	6.99	3.54	2.74	2.56	2.49			49%	61%	63%	64%		
27	6.03	3.66	2.82	2.61	2.44			39%	53%	57%	60%		
28	5.91	3.47	2.75	2.74	2.66	2.56		41%	53%	54%	55%	57%	
29	6.07	3.17	2.59	2.48	2.35			48%	57%	59%	61%		
30	6.08	3.35	2.81	2.69	2.67	2.61	2.55	45%	54%	56%	56%	57%	58%
Mean =	6.31	3.86	2.77	2.63	2.53			39.4%	56.0%	58.2%	59.9%		
COV =	0.07	0.32	0.05	0.06	0 06			0.39	0.04	0.04	0.05		

Table 4-4 Maximum Average Shear Strains (With Internal LOCA)						
Case	Maximum Average Concrete Shear Strains					Strain
#	1 MF	2 MF	3 MF	4 MF	5 MF	Limit
1	0.0009	0.0021	**0.0039**			0.0029
2	0.0021	**0.0069**	**0.0099**			0.0033
3	0.0008	0.0025	0.0037	**0.0071**		0.0047
4	0.0026	**0.0083**	**0.0245**			0.0051
5	0.0014	0.0028	**0.0112**			0.0049
6	0.0012	0.0027	**0.0085**			0.0052
7	0.0017	0.0039	**0.0080**			0.0069
8	0.0037	**0.0053**	**0.0061**			0.0052
9	0.0034	**0.0074**	**0.0114**			0.0038
10	0.0037	**0.0049**	**0.0055**			0.0046
11	0.0032	**0.0051**	**0.0056**			0.0045
12	0.0006	0.0011	0.0021	0.0039	0.0035	0.0056
13	0.0012	0.0050	**0.0069**			0.0057
14	0.0012	0.0023	0.0058	**0.0171**		0.0064
15	0.0012	0.0048	0.0049	**0.0072**		0.0049
16	**0.0072**	**0.0073**	**0.0086**			0.0040
17	0.0017	0.0057	**0.0114**			0.0059
18	0.0007	0.0014	0.0025	0.0037	**0.0053**	0.0042
19	0.0009	0.0020	0.0053	0.0053	**0.0107**	0.0055
20	0.0004	0.0009	0.0020	0.0035	0.0037	0.0067
21	0.0014	0.0035	0.0061	**0.0073**		0.0062
22	0.0019	**0.0067**	**0.0098**			0.0046
23	0.0006	0.0009	0.0014	0.0019	0.0026	0.0048
24	0.0016	**0.0050**	**0.0133**			0.0036
25	0.0016	0.0040	**0.0074**			0.0043
26	0.0016	**0.0048**	**0.0091**			0.0041
27	0.0013	**0.0088**	**0.0207**			0.0053
28	0.0010	0.0015	0.0049	**0.0079**		0.0054
29	0.0019	0.0035	**0.0086**			0.0061
30	0.0006	0.0013	0.0043	0.0056	0.0049	0.0058
Mean =	0.0018	0.0041	0.0078			0.0050
COV =	0.77	0.56	0.65			0.20

Table 4-5 Summary of Average Failure Level and Uncertainties				
	No LOCA		With LOCA	
	Mean	COV	Mean	COV
Multiplication Factor (MF), using Reg. Guide Spectra	3.70	0.41	2.72	0.56
Multiples of g normalized to pga	3.22	0.36	2.42	0.55
Multiples of g normalized to Sa (2-5 Hz)	1.80	0.27	1.28	0.37

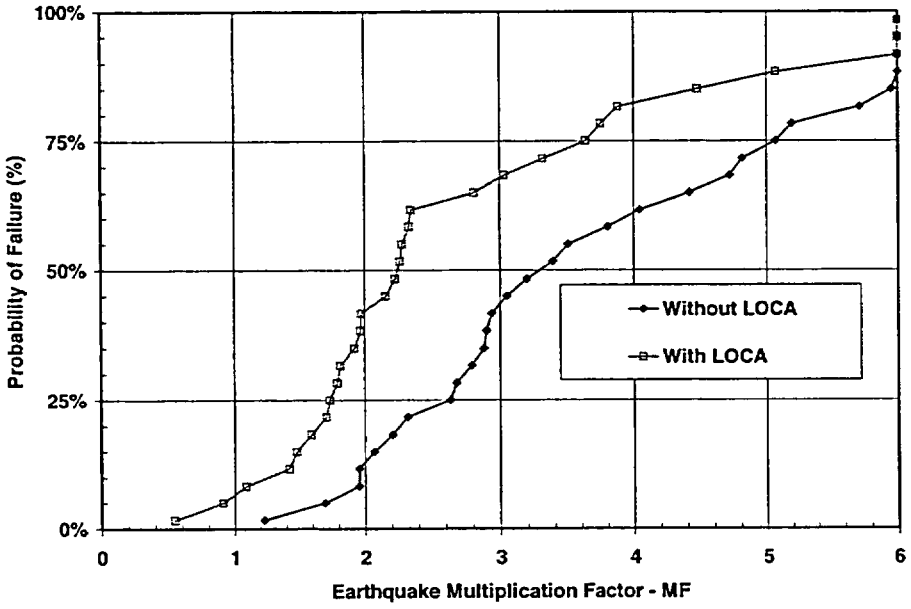

Figure 4.1 Fragility Plot of Failure Data (in terms of MF)

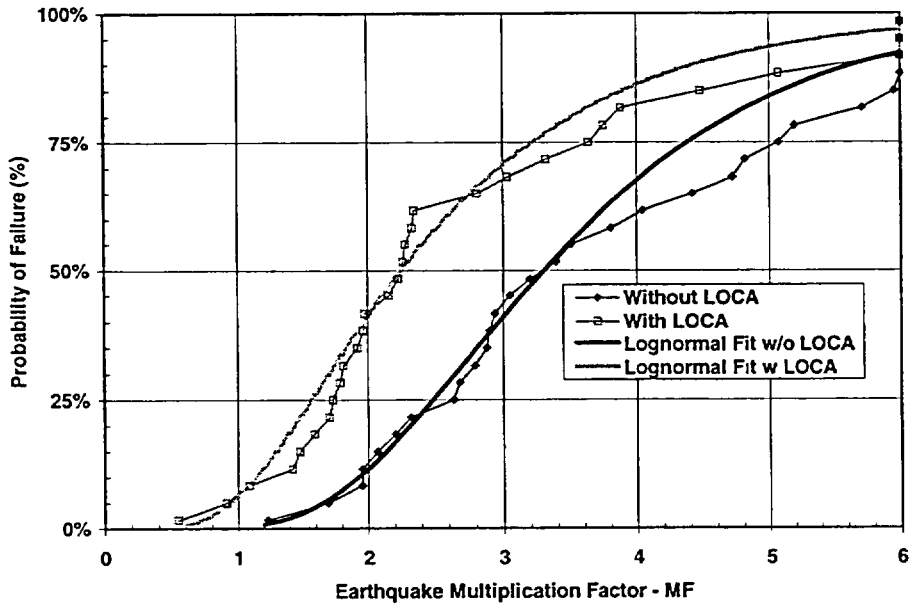

Figure 4.2 Fragility Plots with Fitted Curves (in terms of MF)

Table 4-6 Earthquake Description, Scaling, and Coupled Acceleration									
Case #	Earthquake	Dist (km)	PGA (g)			Scale Fact.	Scale * PGA (g)		Peak Coupled Horizontal (g)
			Vert	Hor-X	Hor-Y		Hor-X	Hor-Y	
1	Cape Mendocino – 1992	8	0.75	1.50	1.04	0.60	0.90	0.62	1.00
2	Chalfant Valley, 1986	41	0.02	0.04	0.04	15.30	0.61	0.61	0.70
3	Coalinga – 1983	11	0.14	0.22	0.19	4.19	0.92	0.80	0.97
4	Coalinga – 1983	34	0.03	0.06	0.10	10.30	0.62	1.03	1.13
5	Coyote Lake – 1979	3	0.12	0.16	0.28	3.92	0.63	1.10	1.15
6	Friuli, Italy – 1976	13	0.06	0.06	0.13	7.10	0.43	0.92	0.99
7	Gazli, USSR – 1976	3	1.26	0.61	0.72	0.86	0.52	0.62	0.73
8	Helena - 1935	8	0.10	0.15	0.17	4.78	0.72	0.81	0.90
9	Imperial Valley - 1979	26	0.21	0.17	0.16	4.18	0.71	0.67	0.77
10	Kobe, Japan – 1995	0.2	0.38	0.29	0.31	1.63	0.47	0.51	0.53
11		49	0.08	0.09	0.11	7.80	0.70	0.86	0.96
12	Landers – 1992	1.1	0.82	0.73	0.79	0.72	0.53	0.57	0.68
13		42	0.04	0.08	0.06	12.80	1.02	0.77	1.03
14	Loma Prieta – 1989	6	0.89	0.56	0.61	0.95	0.53	0.58	0.66
15		21	0.05	0.06	0.08	5.97	0.36	0.48	0.49
16	Mammoth Lakes – 1980	20	0.08	0.11	0.07	9.58	1.05	0.67	1.07
17	Morgan Hill – 1984	0.1	0.39	0.71	1.29	0.94	0.67	1.21	1.25
18		16	0.09	0.07	0.10	6.66	0.47	0.67	0.71
19	Nahanni, Canada - 1985	6	2.09	0.98	1.10	0.75	0.74	0.83	0.93
20		16	0.14	0.15	0.14	2.88	0.43	0.40	0.64
21	Northridge – 1994	8	1.23	1.59	1.29	0.73	1.17	0.95	1.17
22		42	0.07	0.14	0.26	3.77	0.53	0.98	1.06
23	N. Palm Springs – 1986	26	0.10	0.14	0.11	4.52	0.63	0.50	0.72
24	Parkfield – 1966	10	0.14	0.36	0.27	2.94	1.06	0.79	1.09
25	Santa Barbara – 1978	37	0.03	0.07	0.03	13.40	0.94	0.40	1.01
26	San Fernando – 1971	20	0.09	0.09	0.20	4.96	0.45	0.99	1.03
27	Spitak, Armenia – 1988	30	0.12	0.20	0.18	4.04	0.81	0.73	0.88
28	Victoria, Mexico - 1980	35	0.30	0.62	0.59	1.29	0.80	0.76	0.95
29	Whittier Narrows – 1987	9	0.23	0.30	0.20	2.50	0.75	0.50	0.76
30		21	0.12	0.12	0.19	3.55	0.43	0.67	0.75
						Mean =	0.71		0.89
						COV =	0.30		0.22

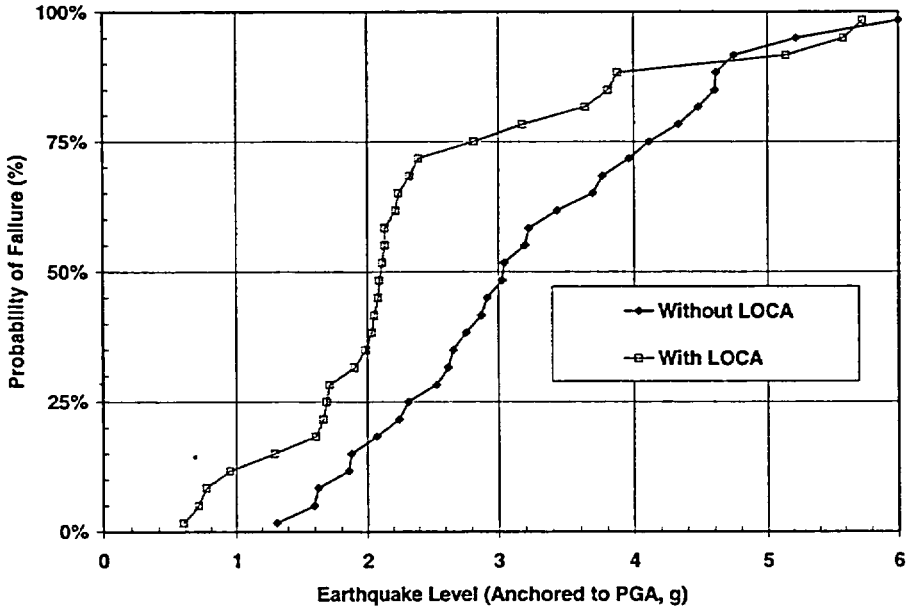

Figure 4.3 Fragility Plot of Failure Data (in terms of PGA)

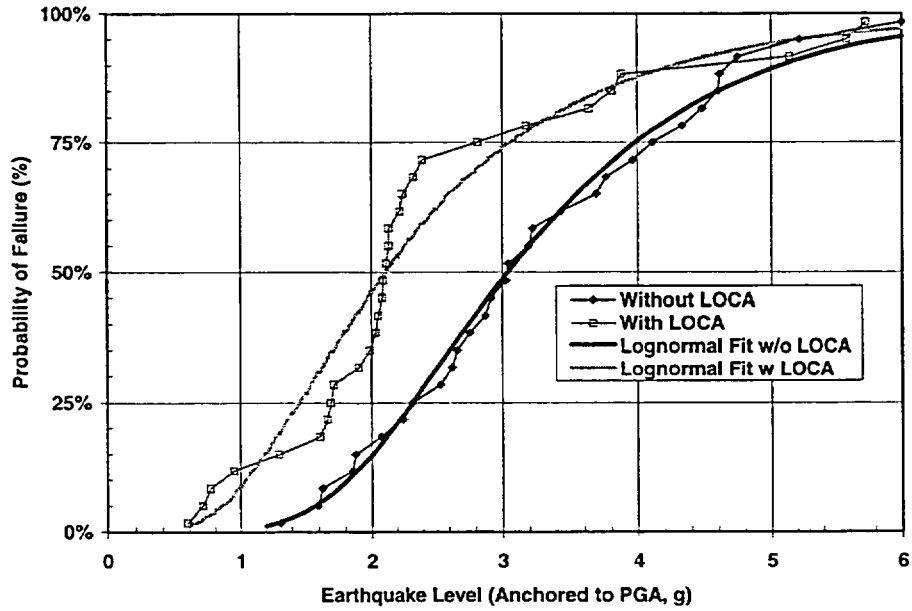

Figure 4.4 Fragility Plots with Fitted Curves (in terms of PGA)

Table 4-7 Earthquake Description and Scaled Spectral Accelerations								
Case #	Earthquake	Dist (km)	Scaled Spectral Acceleration (g) 2 Hz	3 Hz	4 Hz	5 Hz	Average Sa (g) 2-5 Hz	Ratio to Reg Guide Sa 2-5 Hz
1	Cape Mendocino – 1992	8	0.95	1.45	2.06	1.72	1.54	1.97
2	Chalfant Valley, 1986	41	1.96	1.77	1.37	1.65	1.69	1.71
3	Coalinga – 1983	11	1.11	1.90	2.18	3.11	2.07	1.54
4	Coalinga – 1983	34	2.50	2.62	1.61	1.30	2.01	1.54
5	Coyote Lake – 1979	3	2.67	2.59	1.83	1.55	2.16	1.39
6	Friuli, Italy – 1976	13	0.89	1.74	3.46	2.05	2.03	1.72
7	Gazli, USSR – 1976	3	1.27	1.24	0.97	1.22	1.17	2.45
8	Helena - 1935	8	0.96	1.94	1.80	1.57	1.57	1.92
9	Imperial Valley - 1979	26	2.23	2.54	2.15	2.37	2.32	1.22
10	Kobe, Japan – 1995	0.2	0.92	1.09	1.00	0.98	1.00	2.84
11		49	0.77	2.07	2.65	2.72	2.05	1.74
12	Landers – 1992	1.1	0.44	0.69	1.08	1.00	0.80	3.94
13		42	0.75	1.26	2.26	2.84	1.78	2.03
14	Loma Prieta – 1989	6	1.90	1.34	1.22	1.31	1.44	2.03
15		21	0.87	0.96	1.27	1.02	1.03	2.79
16	Mammoth Lakes – 1980	20	1.38	2.76	3.52	2.62	2.57	1.22
17	Morgan Hill – 1984	0.1	1.62	1.89	2.52	1.53	1.89	1.55
18		16	0.59	0.93	1.18	1.80	1.13	2.91
19	Nahanni, Canada - 1985	6	0.70	1.51	1.35	2.58	1.53	2.24
20		16	0.18	0.43	0.43	0.55	0.40	8.27
21	Northridge – 1994	8	1.71	2.46	1.84	2.24	2.06	1.40
22		42	1.53	1.91	2.09	2.31	1.96	1.47
23	N. Palm Springs – 1986	26	0.44	0 65	0.98	0.98	0.76	4.08
24	Parkfield – 1966	10	1.46	2.89	2.93	2.68	2.49	1.22
25	Santa Barbara – 1978	37	1.19	1.77	3.27	2.31	2.13	1.50
26	San Fernando – 1971	20	1.10	2.96	3.44	2.67	2.54	1.32
27	Spitak, Armenia – 1988	30	1.87	2.52	1.91	1.79	2.02	1.42
28	Victoria, Mexico - 1980	35	1.38	1.11	1.38	1.49	1.34	2.14
29	Whittier Narrows – 1987	9	2.26	1.42	1.27	1.86	1.70	1.77
30		21	0.26	0.62	0.72	1.75	0.84	5.09
	Mean =		1.26	1.70	1.86	1.85	1.67	2.28
	COV =		0.52	0.43	0.46	0.36	0.44	0.64

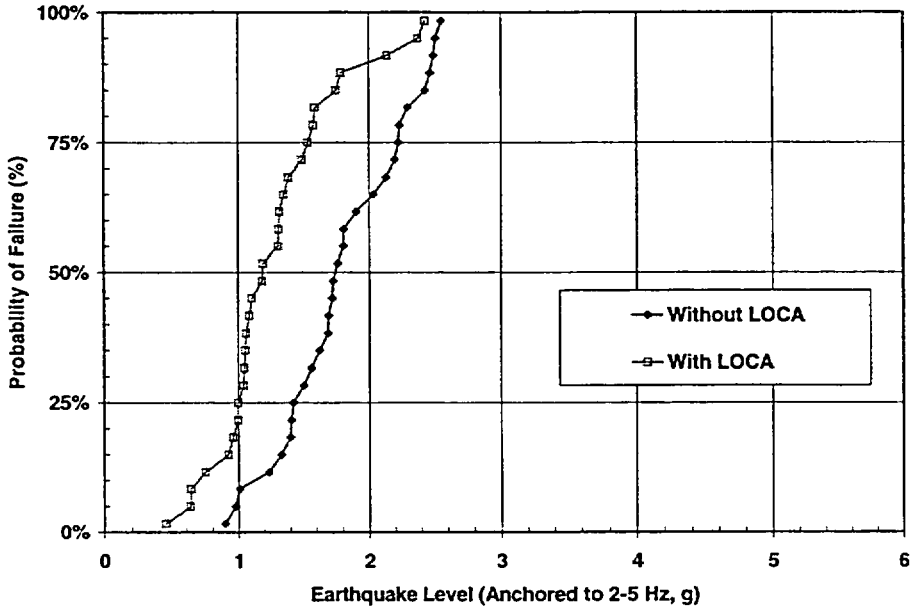

Figure 4.5 Fragility Plot of Failure Data (in terms of Sa, 2-5Hz)

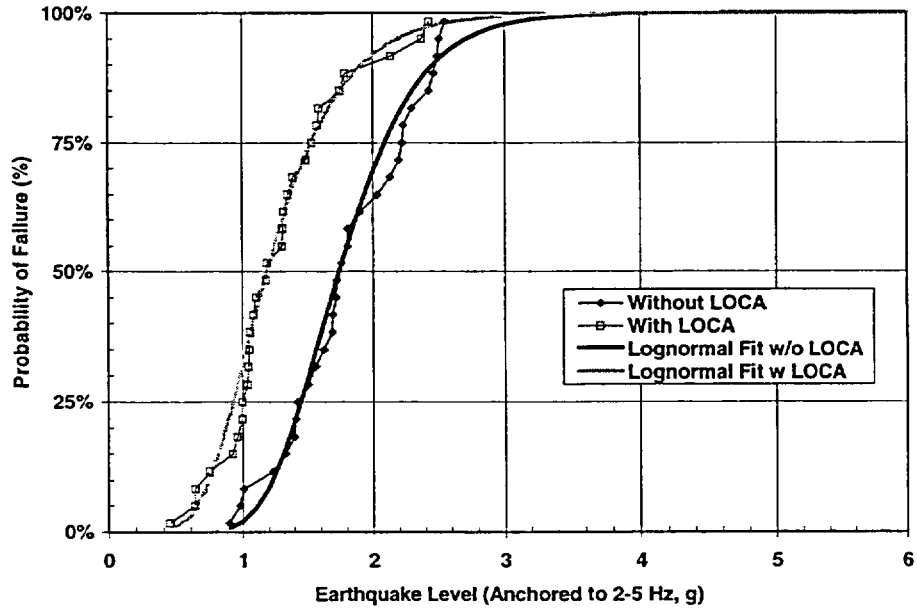

Figure 4.6 Fragility Plots with Fitted Curves (in terms of Sa, 2-5 Hz)

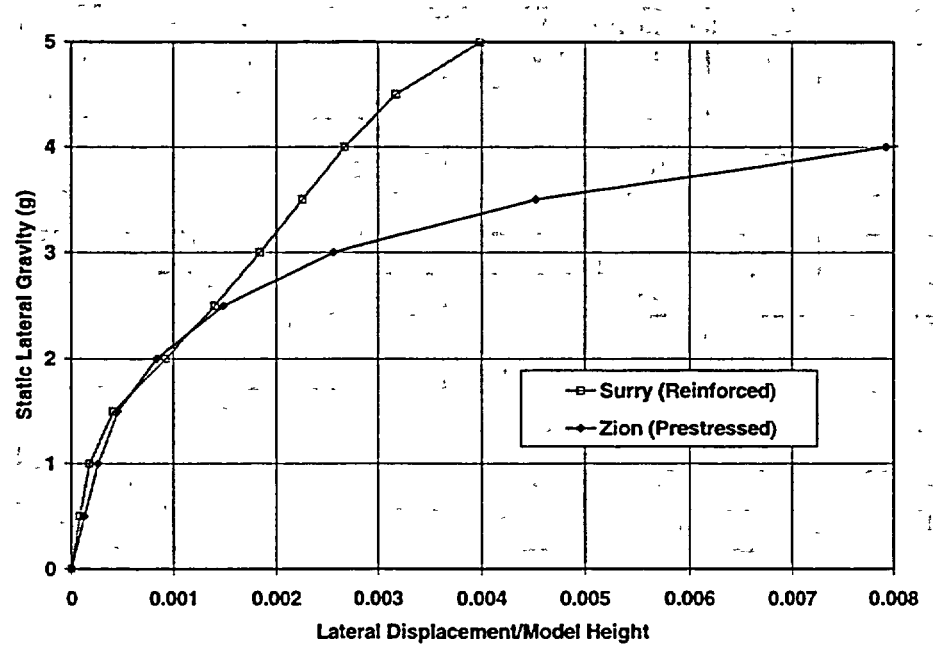

Figure 4.7 Static Pushover Comparison of Surry and Zion Models

Table 4-8 Modal Frequency Reduction Comparison									
LOCA	Plant	Variable	Initial	1st-Bending Frequency			Reduction Percentage		
			Freq.	1 MF	2 MF	3 MF	1 MF	2 MF	3 MF
No	Zion	Mean =	4.42	3.68	3.05	2.68	16.9%	31.0%	39.4%
		COV =	0.07	0.14	0.16	0.18	0.52	0.32	0.26
	Surry	Mean =	6.31	4.48	3.79	3.36	28.9%	39.8%	46.7%
		COV =	0.07	0.16	0.15	0.20	0.38	0.23	0.23
Yes	Zion	Mean =	4.42	3.12	2.44	2.10	29.4%	44.7%	52.3%
		COV =	0.07	0.19	0.17	0.19	0.40	0.21	0.18
	Surry	Mean =	6.31	2.77	2.63	2.53	56.0%	58.2%	59.9%
		COV =	0.07	0.05	0.06	0.06	0.04	0.04	0.05

Table 4-9 Maximum Average Shear Strains Comparison						
LOCA	Plant	Variable	Max. Average Concrete Shear Strains			Strain
			1 MF	2 MF	3 MF	Limit
No	Zion	Mean =	0.0012	0.0051	0.0140	0.0050
		COV =	0.81	1.13	1.57	0.20
	Surry	Mean =	0.0010	0.0023	0.0047	0.0050
		COV =	0.63	0.59	0.65	0.20
Yes	Zion	Mean =	0.0017	0.0055	0.0118	0.0050
		COV =	0.75	0.89	0.84	0.20
	Surry	Mean =	0.0018	0.0041	0.0078	0.0050
		COV =	0.77	0.56	0.65	0.20

Table 4-10 Comparison of Average Failure Level and Uncertainties								
	No LOCA				With LOCA			
	Zion		Surry		Zion		Surry	
	Mean	COV	Mean	COV	Mean	COV	Mean	COV
Multiplication Factor (MF), using Reg. Guide Spectra	2.77	0.55	3.70	0.41	2.56	0.58	2.72	0.56
Multiples of g normalized to pga	2.34	0.48	3.22	0.36	2.17	0.50	2.42	0.55
Multiples of g normalized to Sa (2-5 Hz)	1.29	0.35	1.80	0.27	1.15	0.29	1.28	0.37

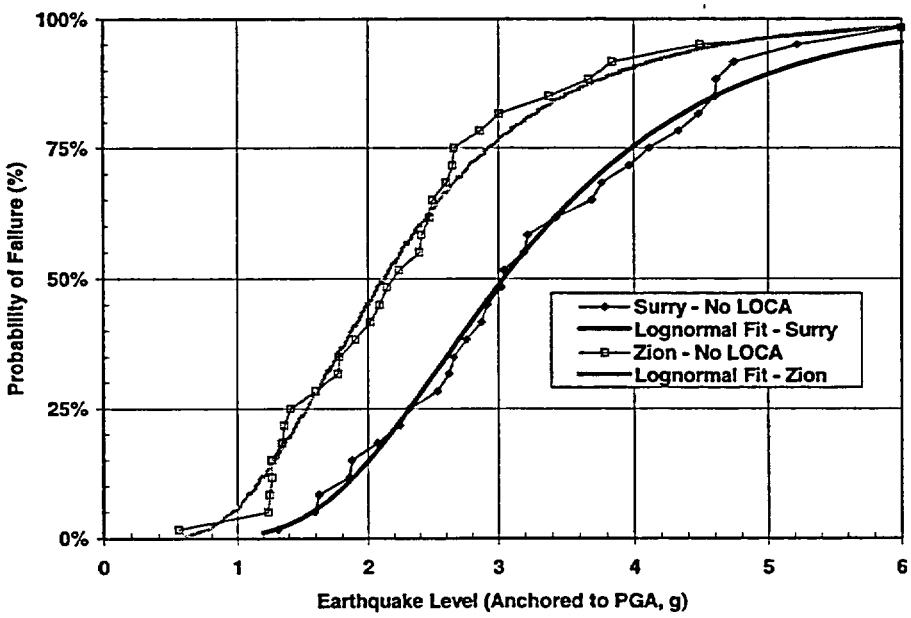

Figure 4.8 Fragility Plot Comparison of Surry and Zion (in terms of PGA)

5. Conclusions and Recommendations

5.1 Background

The NUPEC scale-model testing presented a unique opportunity to evaluate analytical methods and the ability to calculate the seismic response of an RCCV model. Based on the test results, some very general qualitative assessments were drawn of the structural and functional integrity of a U.S. containment (Cherry et al., 2001). The accompanying analysis was successful in capturing much of the model response and behavior observed during the tests.

The current program used finite element models similar to those for the NUPEC tests, and seeks to learn the response of U.S. containments. The objective of the calculations reported herein focused on the question, "What is the analytical predicted behavior and structural capacity of an actual reinforced concrete containment structure using the most recently developed and validated analysis tools?" This section summarizes the results of the analytical modeling of the Surry containment, resulting frequency reductions, and structural failure probabilities. Final comments and recommendations for additional, related work are then presented.

5.2 Results and Lessons Learned

The Surry nuclear power plant containment structure was modeled in detail with 3-D solid finite elements. Approximately the same amount of detail used in the RCCV seismic model (Cherry et al., 2001) was incorporated into this full-scale model of Surry. In addition, the same concrete material model was used in both analyses. After the Surry model was completed and its mass and stiffness properties determined, a much simpler (coarse) model was developed. This was necessary because the detailed Surry model was much too large to perform the multiple number of analyses necessary in a probabilistic failure study.

The possibility of using a nonlinear beam model or a lumped-mass/spring model was examined. It was found that neither could model both nonlinear shear stiffness correctly and include hysteresis effects to account for accumulating damage. Using a coarse grid of solid elements meets both of the requirements, with a slightly more complex model. This Coarse Model was compared to the Original Model and all the structural properties (i.e., total mass, center of mass, moment of inertia, major modal frequencies, static pushover, etc.) were nearly identical or very similar.

Next, the containment material properties and other parameters to be utilized in the analysis were assigned. Both a mean value and an uncertainty were assigned to each and keyed into an LHS process, resulting in 30 different sets of input parameters for the analysis. In addition, 30 different earthquake time histories were obtained and scaled for input into the dynamic analysis of the model.

Two separate loading cases were analyzed. The first case increased earthquake levels without any internal pressure. The second case increased earthquake levels while the containment vessel was loaded internally to the design pressure. Thirty seismic analyses (at various seismic levels) were performed to predict the failure earthquake of the Coarse Model using the various parameters specified by the LHS plan. For each of the two loading cases, 30 runs were performed under a MF=1.0, 2.0, 3.0, 4.0, and finally a MF=5.0 input earthquake.

After each analysis run, the modal frequencies were computed to observe the amount of damage for increasing earthquake inputs. For the case with no internal pressure, the frequencies dropped about 29% after the level MF=1.0 input, 40% after the level MF=2.0 input, and 47% after the level MF=3.0 input. When an internal LOCA pressure was applied, the frequency dropped 40%. It further dropped about 56% after the level MF=1.0 input, 58% after the level MF=2.0 input, and 60% after the level MF=3.0 input. This is similar to what happened during the RCCV model test. Significant additional cracking occurred in the concrete when the vessel was pressurized to design pressure and the design basis seismic load was applied. As a result of this combined test, the resonant frequency of the vessel reduced significantly.

For each loading case, the peak average shear strains were calculated for each analysis, as well as the peak concrete, rebar, and tendon strains. In each case, the predicted failure was caused by concrete shear. The average failure level in MFs, or multiplication factors of various earthquakes enveloped by the Regulatory Guide 1.60 design response spectra, was relatively high; more than 2.5 times MF with and without LOCA pressure. The case with LOCA had a much lower mean (2.72 compared to 3.70 without LOCA).

When the failure levels were based on spectra anchored to PGA, the average failure level in g was lower than the results in terms of MFs. The means were still reasonably high, above 2.4 g with and without LOCA pressure. The case with LOCA had a much lower mean (2.42g compared to 3.22g without LOCA).

For failure levels based on spectra anchored to Sa in the 2-5 Hz range, the average failure level in g Sa was much lower than the results in terms of MFs or when spectra was anchored to PGA. The case with LOCA had a lower mean; 1.28g Sa compared to 1.80g Sa without LOCA pressure.

Although the mean prediction of structural failure is reasonably high (~2.4g PGA or 1.3g Sa), the large uncertainties yielded some probability of failure at only 1g when a LOCA pressure was applied (~5-25% probability of failure). This large uncertainty is the result of using so many different time history inputs. In some PSAs, these large 'tailing' failure levels can significantly affect the overall plant risk when integrated with probabilistic seismic hazard curves.

In addition, the results of the reinforced concrete containment analysis were compared to a previous fragility analysis of a prestressed concrete containment. A comparison between the analysis results demonstrates that for these two specific containments, the reinforced containment showed a higher resistance to failure, but encountered premature damage in the concrete.

These results show, in general, how robust a reinforced concrete containment structure is when it is modeled on a rigid rock foundation. The most significant variable in the response is the variability in the input earthquakes. Modeling on a rock site will produce higher concrete stresses and strains than for a less rigid site model, resulting in a conservative estimate of the reinforced concrete containment's structural capacity. This should not be confused with the containment's functional capacity. To determine the containment's functional capacity, all failure modes and types, on a plant-specific case, must be examined and include basemat uplift, excessive distortion of piping, and effects of impact with other nearby structures. Modeling SSI will significantly impact the frequencies, mode shapes of the structure, and input earthquakes. Based on these results, response on a soil site will most likely be dominated by SSI and uplift, and the concrete will not be the failure mode, in other words, other things will probably fail before the reinforced concrete structure fails.

The results from this work also corroborate previous work on the seismic capacity of light water containments (Amin et al., 1989, and Clauss et al., 1989). These studies found that containments were typically very robust. Capacities ranged from 0.3g to 1.0g (scaled to PGA) and were usually at least three times the SSE for each site. The only reinforced concrete containment studied was the Clinton Nuclear Power Plant containment structure and it was determined to have a structural capacity of approximately 1.0g. These capacities are not mean or median values; instead, they are described as 'conservative' lower bound capacities.

5.3 Recommendations for Future Work

An extension of this work would expand the current Zion or Surry fragility analyses to include SSI and basemat uplift. This would allow for inclusion of additional failure modes and would be more representative of actual concrete containments in the U.S. Allowing basemat uplift and modeling SSI will significantly impact the frequencies, mode shapes, and even the input earthquakes. Based on the results of this report, failure will more likely be dominated by SSI effects and/or basemat uplift. In addition, analyzing containments with SSI and uplift would produce results more applicable for a probabilistic risk study because it would include most of the predominant failure modes of a concrete containment. However, some failure modes will always be plant-specific or require very detailed modeling.

6. References

Amin, M., P. K. Agrawal, and T. J. Ahl, *An Analytical Study of the Seismic Threat to Containment Integrity,* NUREG/CR-5098, SAND88-7018, Sandia National Laboratories, Albuquerque, NM, 1989.

Butler, T. A., and L. E. Fugelso, *Response of the Surry and Indian Point Containment Buildings to Severe accident Pressures,* NUREG/CR-2569, LA-9301-MS, Los Alamos National Laboratory, 1982.

Cherry, J. L., R. J. James, L. Zhang, and Y. R. Rashid, *Seismic Analysis of a Reinforced Concrete Containment Vessel Model,* NUREG/CR-6707, SAND2001/0022P, Sandia National Laboratories, Albuquerque, NM, 2001.

Clauss, D. B. and W. A. von Riesemann, "Investigation of the Limit States for LWR Containments" *Structural Mechanics in Reactor Technology,* 10th International Conference, Volume K2, pp 509-514, 1989.

Hibbitt, D. et al., *ABAQUS/Standard, Version 5.7 User's Manual,* Hibbitt, Karlsson, and Sorensen, Inc., Pawtucket, Rhode Island, 1997.

James, R. J. et al., *ANACAP-U, ANATECH Concrete Analysis Package, Version 2.5, User's Manual,* ANATECH Corp., San Diego, CA, September 1997.

James, R. J., L. Zhang, Y. R. Rashid, and J. Cherry, *Seismic Analysis of a Prestressed Concrete Containment Vessel Model,* NUREG/CR-6639, SAND99-1464, Sandia National Laboratories, Albuquerque, NM, 1999.

Klamerus, E. W. and J. L. Cherry, *Structural Seismic Fragility Analysis of the Zion Containment,* NUREG/CR-6740, SAND2001-2504P, Sandia National Laboratories, Albuquerque, NM, 2001.

McKay, M. D., W. J. Conover, and R. J. Beckman, "A Comparison of Three Methods for Selecting Values of Input Variables in the Analysis of Output from a Computer Code," *Technometrics,* Vol. 21, pp 239-245, 1979.

NUPEC Summary Report – 2001 (translation of excerpts), *Proving Tests on the Seismic Reliability for Nuclear Power Plant, Seismic Proving Test of Reinforced Concrete Containment Vessel (RCCV),* Nuclear Power Engineering Corporation, Executive Manager Kunio Terada, 2001.

NUREG-1150: *Severe Accident Risks: An Assessment for five U.S. Nuclear Power Plants,* U.S. Nuclear Regulatory Commission, Washington, DC, December1990.

Pananos, W. J. and C. F. Reeves, *Containment Integrity at Surry Nuclear Power Station,* TP-84-13, Stone and Webster Engineering Corporation, Boston MA, February 1984.

Sasaki, Y. S. Tsurumaki, H. Akiyama, K. Sato, and H. Eto, *Seismic Proving test of a Prestressed Concrete Containment Vessel,* ASME/JSME Joint PVP Conference, San Diego, CA, 1998.

Appendix A

Earthquake Time Histories

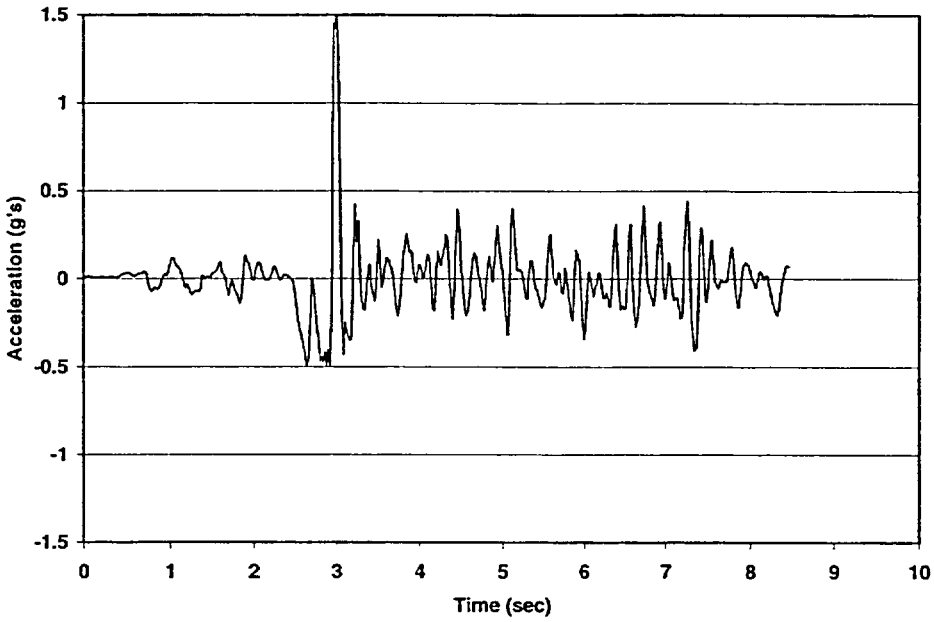

Figure A.1 Time History #1 (Cape Mendocino) Horizontal - X

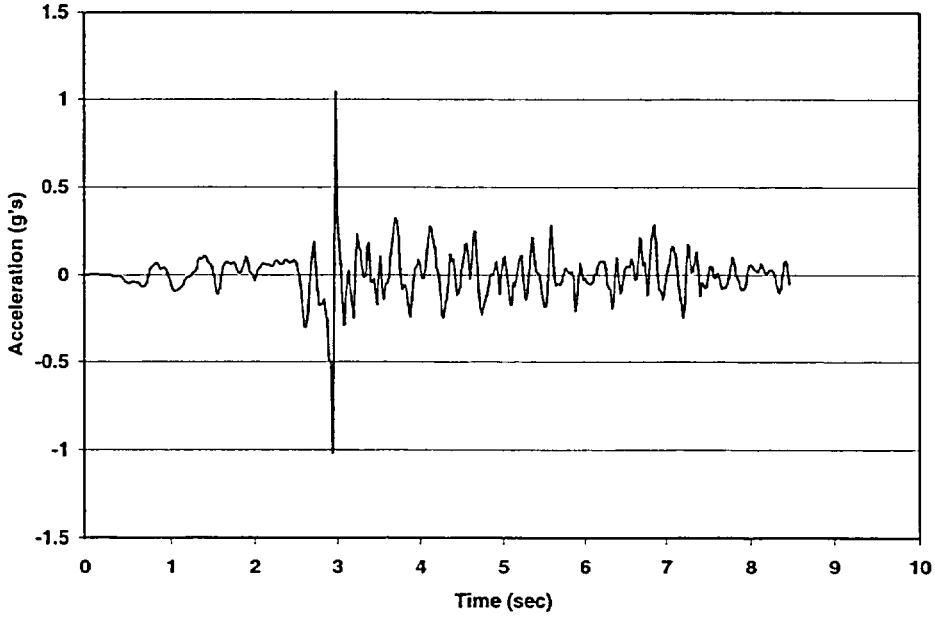

Figure A.2 Time History #1 (Cape Mendocino) Horizontal - Y

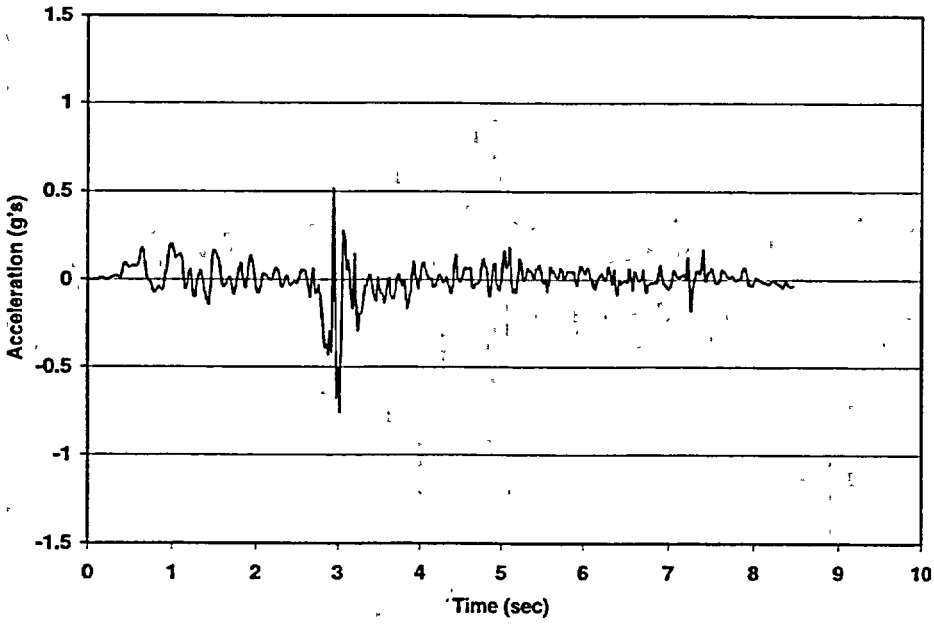

Figure A.3 Time History #1 (Cape Mendocino) Vertical - Z

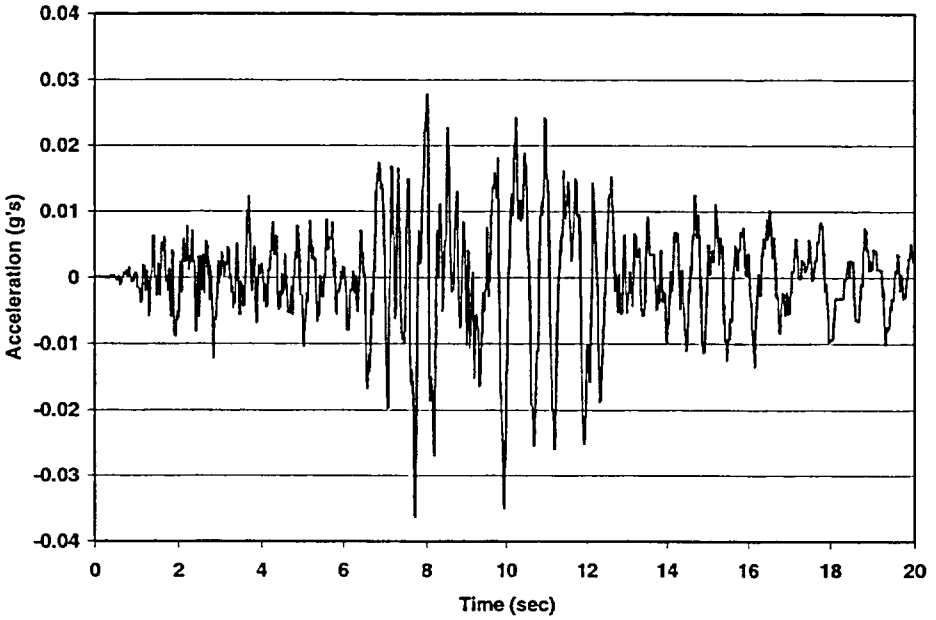

Figure A.4 Time History #2 (Chalfant Valley) Horizontal - X

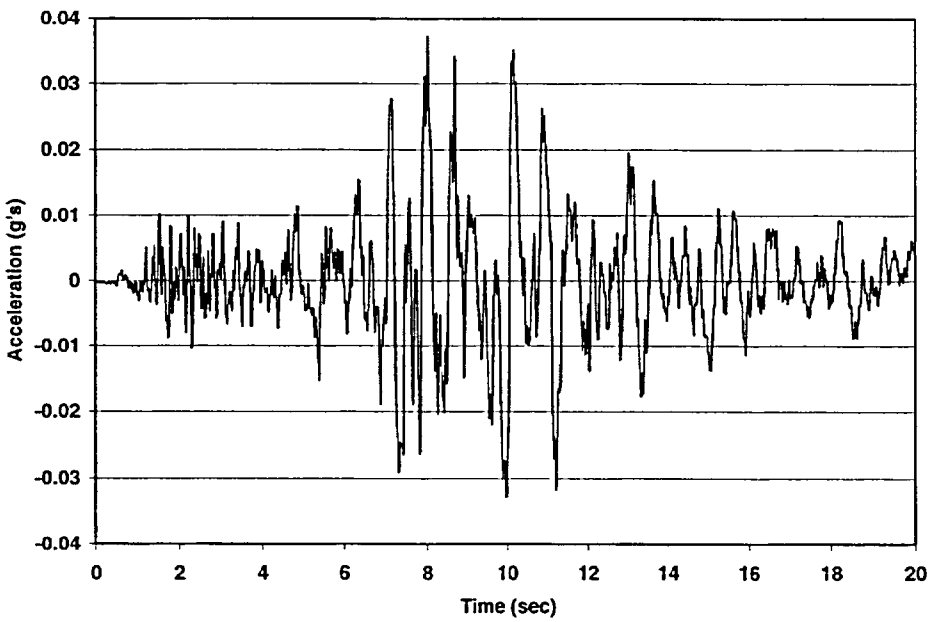

Figure A.5 Time History #2 (Chalfant Valley) Horizontal - Y

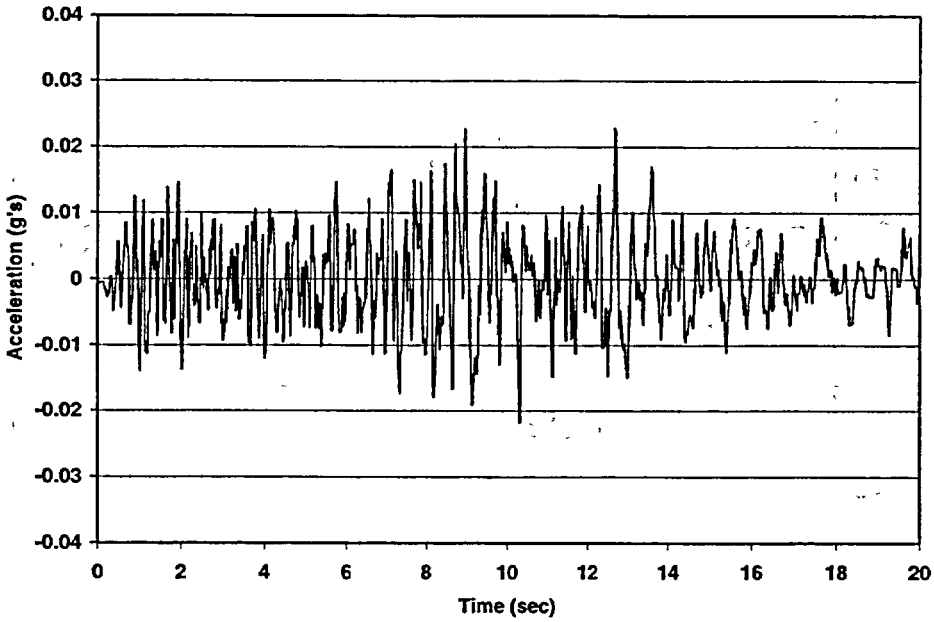

Figure A.6 Time History #2 (Chalfant Valley) Vertical - Z

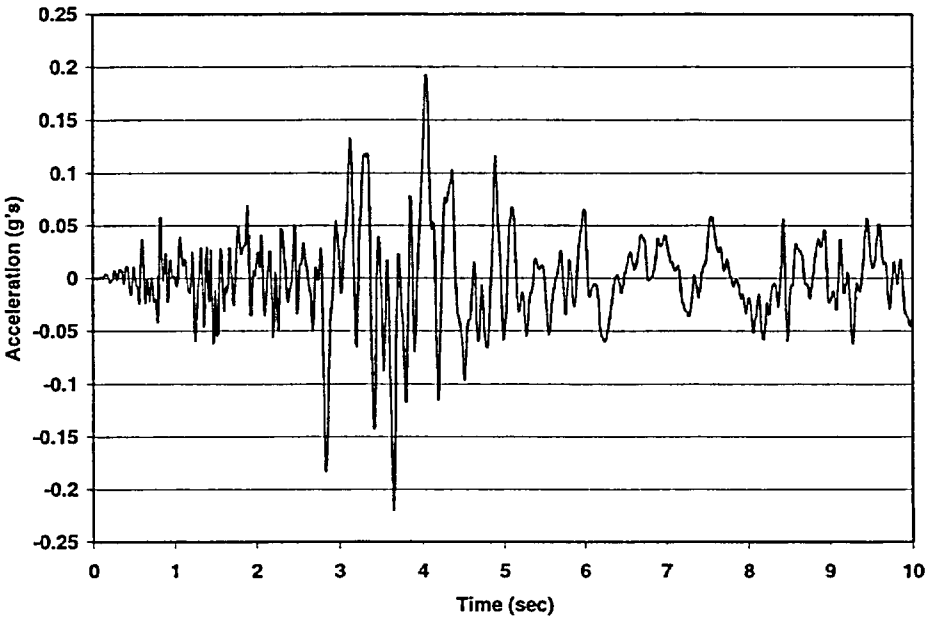

Figure A.7 Time History #3 (Coalinga – 11km) Horizontal - X

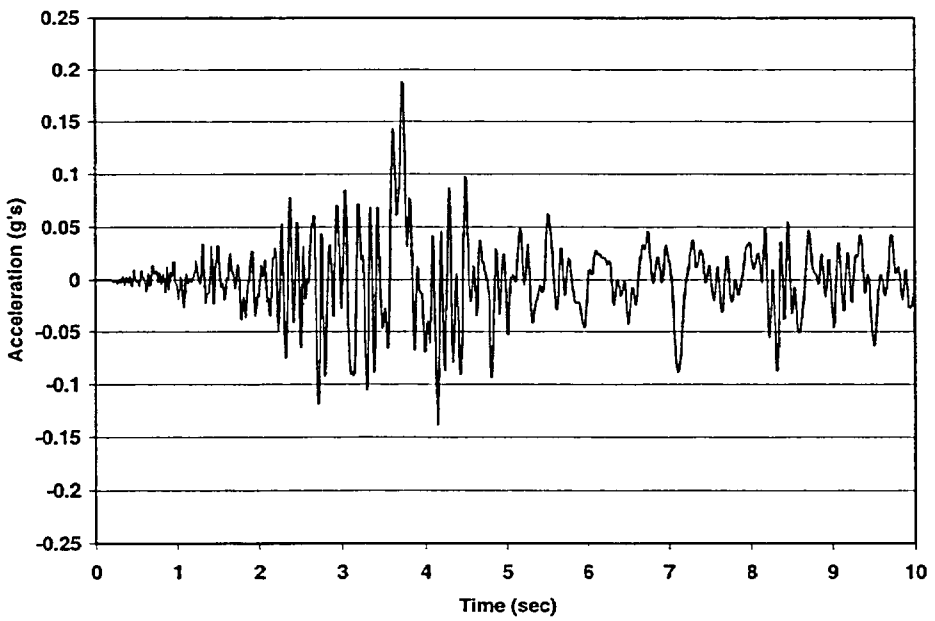

Figure A.8 Time History #3 (Coalinga – 11km) Horizontal - Y

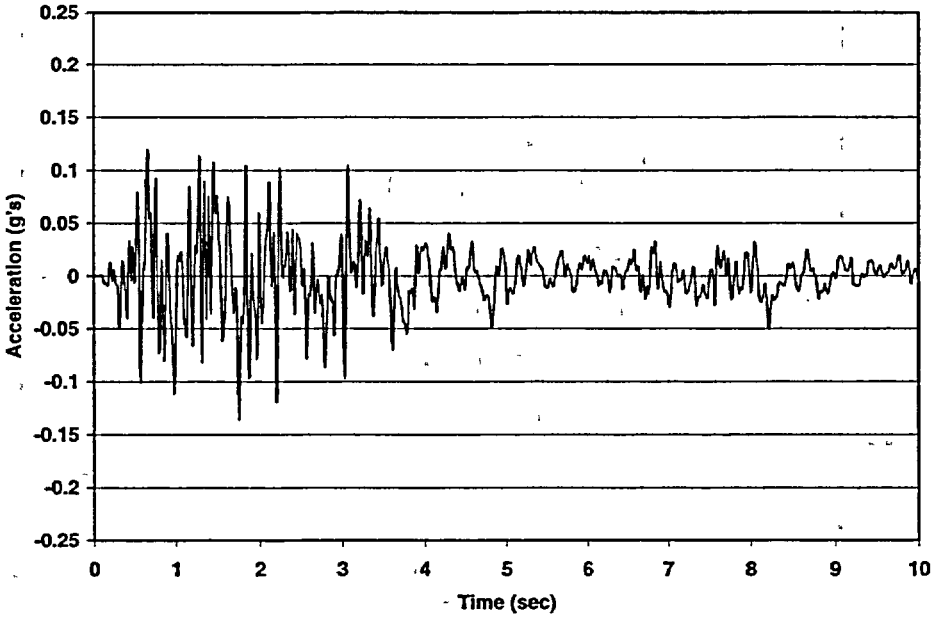

Figure A.9 Time History #3 (Coalinga – 11km) Vertical - Z

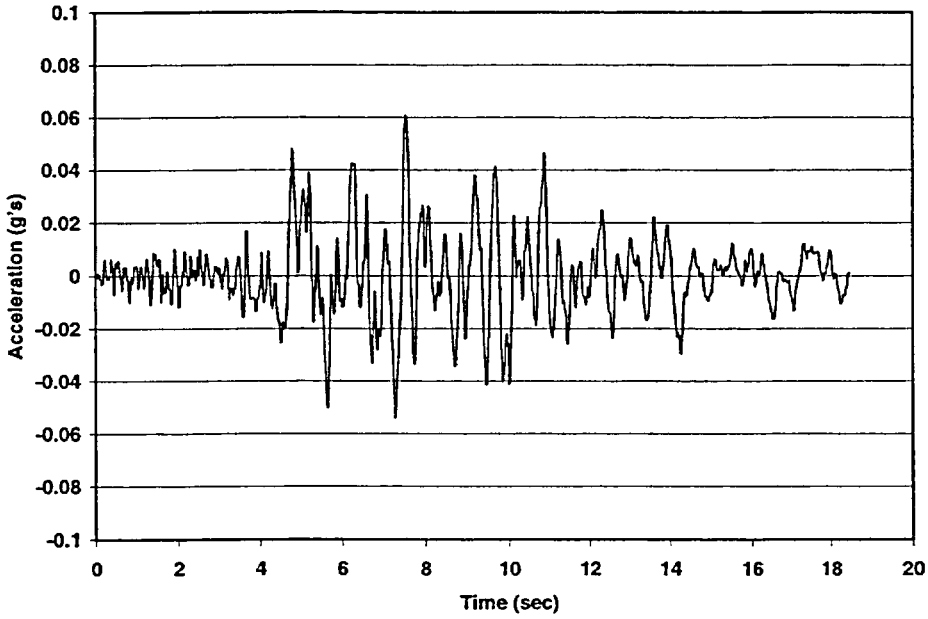

Figure A.10 Time History #4 (Coalinga – 34km) Horizontal - X

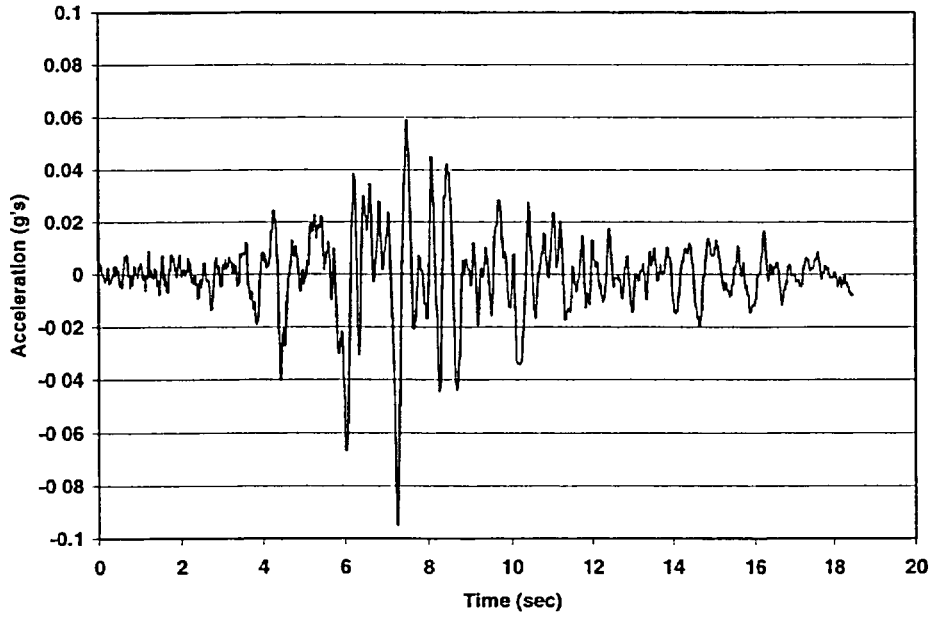

Figure A.11 Time History #4 (Coalinga – 34km) Horizontal - Y

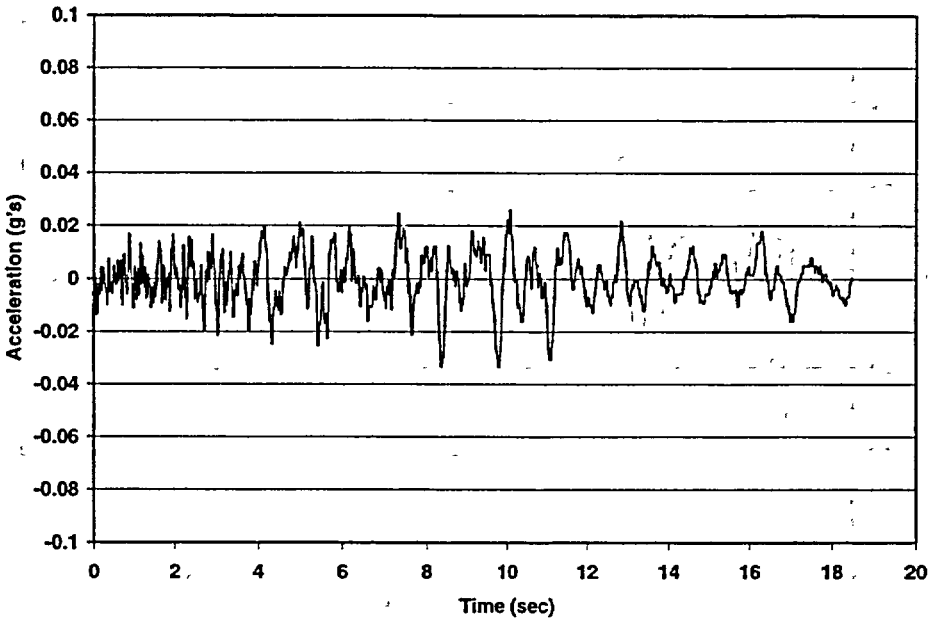

Figure A.12 Time History #4 (Coalinga – 34km) Vertical - Z

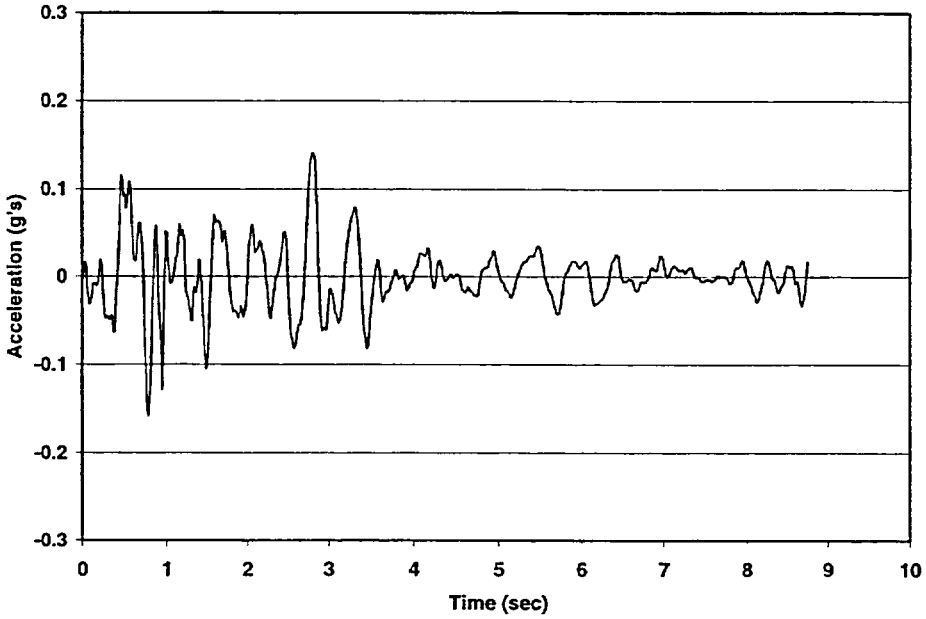

Figure A.13 Time History #5 (Coyote Lake) Horizontal - X

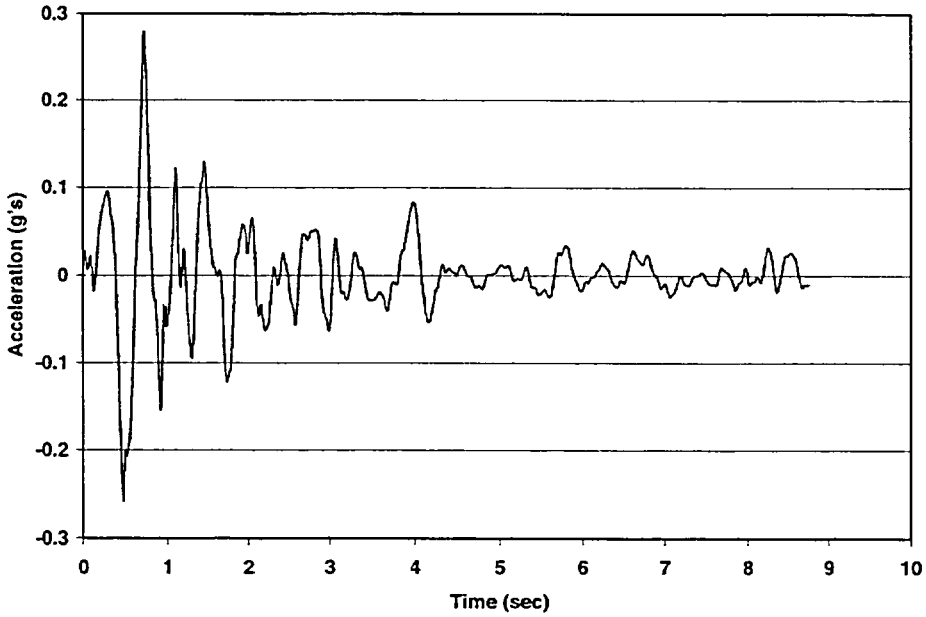

Figure A.14 Time History #5 (Coyote Lake) Horizontal - Y

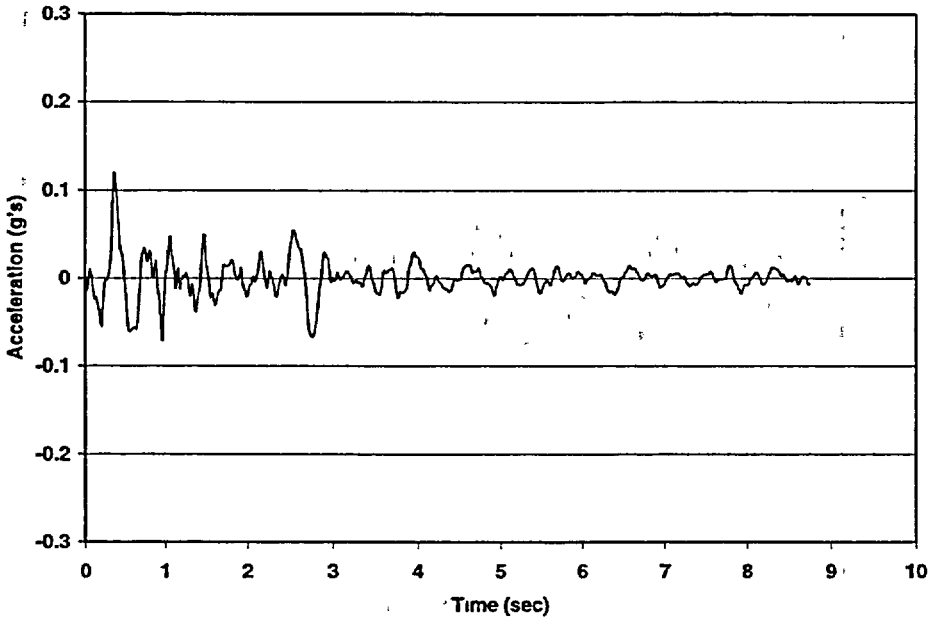

Figure A.15 Time History #5 (Coyote Lake) Vertical - Z

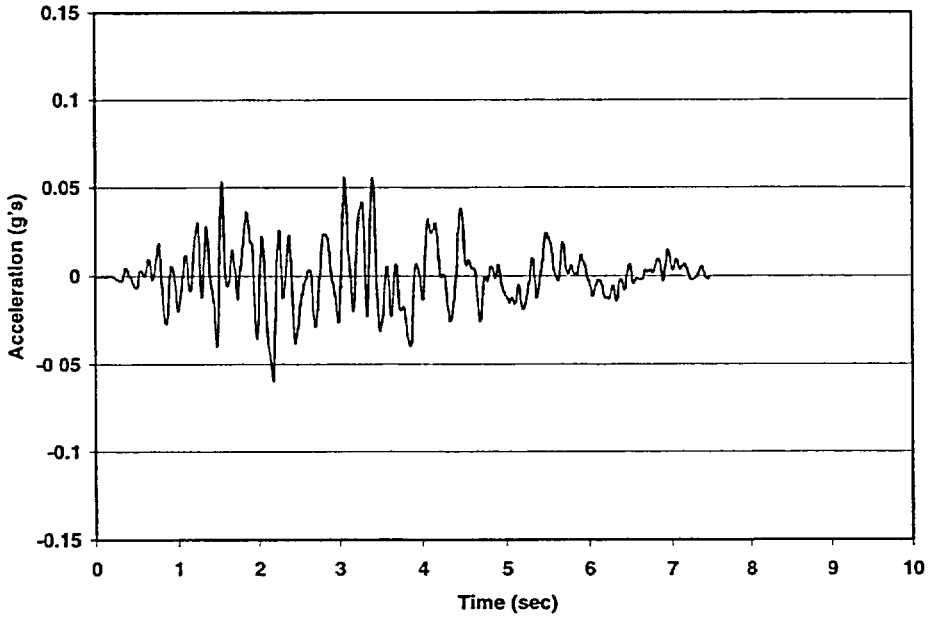

Figure A.16 Time History #6 (Friuli, Italy) Horizontal - X

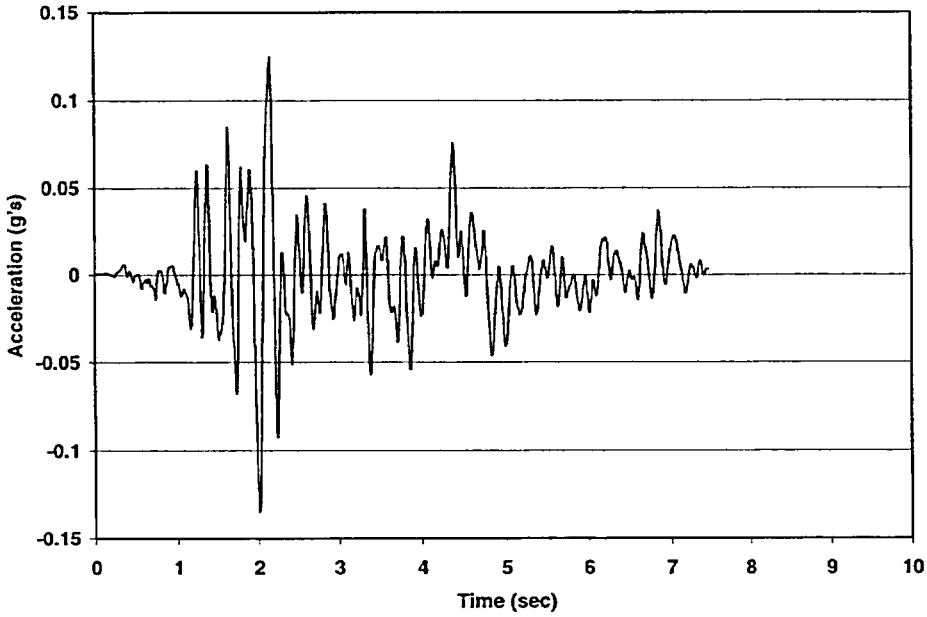

Figure A.17 Time History #6 (Friuli, Italy) Horizontal - Y

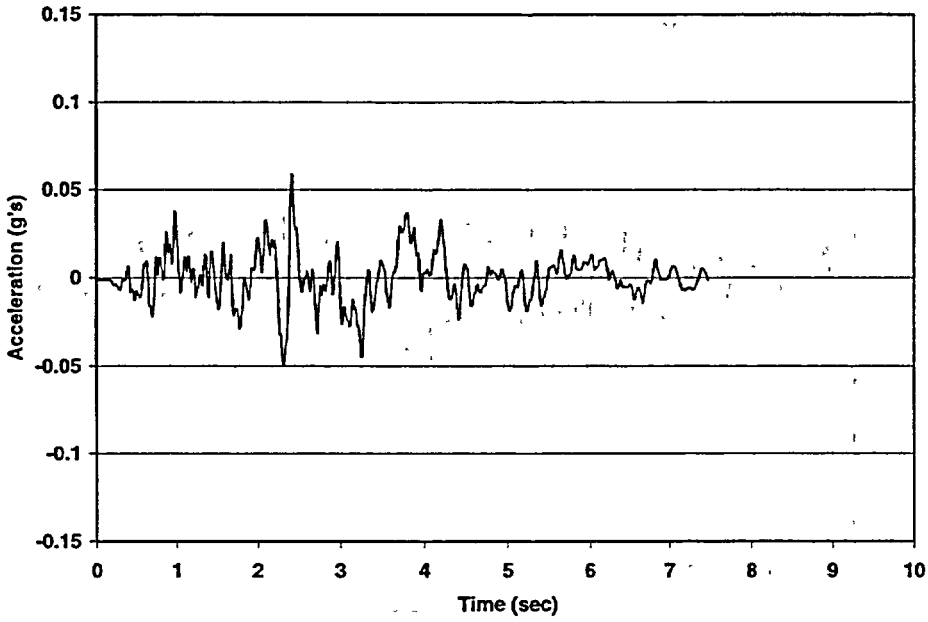

Figure A.18 Time History #6 (Friuli, Italy) Vertical - Z

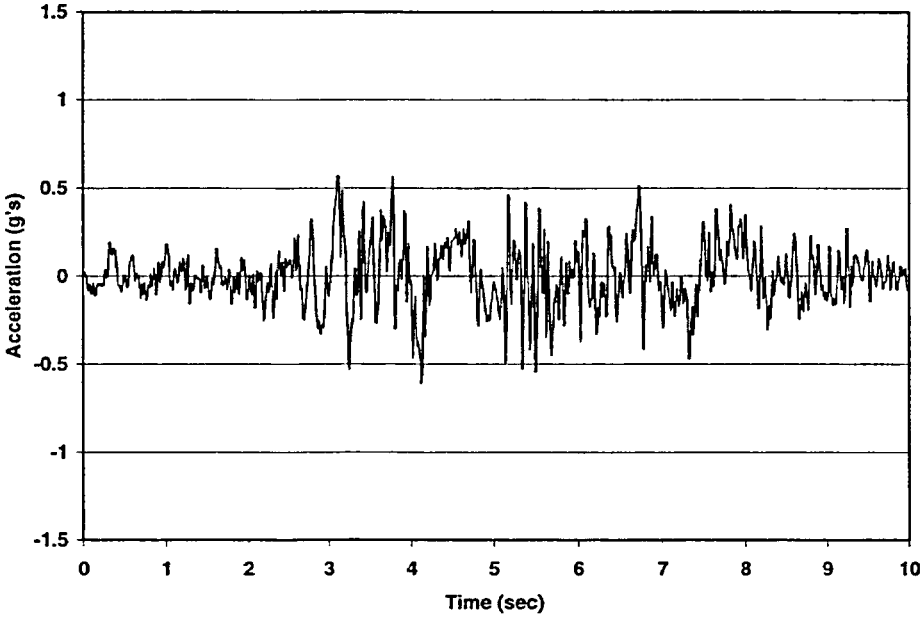

Figure A.19 Time History #7 (Gazli, USSR) Horizontal - X

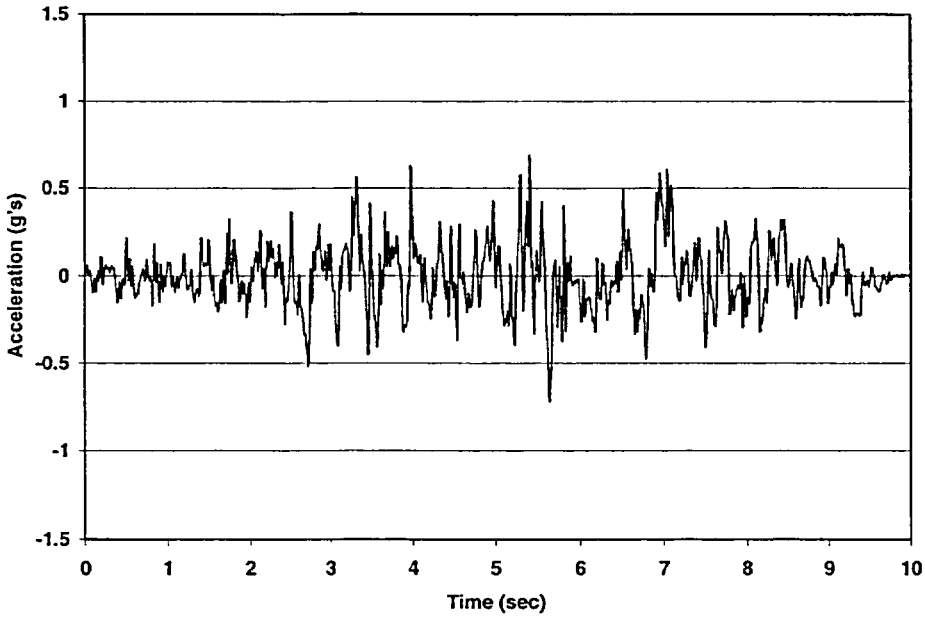

Figure A.20 Time History #7 (Gazli, USSR) Horizontal - Y

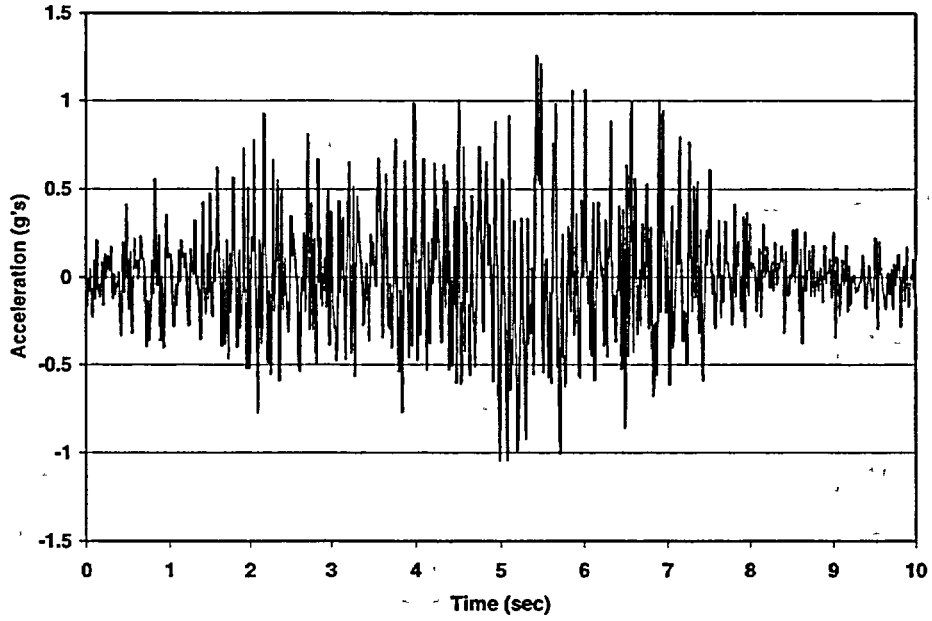

Figure A.21 Time History #7 (Gazli, USSR) Vertical - Z

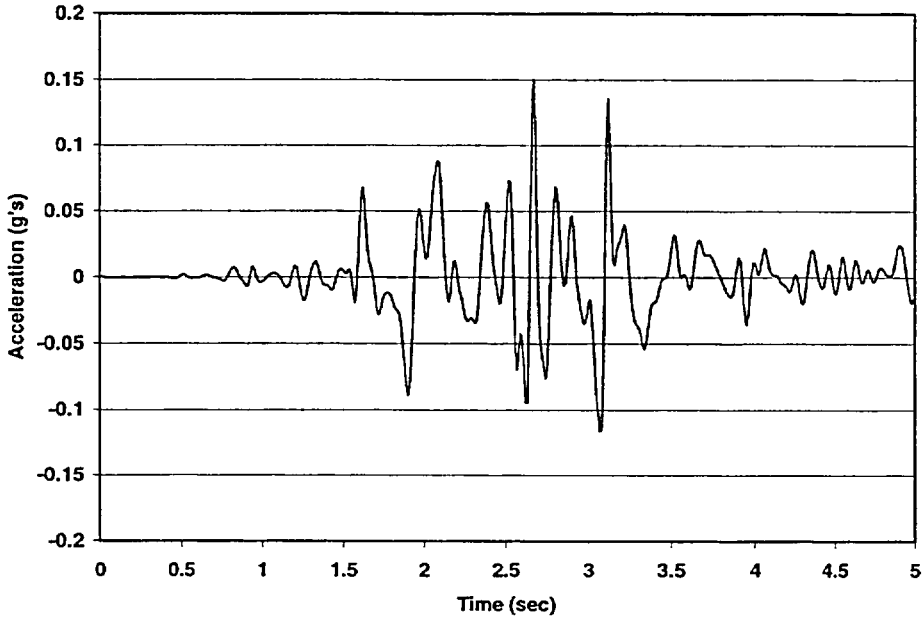

Figure A.22 Time History #8 (Helena) Horizontal - X

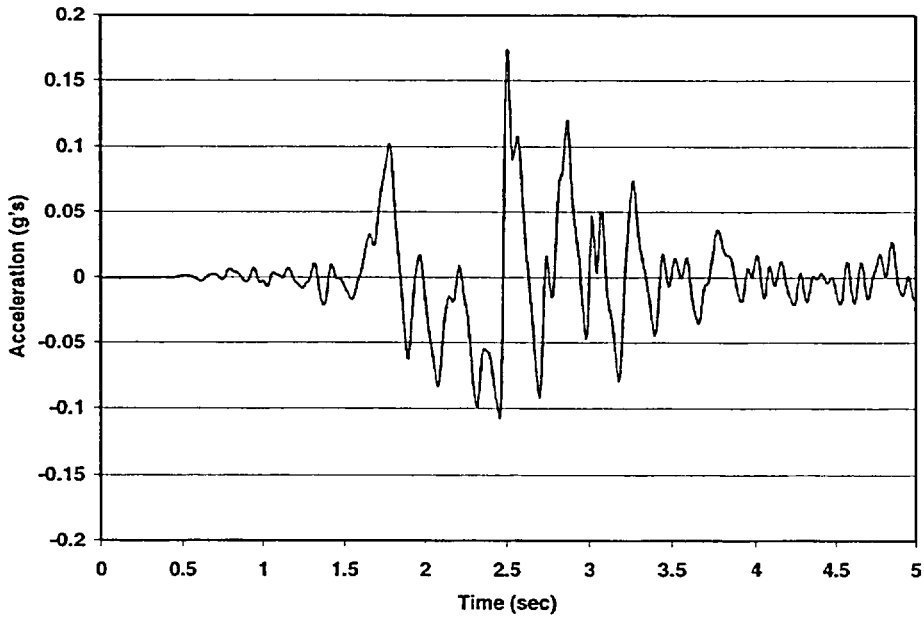

Figure A.23 Time History #8 (Helena) Horizontal - Y

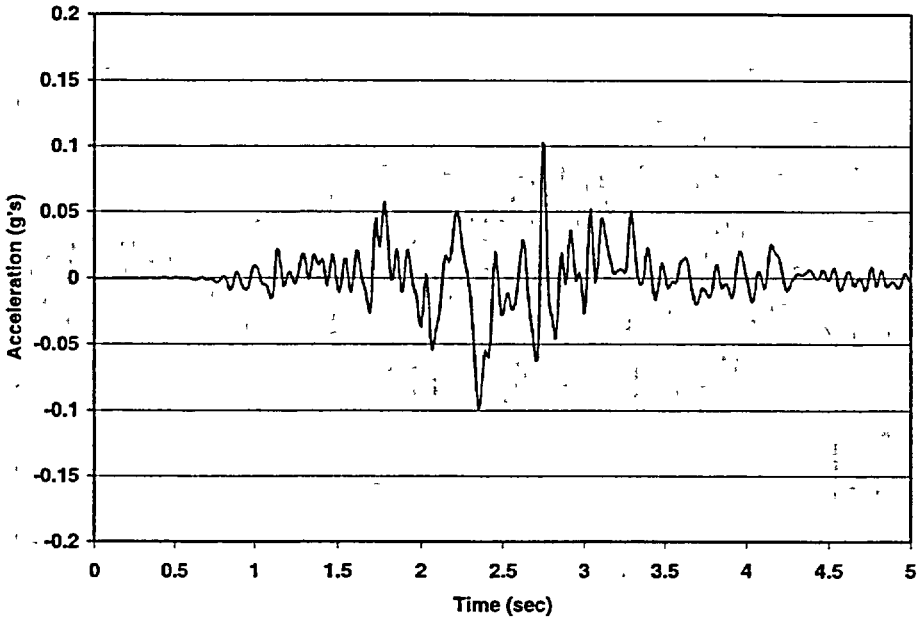

Figure A.24 Time History #8 (Helena) Vertical - Z

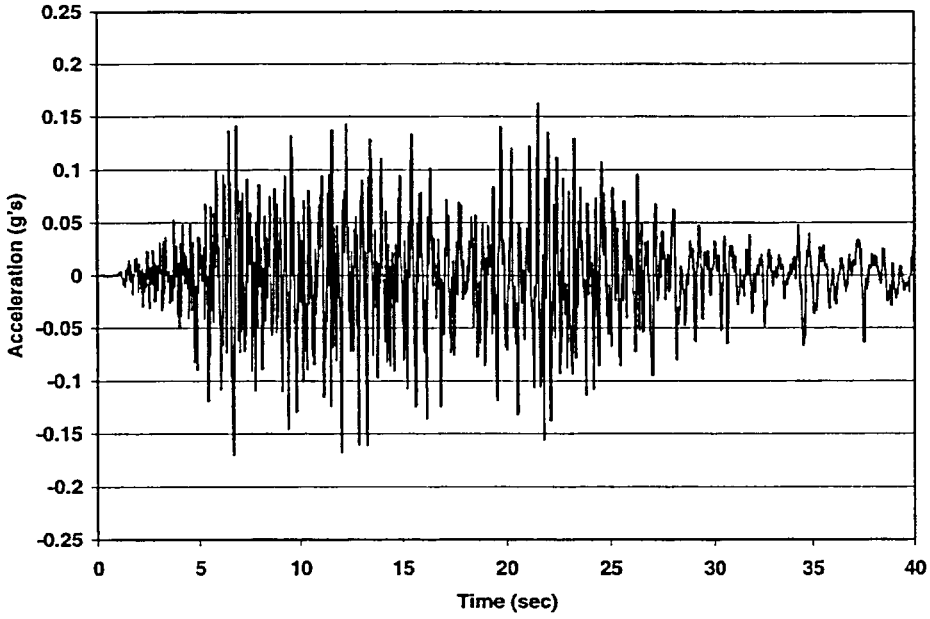

Figure A.25 Time History #9 (Imperial Valley) Horizontal - X

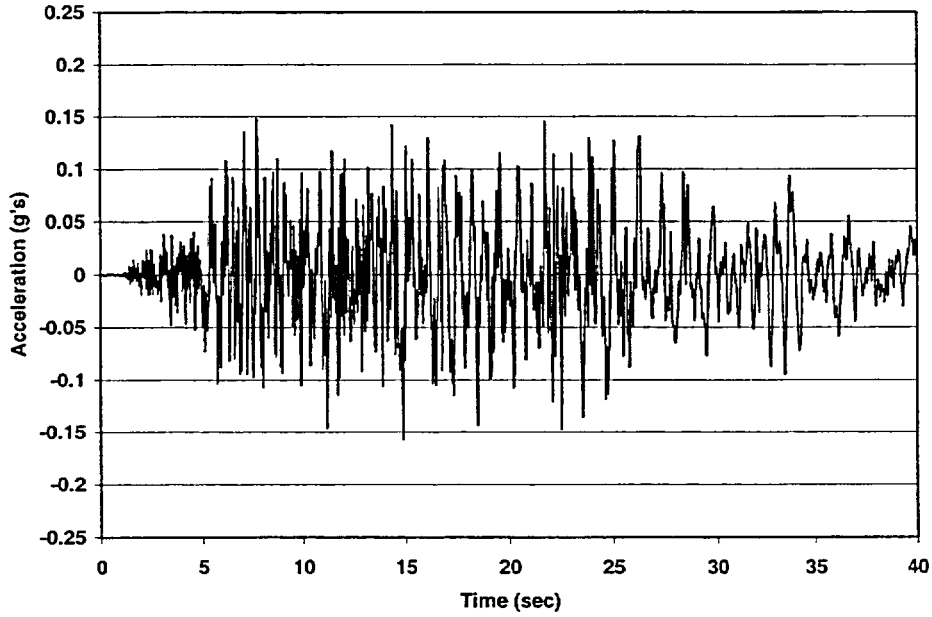

Figure A.26 Time History #9 (Imperial Valley) Horizontal - Y

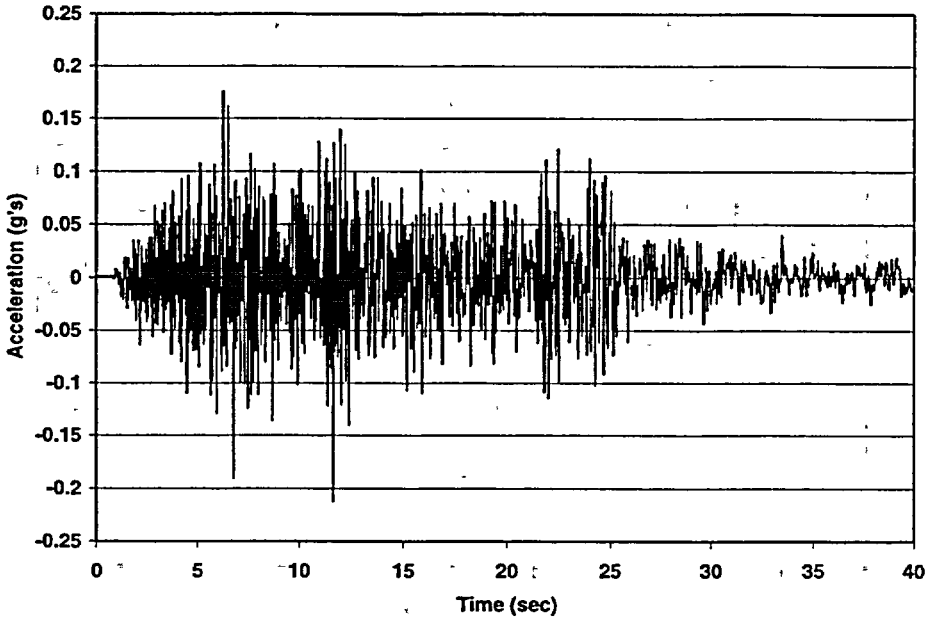

Figure A.27 Time History #9 (Imperial Valley) Vertical - Z

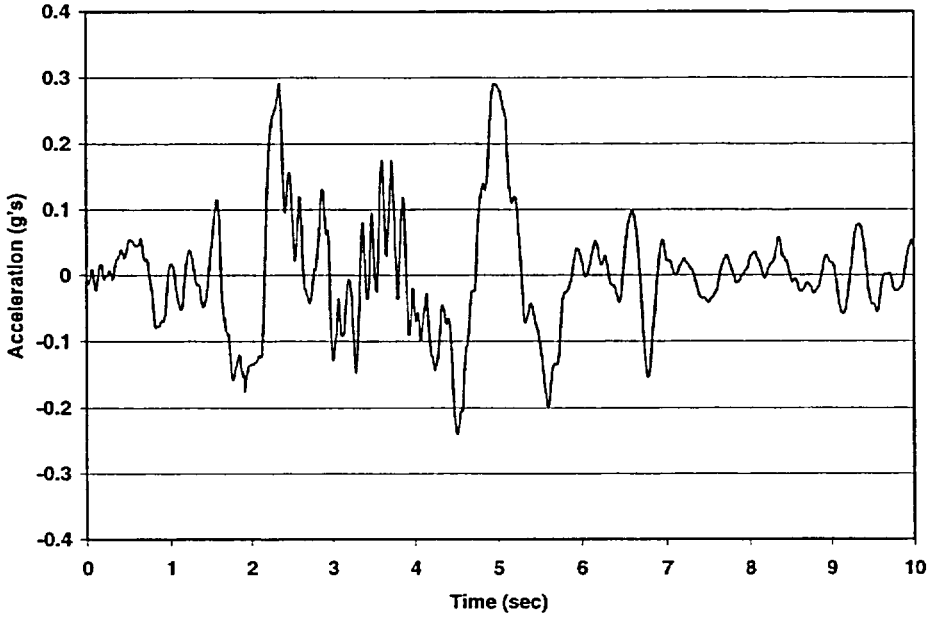

Figure A.28 Time History #10 (Kobe, Japan – 0.2km) Horizontal - X

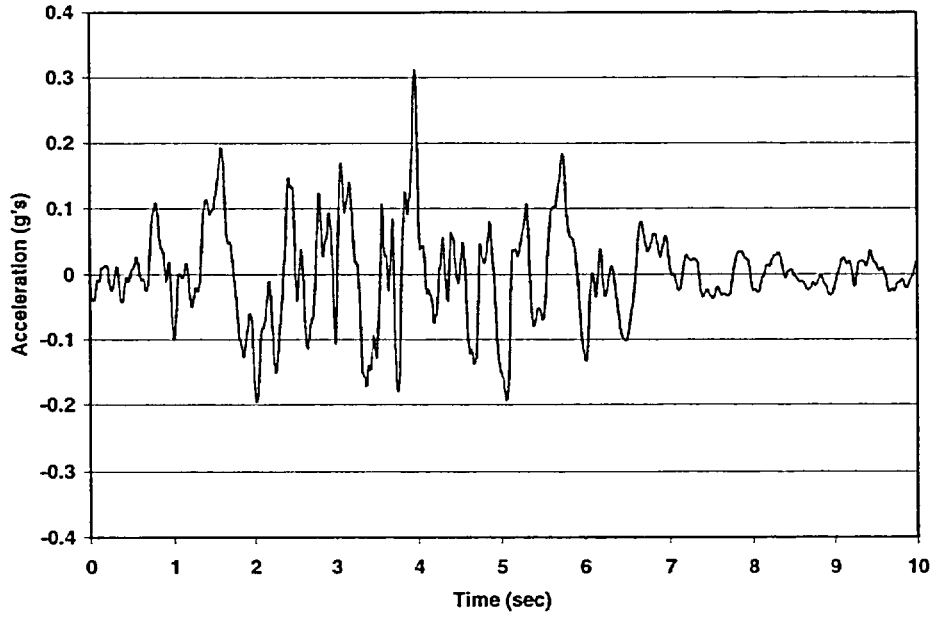

Figure A.29 Time History #10 (Kobe, Japan – 0.2km) Horizontal - Y

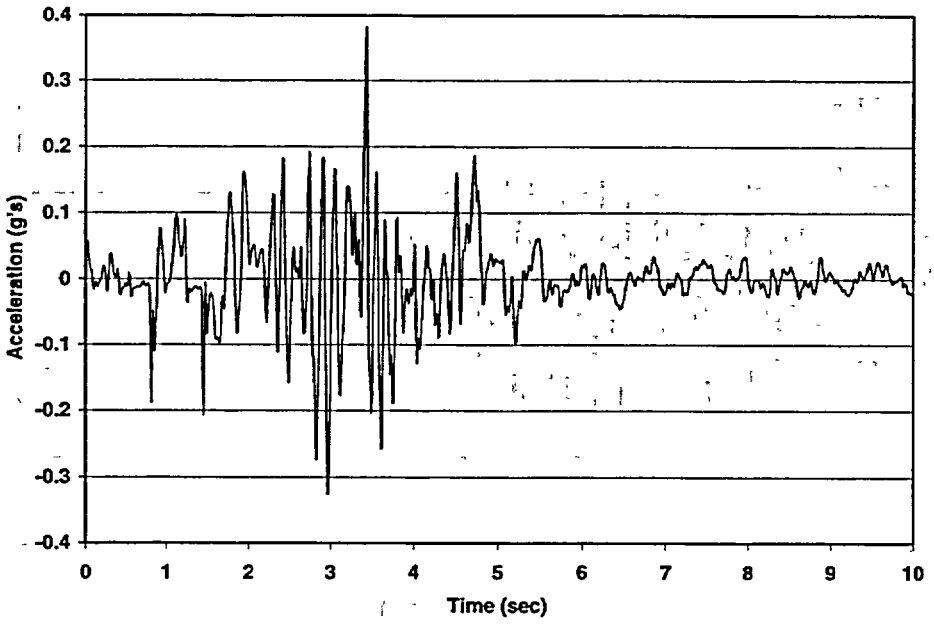

Figure A.30 Time History #10 (Kobe, Japan – 0.2km) Vertical - Z

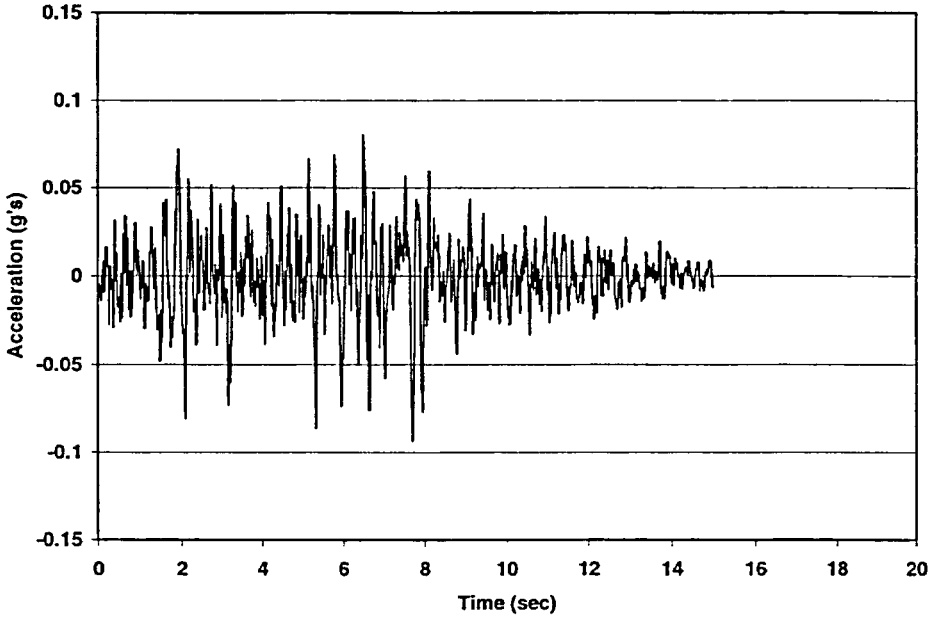

Figure A.31 Time History #11 (Kobe, Japan – 49km) Horizontal - X

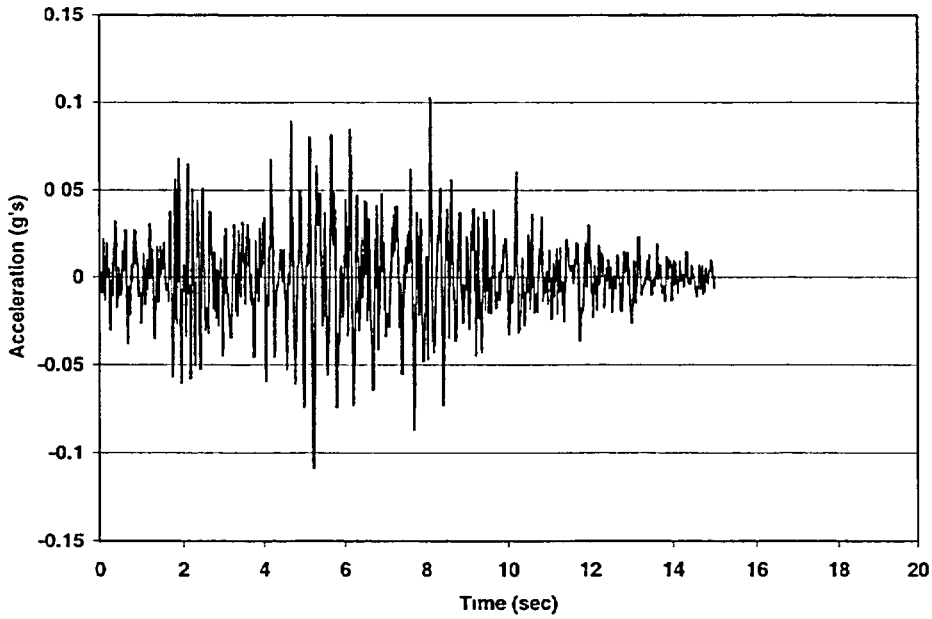

Figure A.32 Time History #11 (Kobe, Japan – 49km) Horizontal - Y

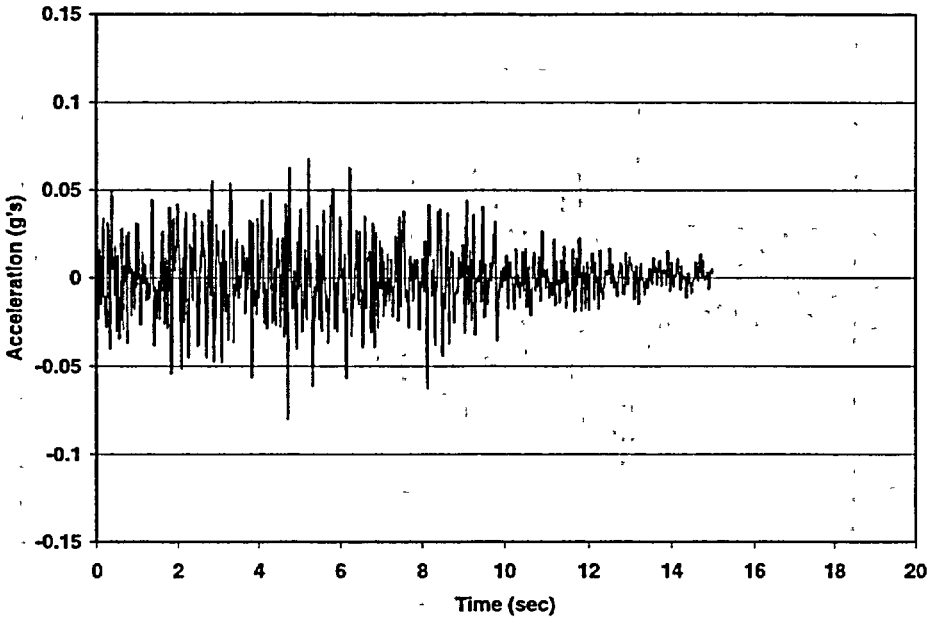

Figure A.33 Time History #11 (Kobe, Japan – 49km) Vertical - Z

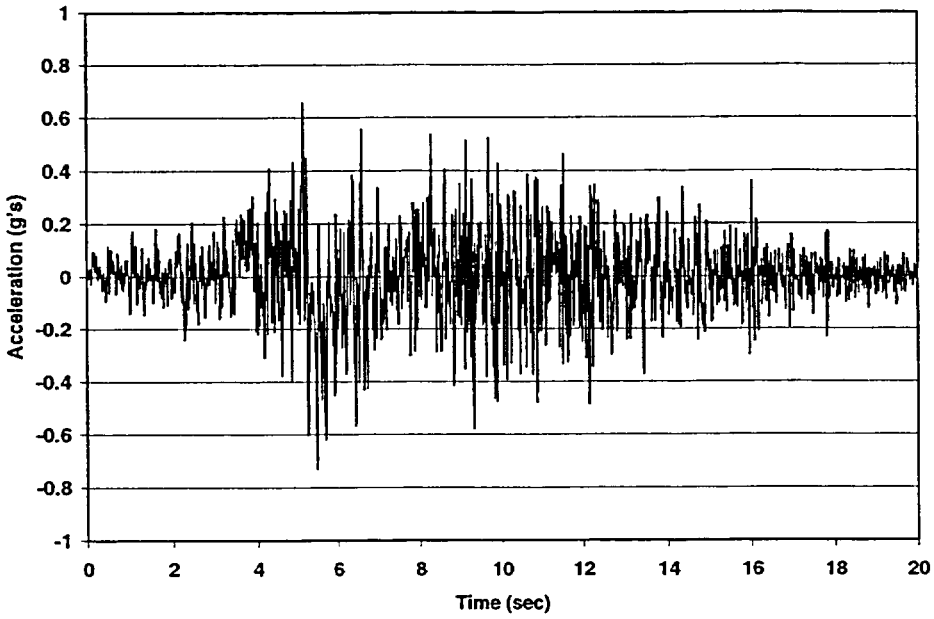

Figure A.34 Time History #12 (Landers – 1.1km) Horizontal - X

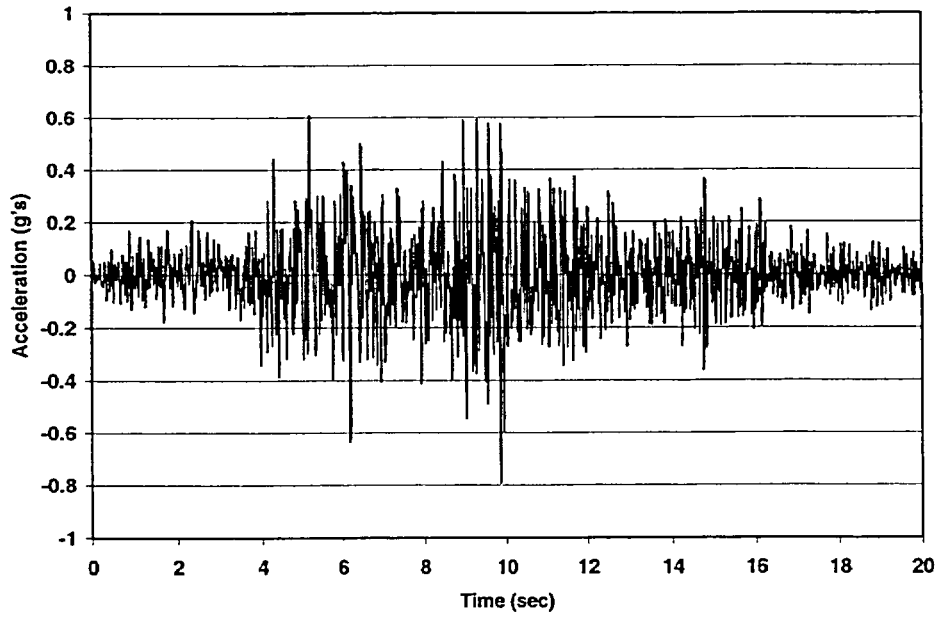

Figure A.35 Time History #12 (Landers – 1.1km) Horizontal - Y

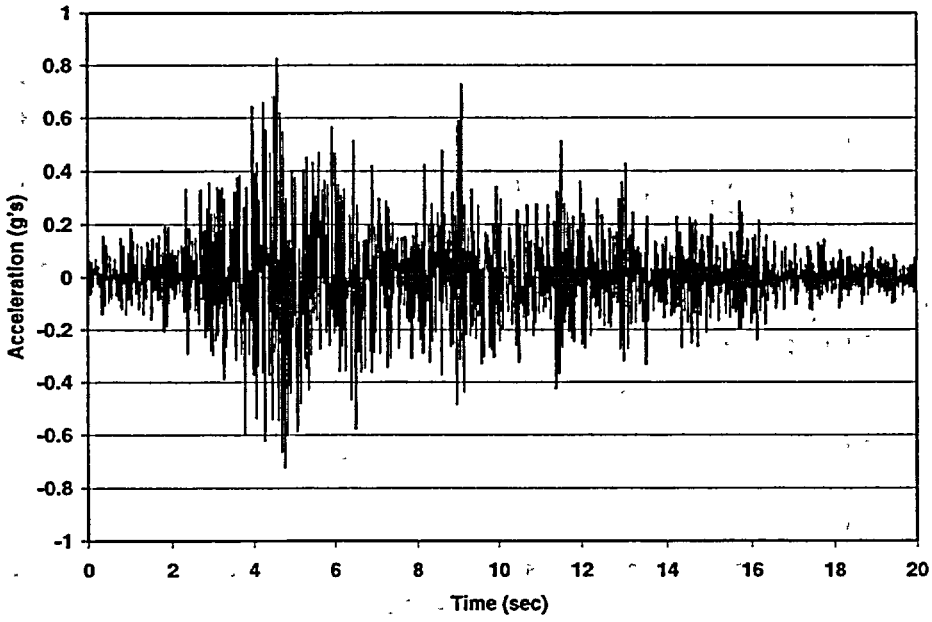

Figure A.36 Time History #12 (Landers – 1.1km) Vertical - Z

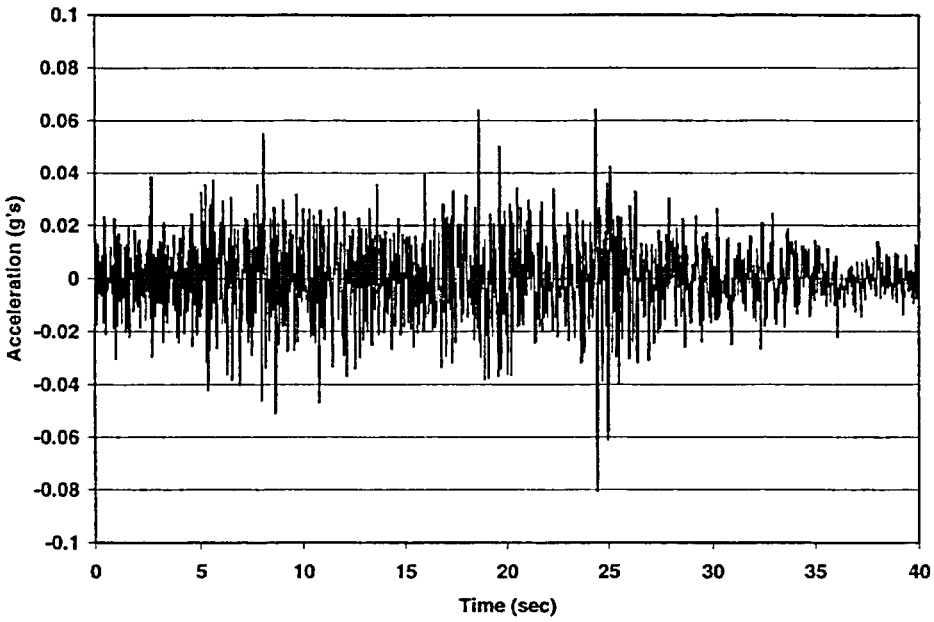

Figure A.37 Time History #13 (Landers – 42km) Horizontal - X

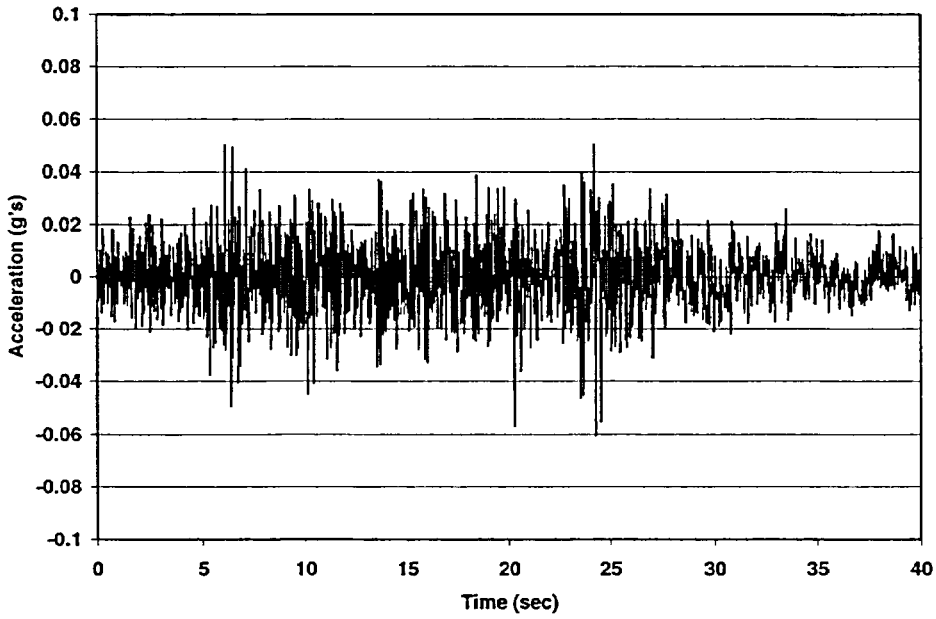

Figure A.38 Time History #13 (Landers – 42km) Horizontal - Y

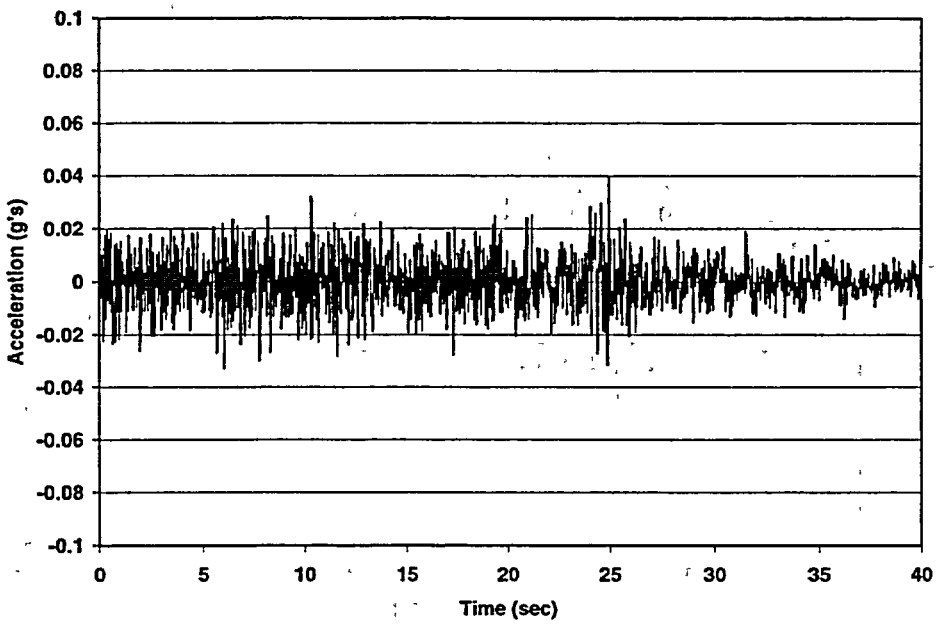

Figure A.39 Time History #13 (Landers – 42km) Vertical - Z

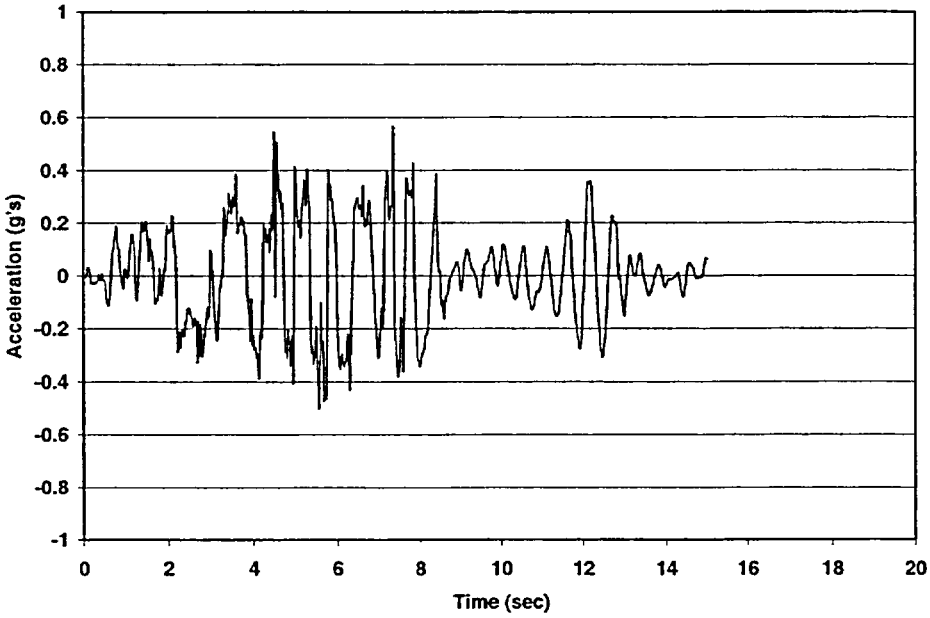

Figure A.40 Time History #14 (Loma Prieta – 6km) Horizontal - X

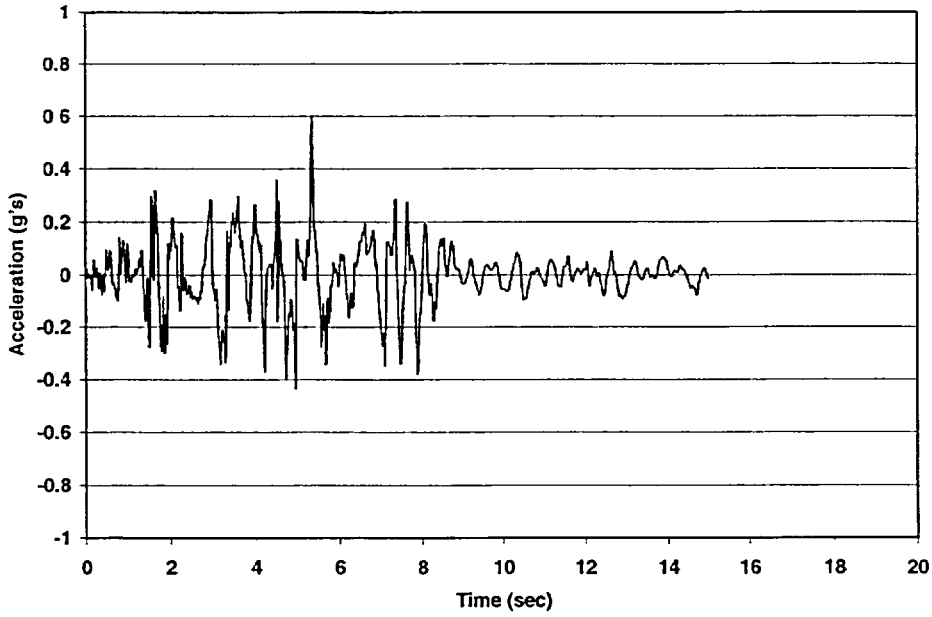

Figure A.41 Time History #14 (Loma Prieta – 6km) Horizontal - Y

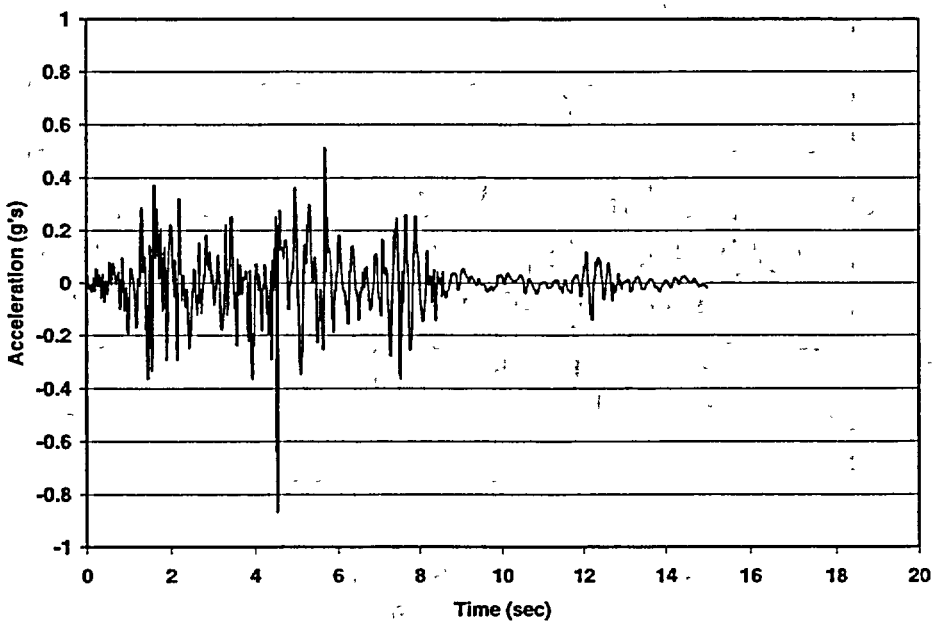

Figure A.42 Time History #14 (Loma Prieta – 6km) Vertical - Z

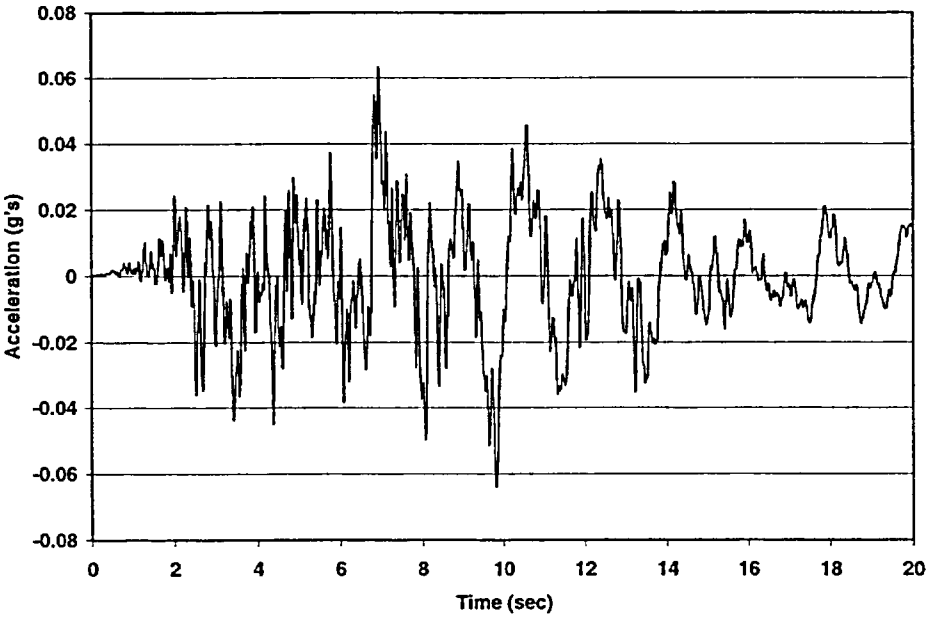

Figure A.43 Time History #15 (Loma Prieta – 21km) Horizontal - X

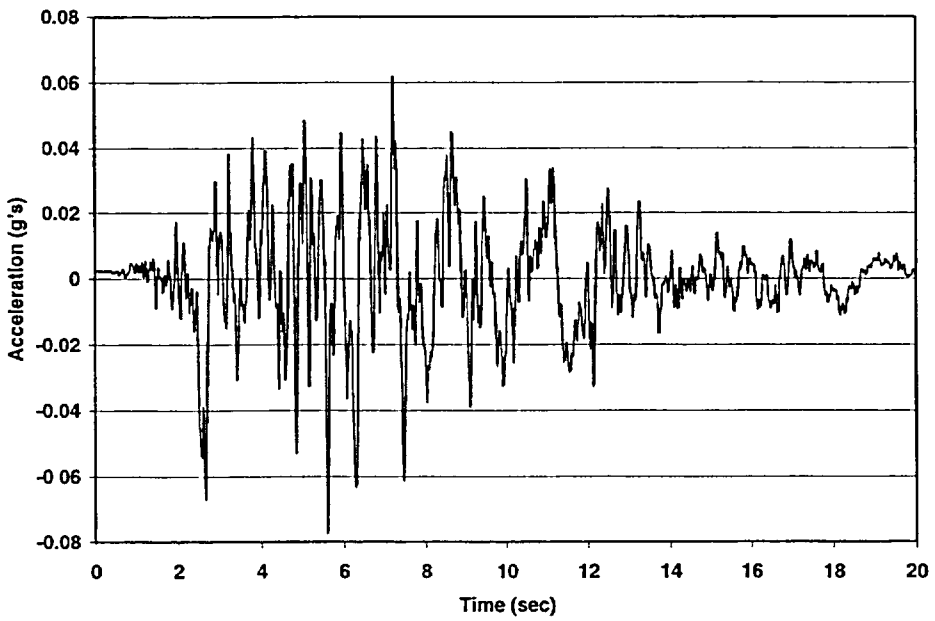

Figure A.44 Time History #15 (Loma Prieta – 21km) Horizontal - Y

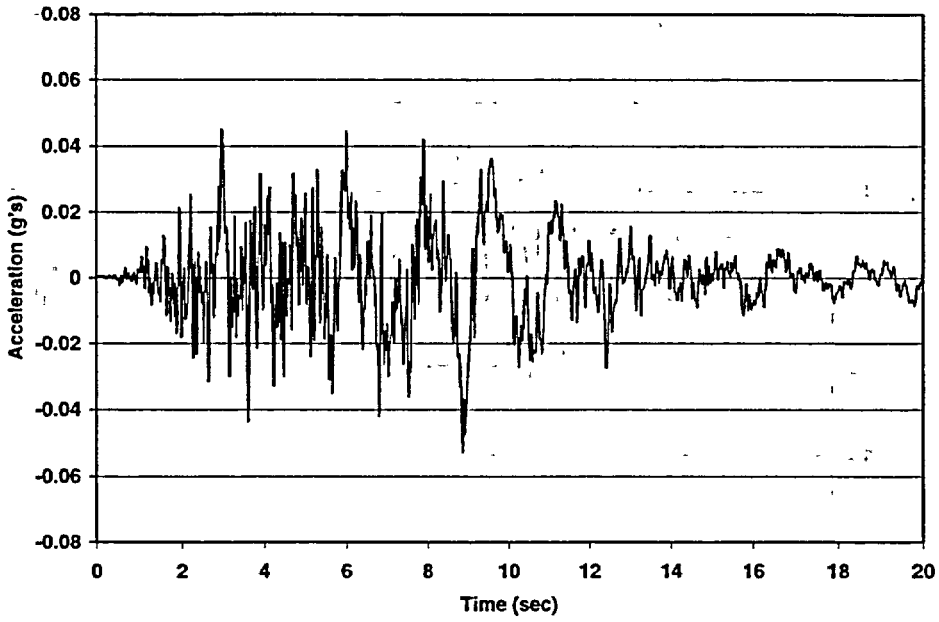

Figure A.45 Time History #15 (Loma Prieta – 21km) Vertical - Z

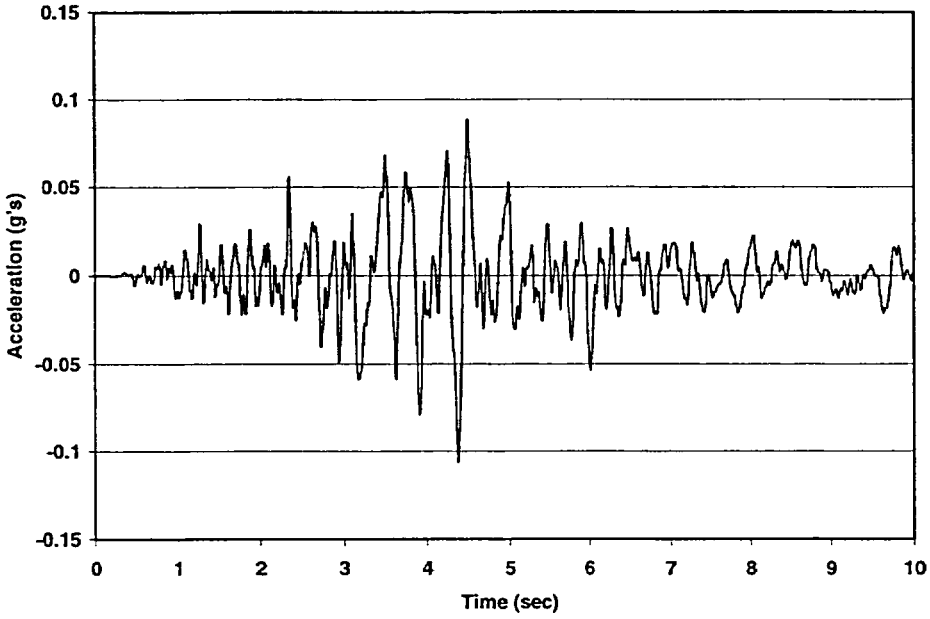

Figure A.46 Time History #16 (Mammoth Lakes) Horizontal - X

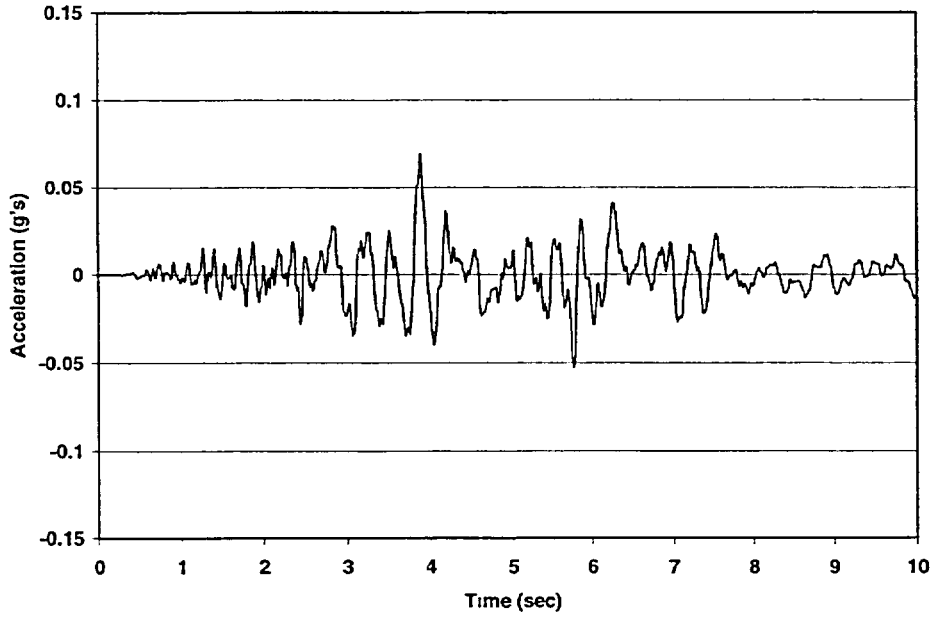

Figure A.47 Time History #16 (Mammoth Lakes) Horizontal - Y

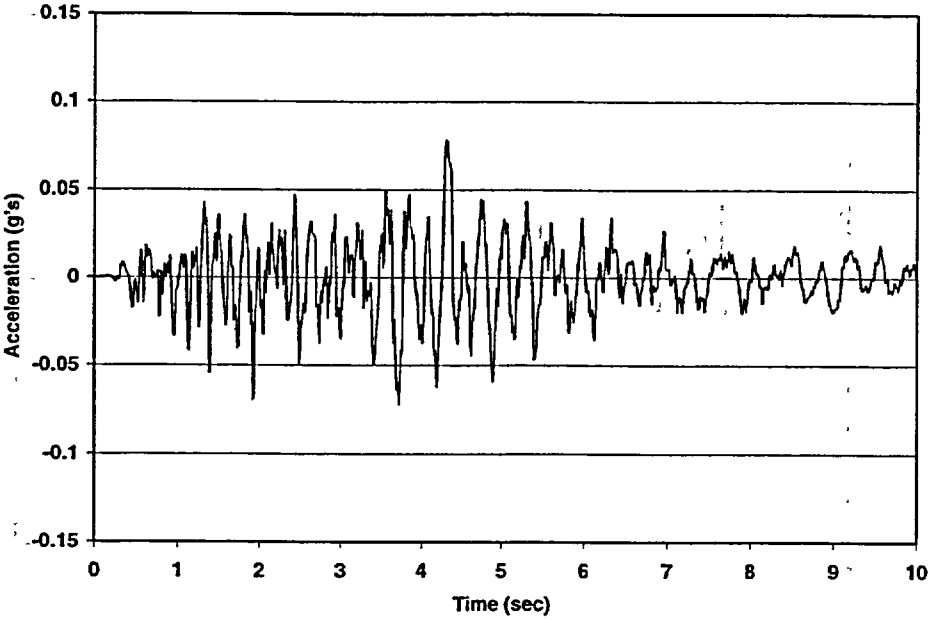

Figure A.48 Time History #16 (Mammoth Lakes) Vertical - Z

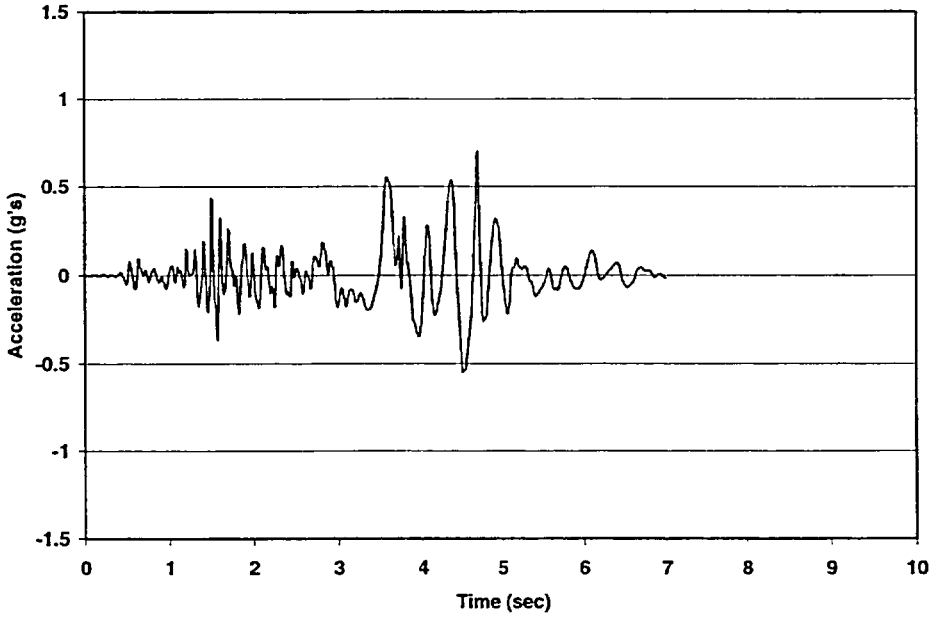

Figure A.49 Time History #17 (Morgan Hill – 0.1km) Horizontal - X

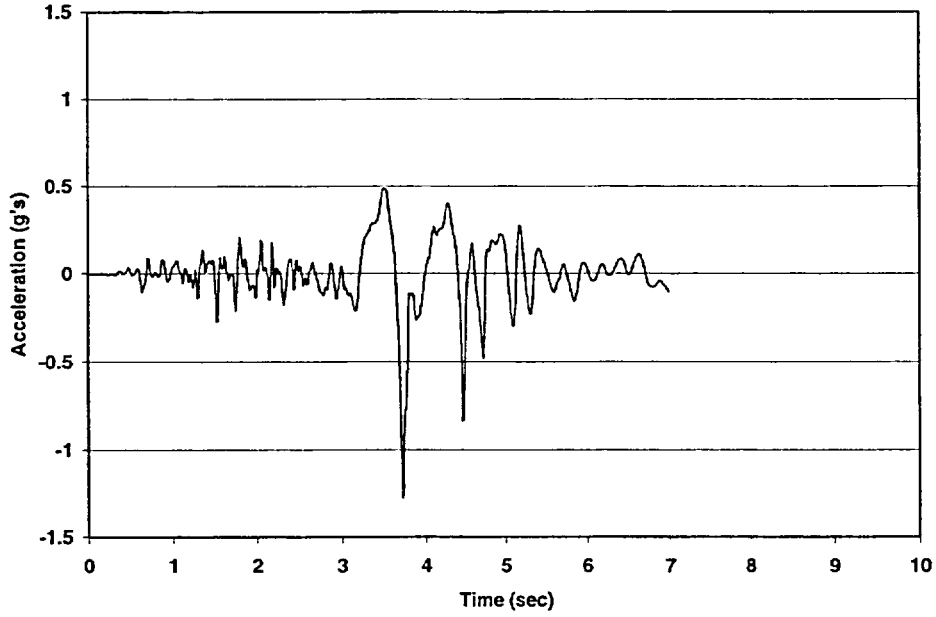

Figure A.50 Time History #17 (Morgan Hill – 0.1km) Horizontal - Y

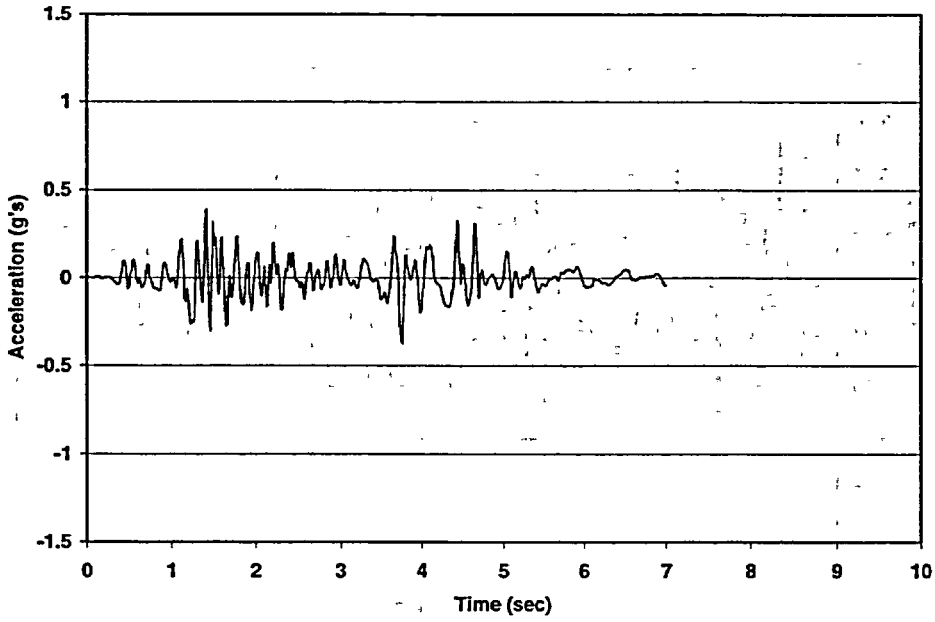

Figure A.51 Time History #17 (Morgan Hill – 0.1km) Vertical - Z

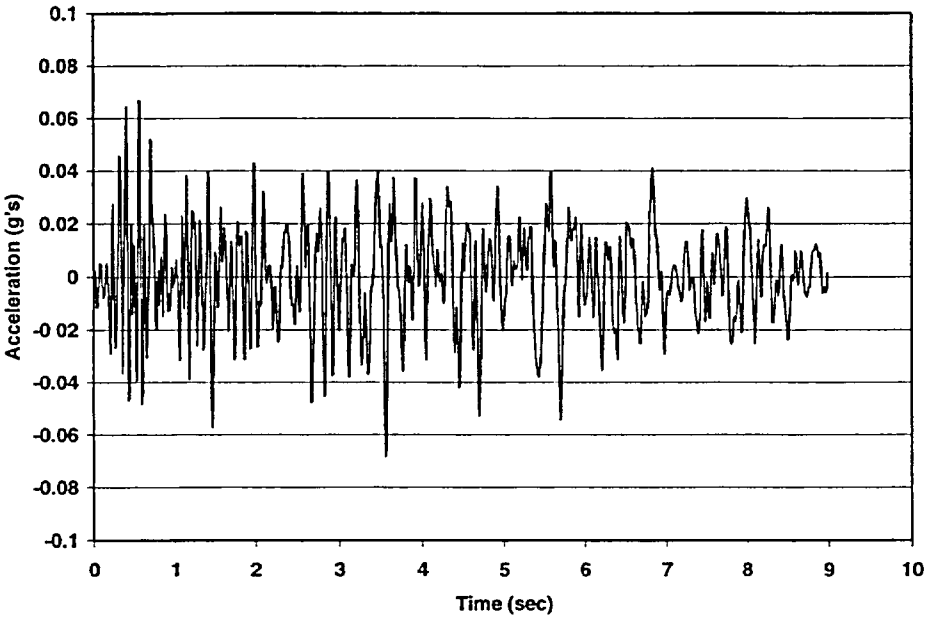

Figure A.52 Time History #18 (Morgan Hill – 16km) Horizontal - X

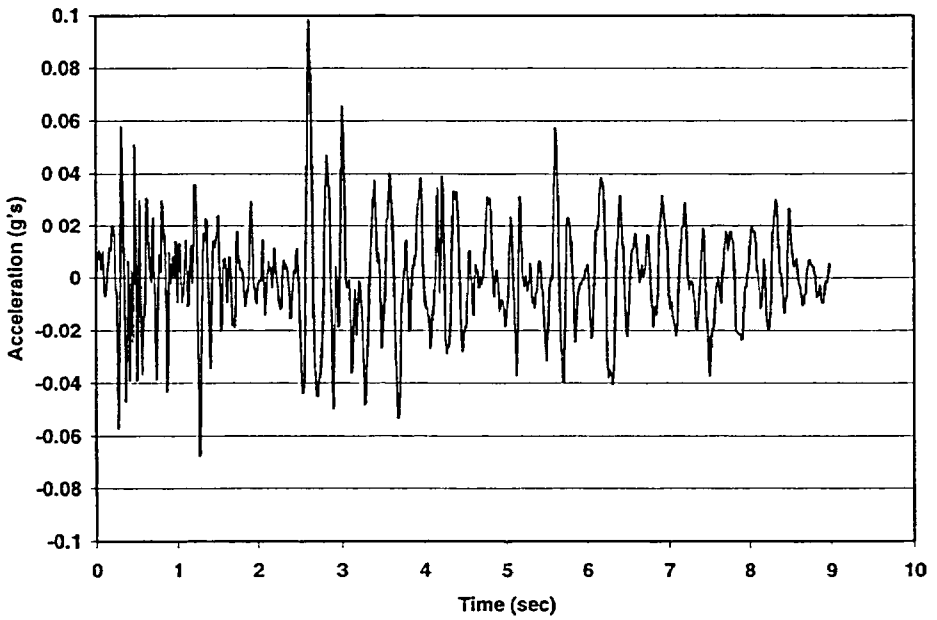

Figure A.53 Time History #18 (Morgan Hill – 16km) Horizontal - Y

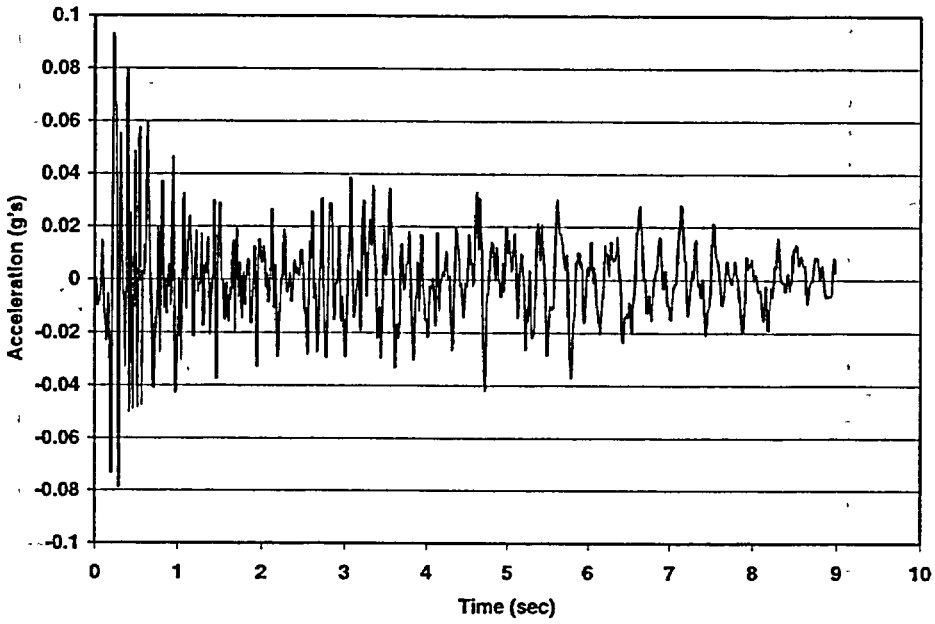

Figure A.54 Time History #18 (Morgan Hill – 16km) Vertical - Z

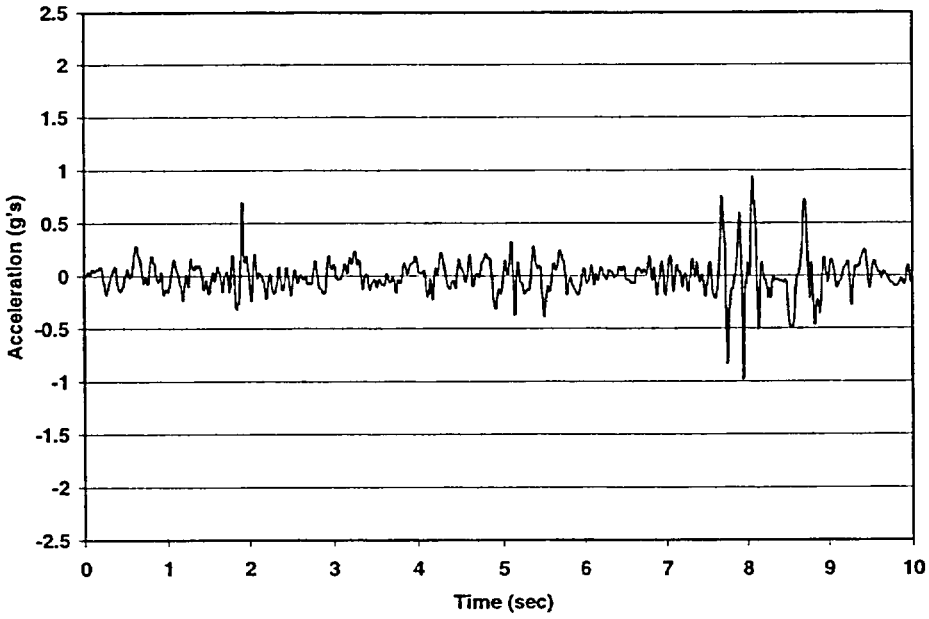

Figure A.55 Time History #19 (Nahanni, Canada – 6km) Horizontal - X

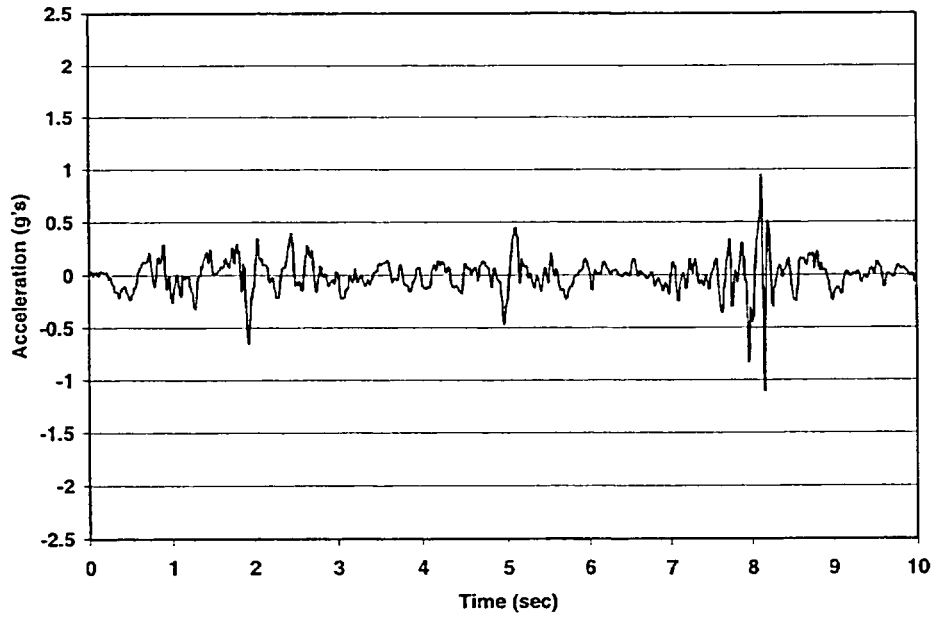

Figure A.56 Time History #19 (Nahanni, Canada – 6km) Horizontal - Y

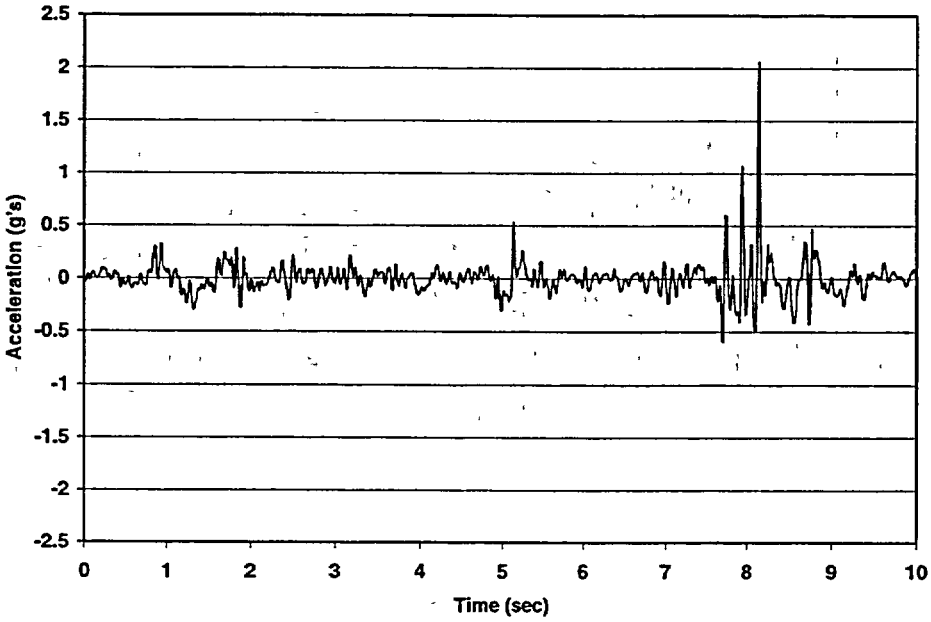

Figure A.57 Time History #19 (Nahanni, Canada – 6km) Vertical - Z

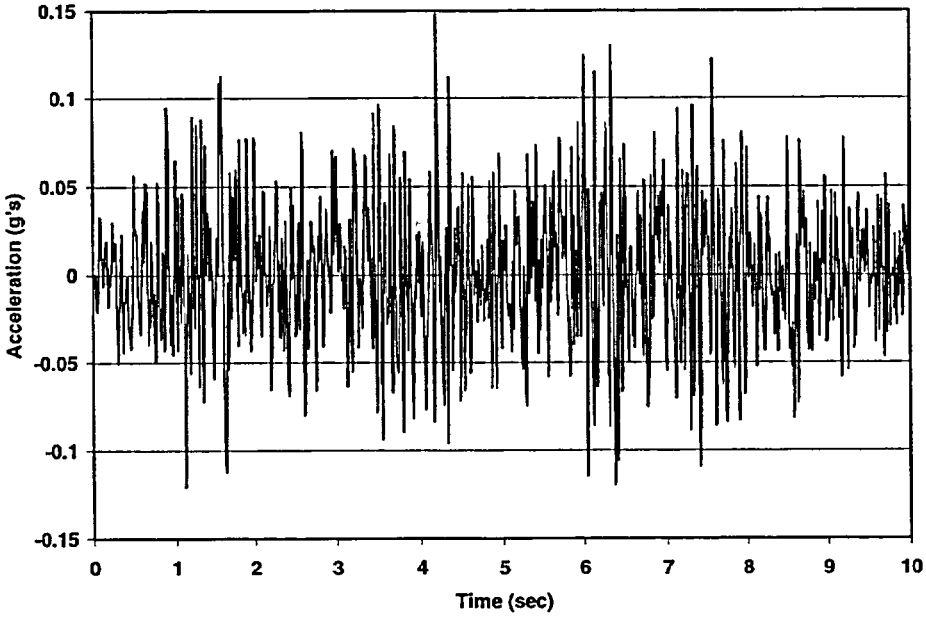

Figure A.58 Time History #20 (Nahanni, Canada – 16km) Horizontal - X

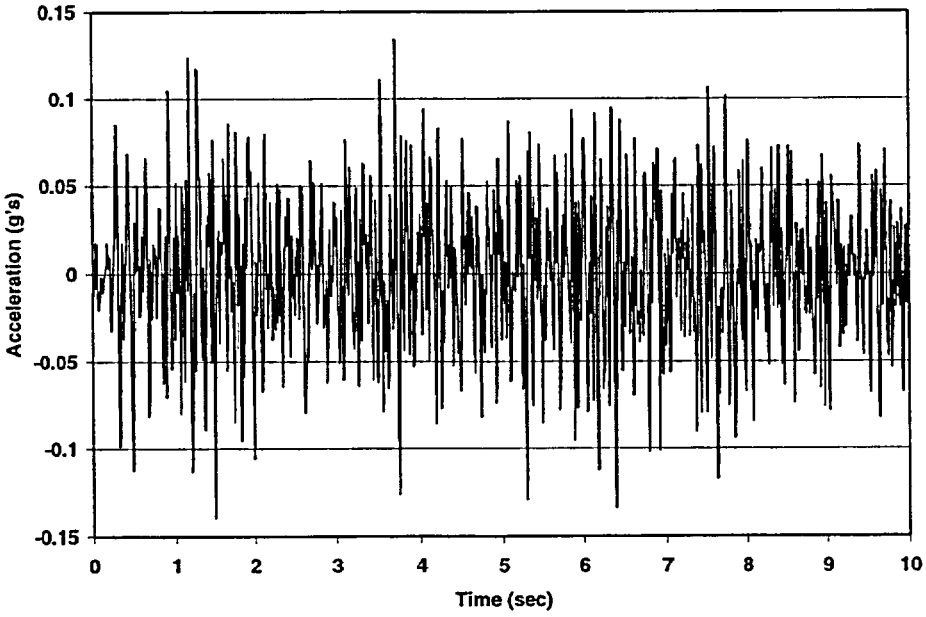

Figure A.59 Time History #20 (Nahanni, Canada – 16km) Horizontal - Y

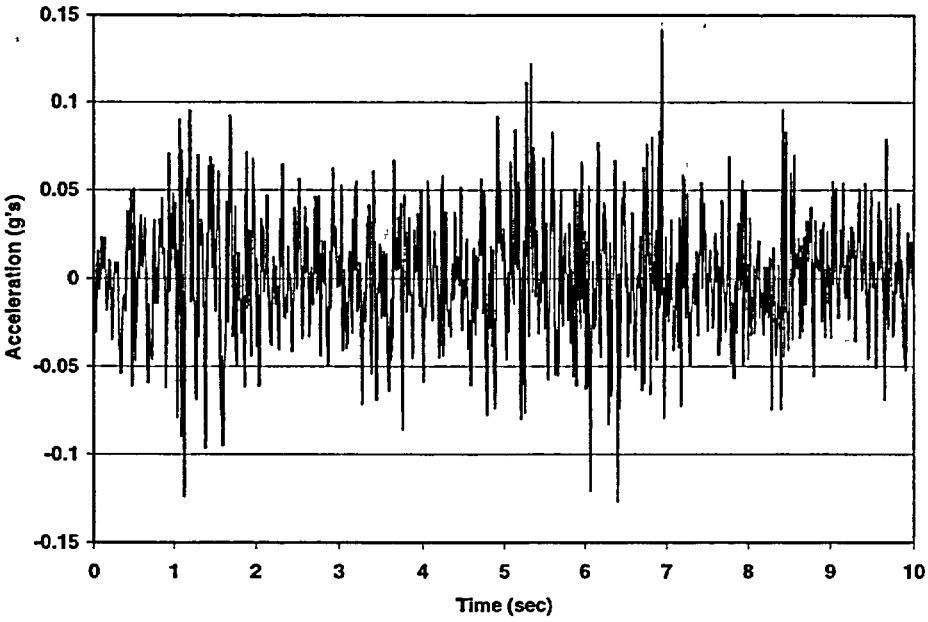

Figure A.60 Time History #20 (Nahanni, Canada – 16km) Vertical - Z

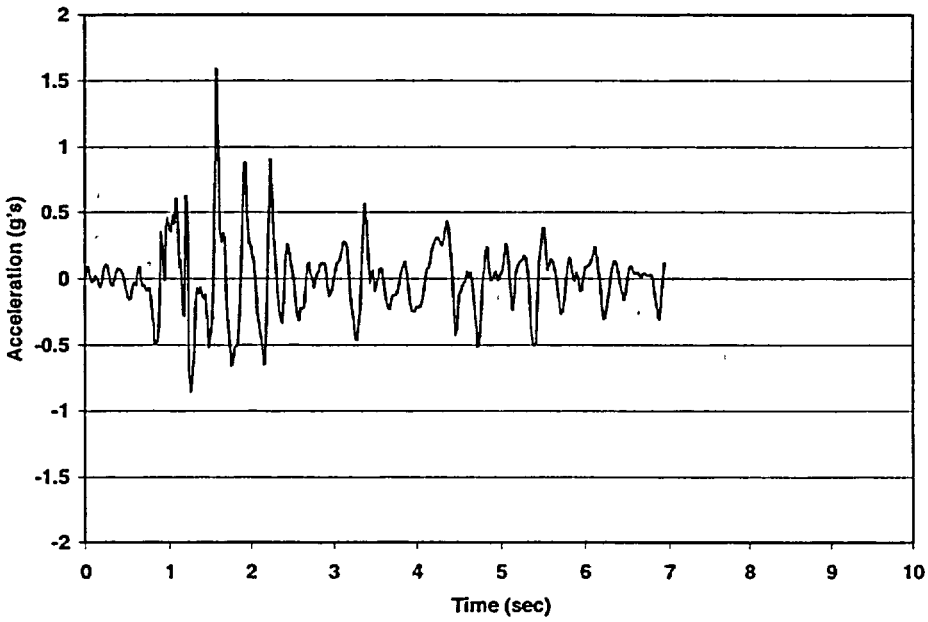

Figure A.61 Time History #21 (Northridge – 8km) Horizontal - X

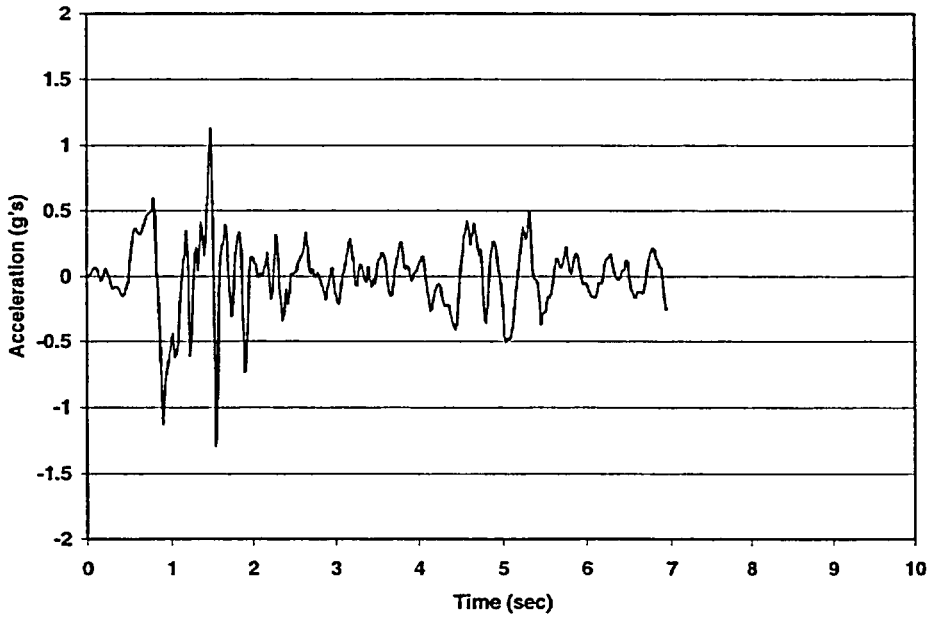

Figure A.62 Time History #21 (Northridge – 8km) Horizontal - Y

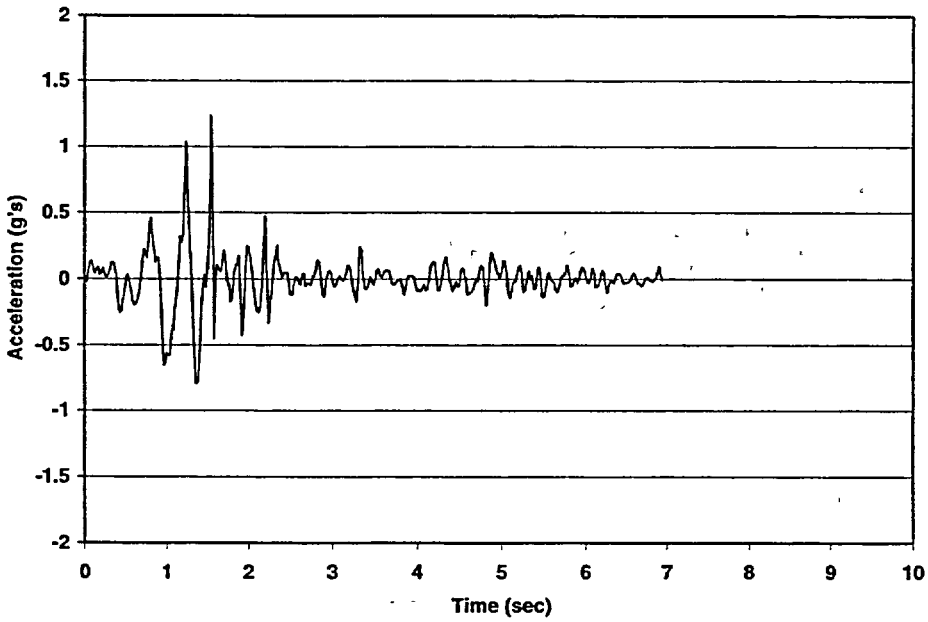

Figure A.63 Time History #21 (Northridge – 8km) Vertical - Z

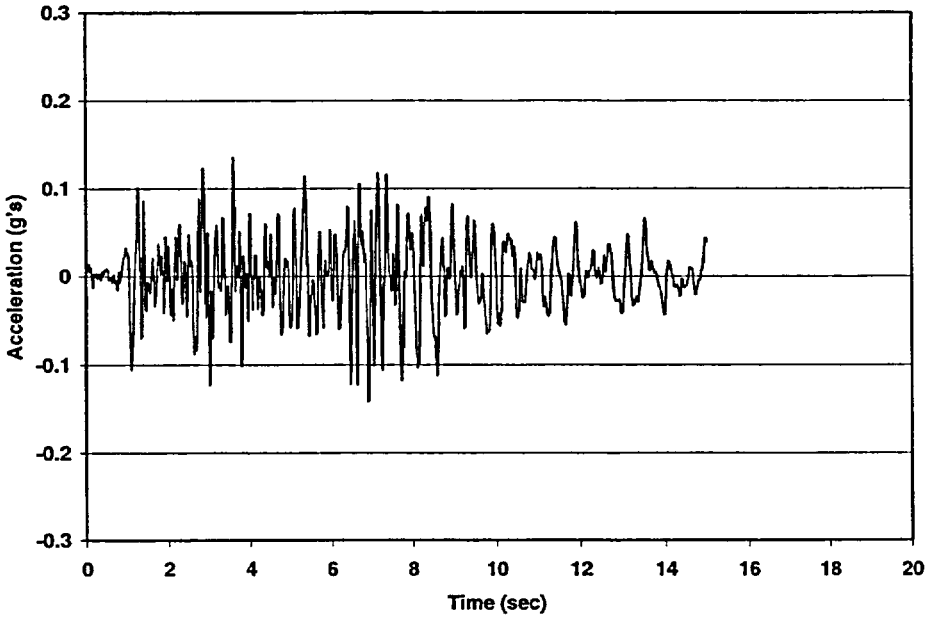

Figure A.64 Time History #22 (Northridge – 42km) Horizontal - X

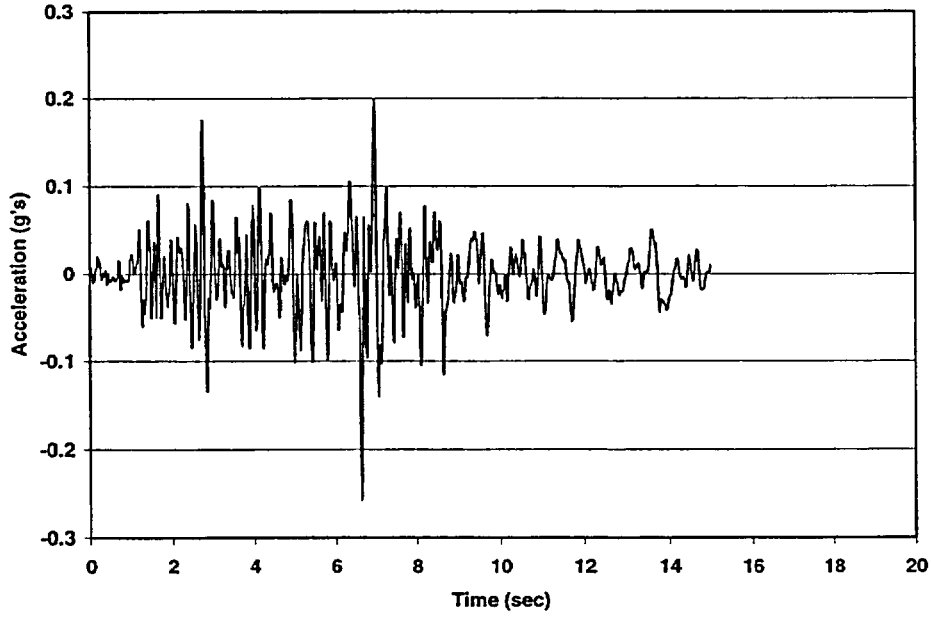

Figure A.65 Time History #22 (Northridge – 42km) Horizontal - Y

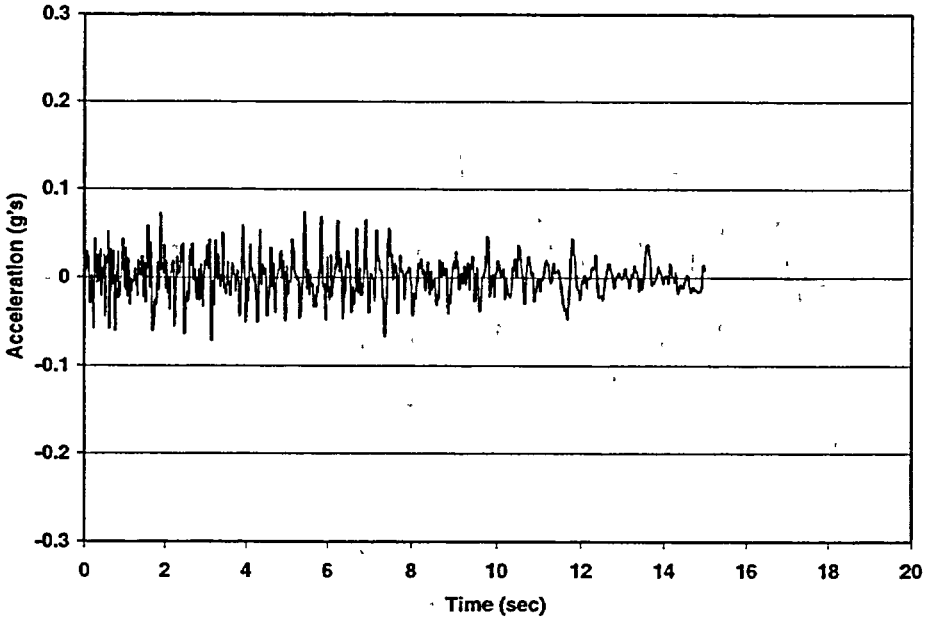

Figure A.66 Time History #22 (Northridge – 42km) Vertical - Z

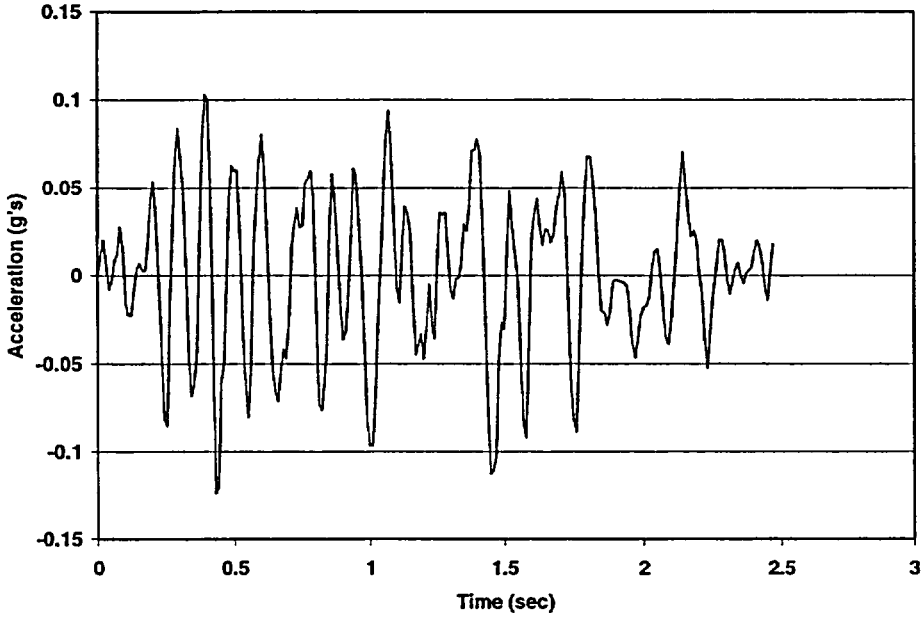

Figure A.67 Time History #23 (N. Palm Springs) Horizontal - X

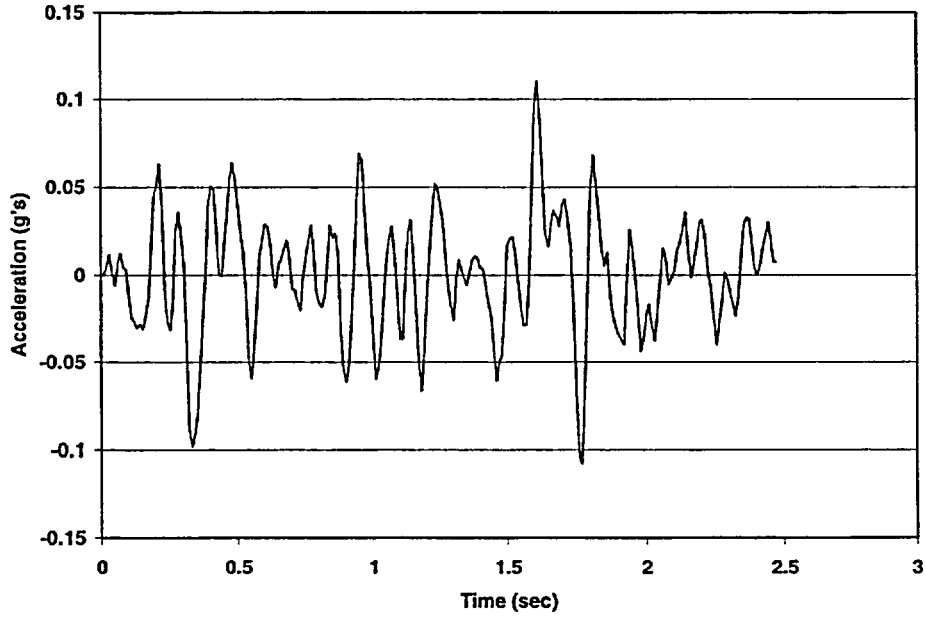

Figure A.68 Time History #23 (N. Palm Springs) Horizontal - Y

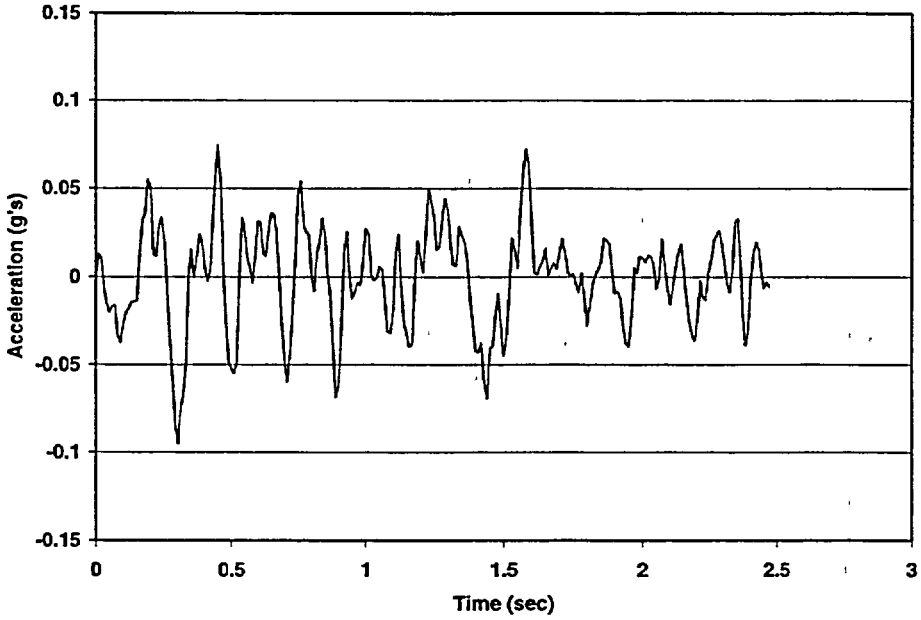

Figure A.69 Time History #23 (N. Palm Springs) Vertical - Z

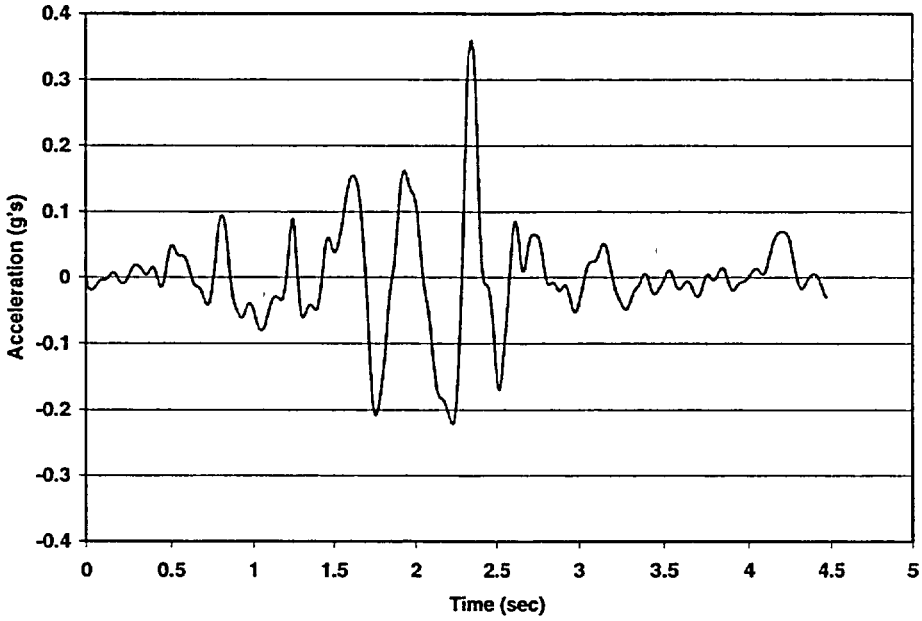

Figure A.70 Time History #24 (Parkfield) Horizontal - X

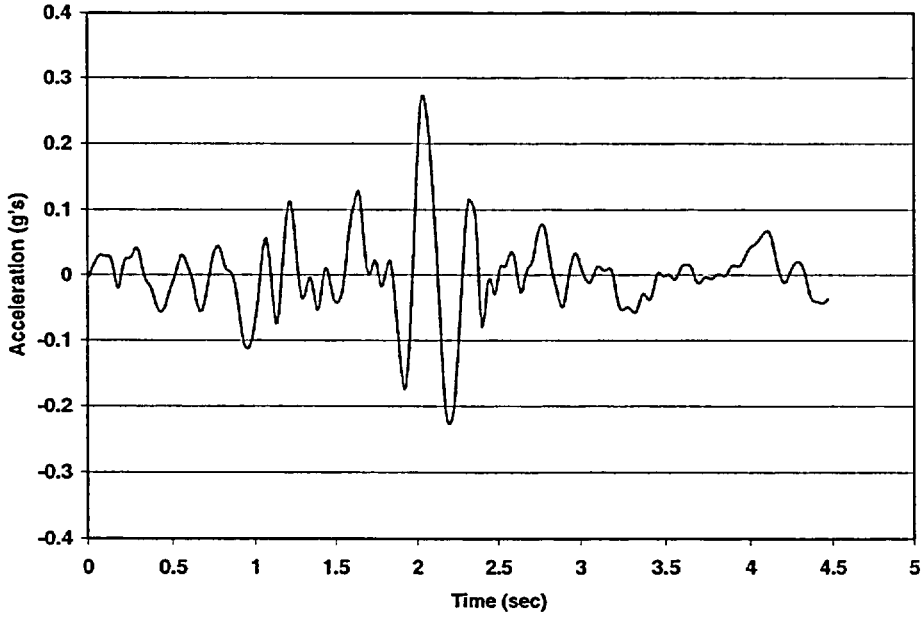

Figure A.71 Time History #24 (Parkfield) Horizontal - Y

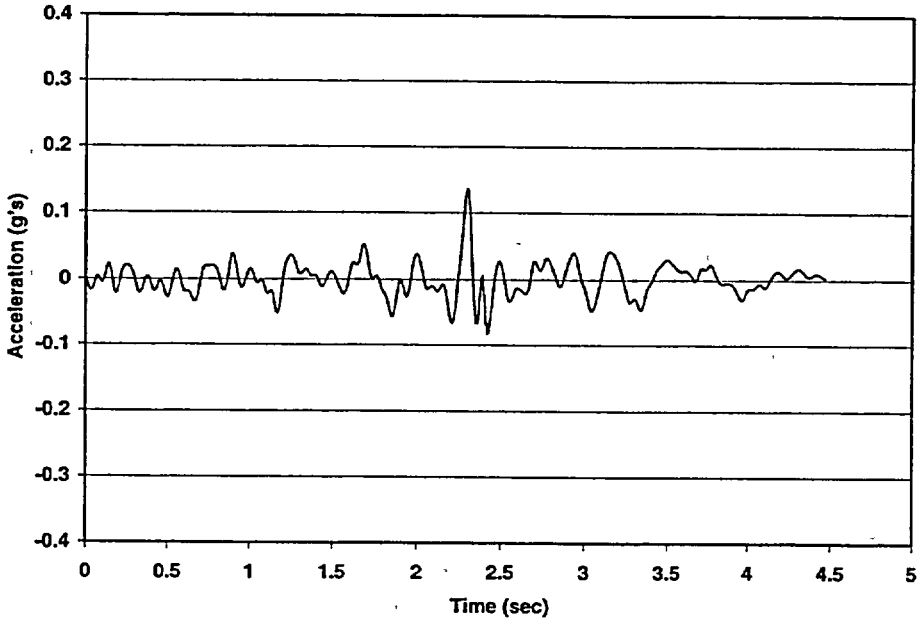

Figure A.72 Time History #24 (Parkfield) Vertical - Z

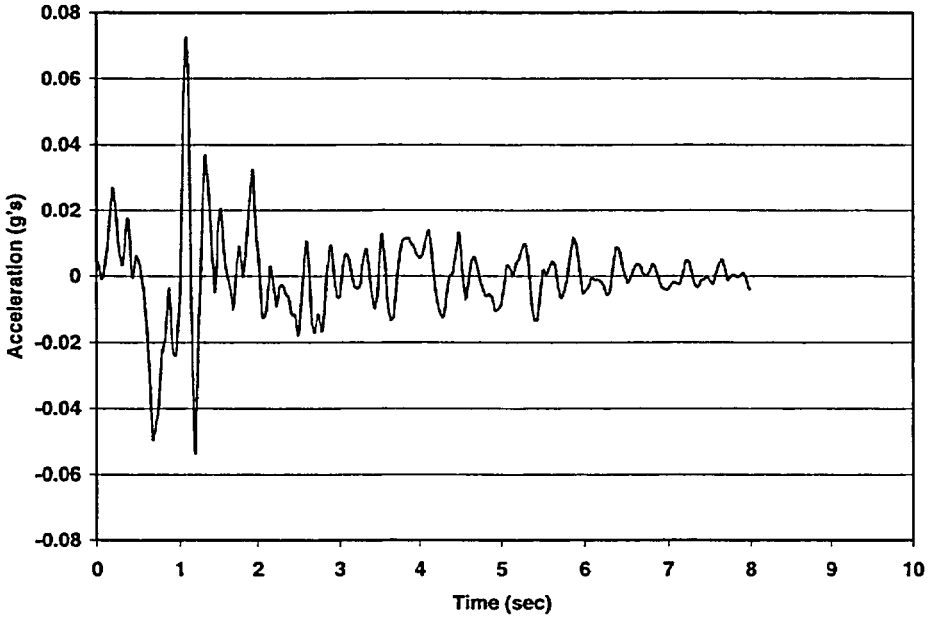

Figure A.73 Time History #25 (Santa Barbara) Horizontal - X

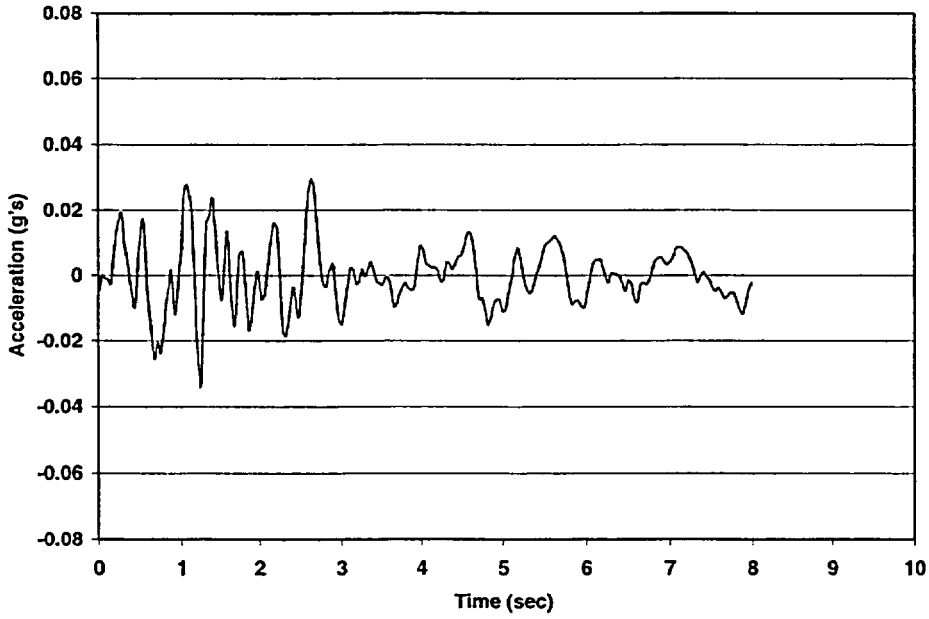

Figure A.74 Time History #25 (Santa Barbara) Horizontal - Y

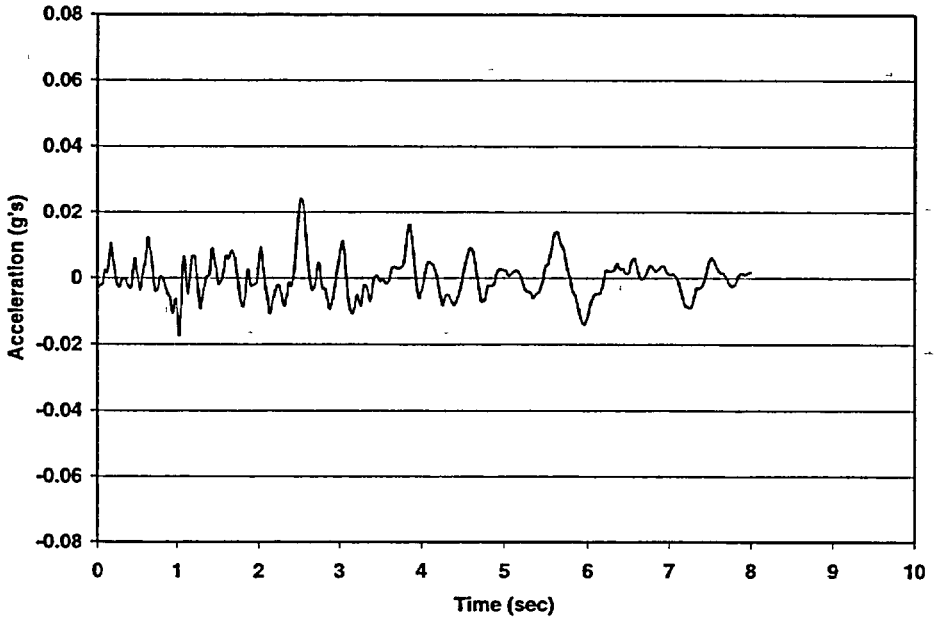

Figure A.75 Time History #25 (Santa Barbara) Vertical - Z

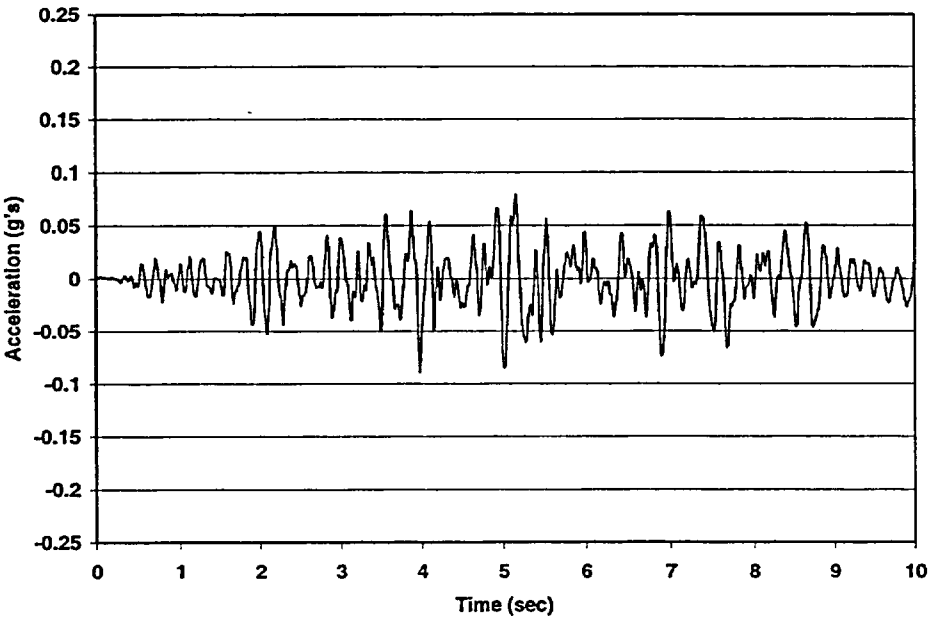

Figure A.76 Time History #26 (San Fernando) Horizontal - X

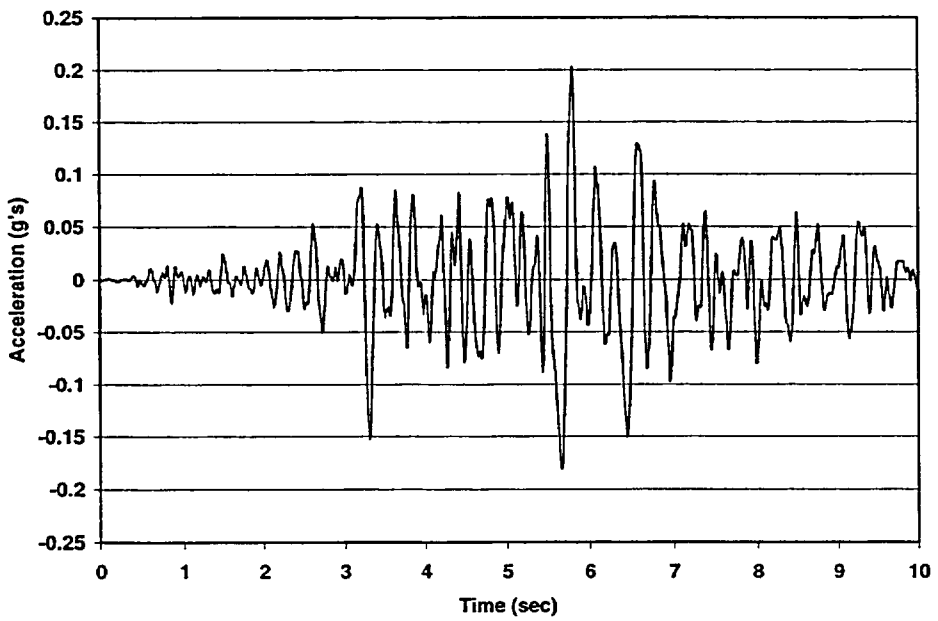

Figure A.77 Time History #26 (San Fernando) Horizontal - Y

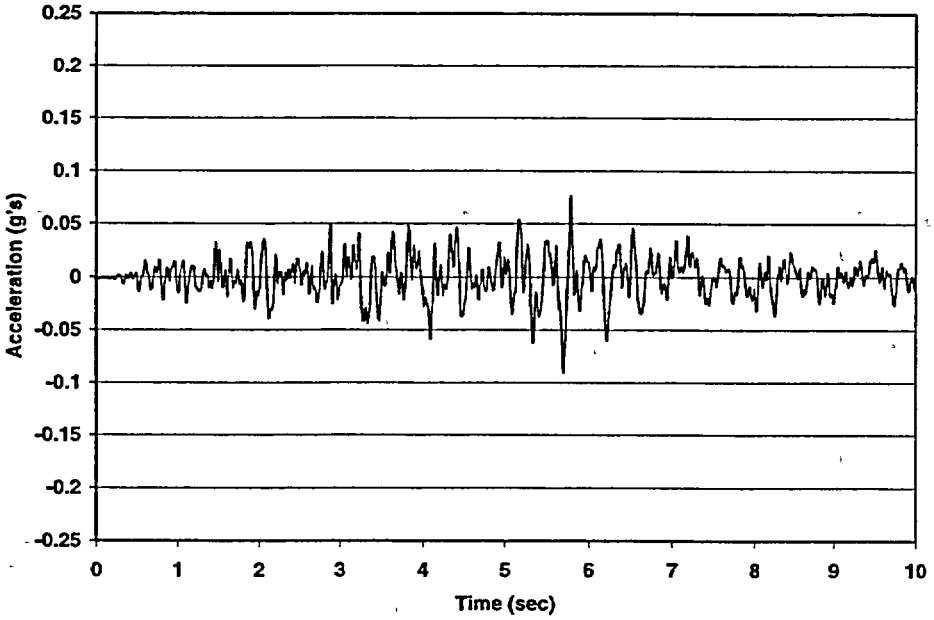

Figure A.78 Time History #26 (San Fernando) Vertical - Z

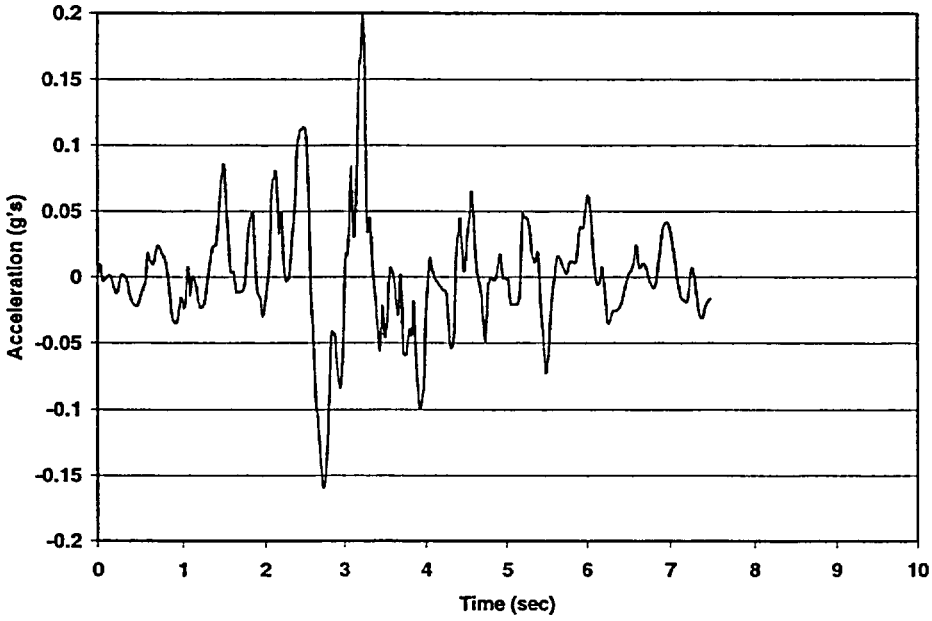

Figure A.79 Time History #27 (Spitak, Armenia) Horizontal - X

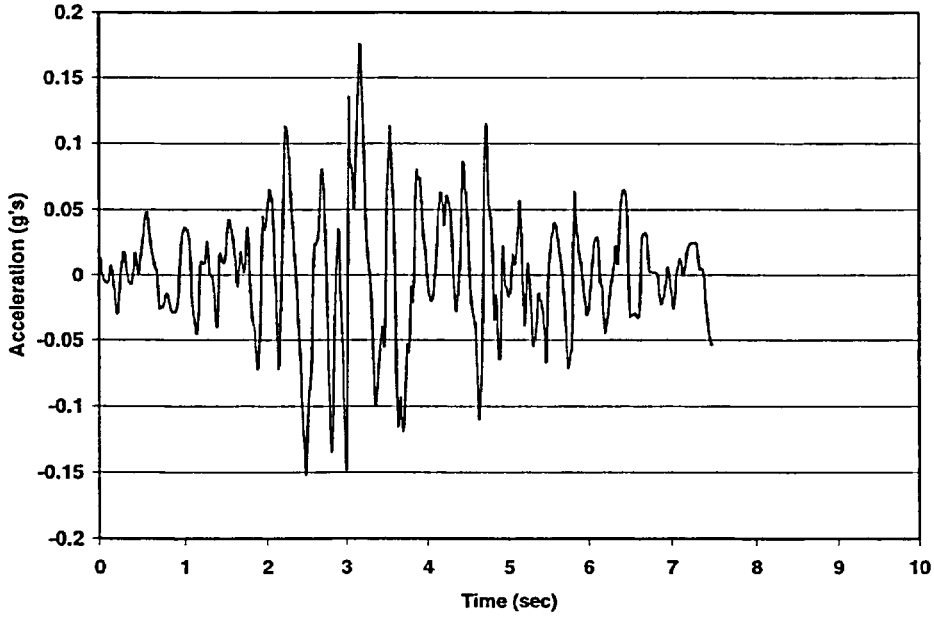

Figure A.80 Time History #27 (Spitak, Armenia) Horizontal - Y

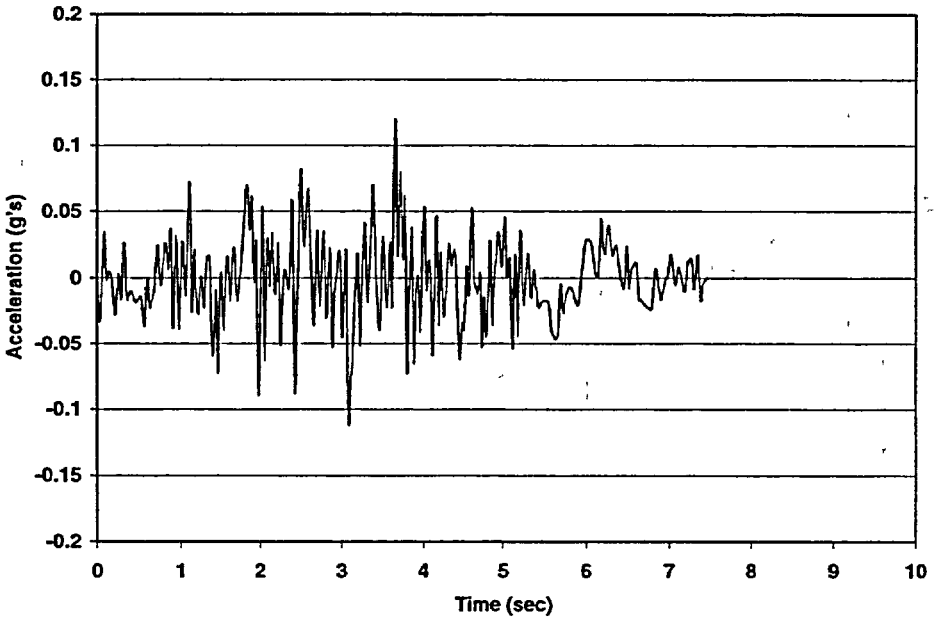

Figure A.81 Time History #27 (Spitak, Armenia) Vertical - Z

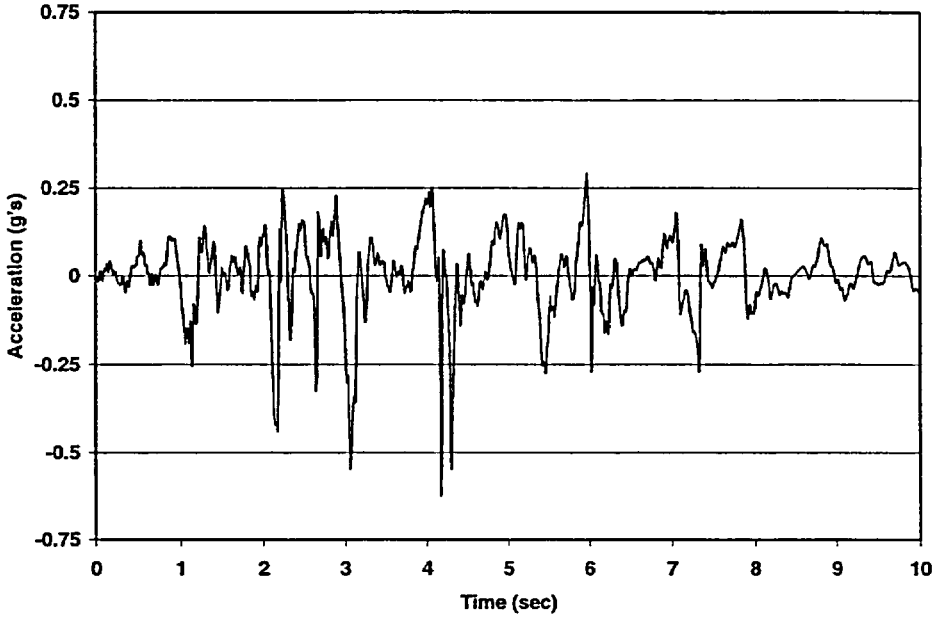

Figure A.82 Time History #28 (Victoria, Mexico) Horizontal - X

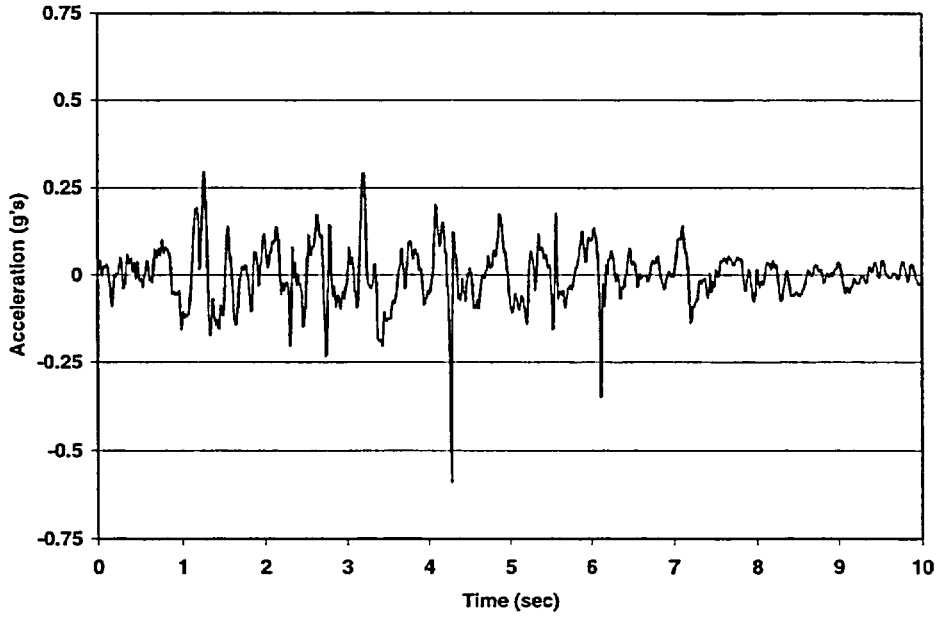

Figure A.83 Time History #28 (Victoria, Mexico) Horizontal - Y

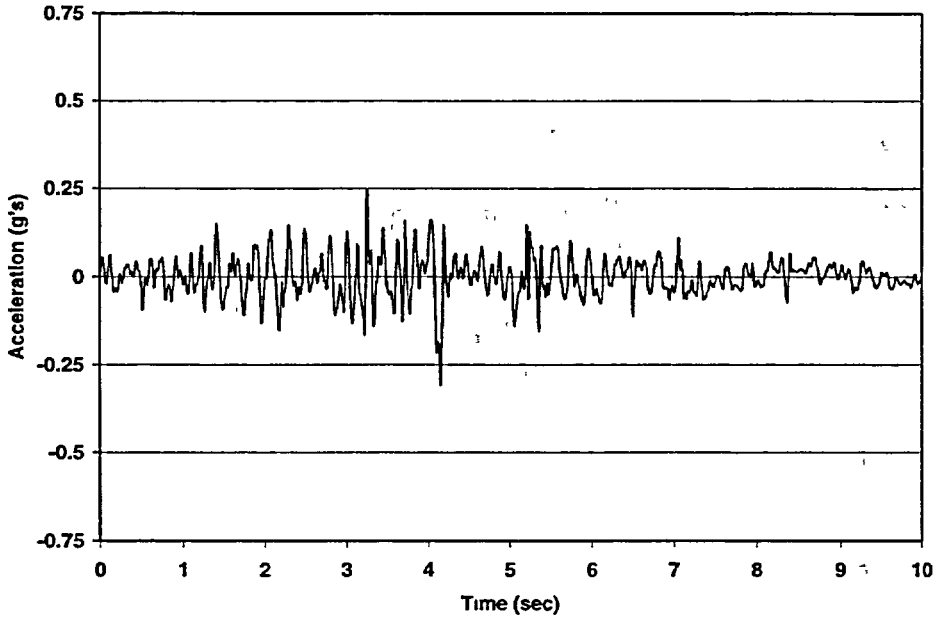

Figure A.84 Time History #28 (Victoria, Mexico) Vertical - Z

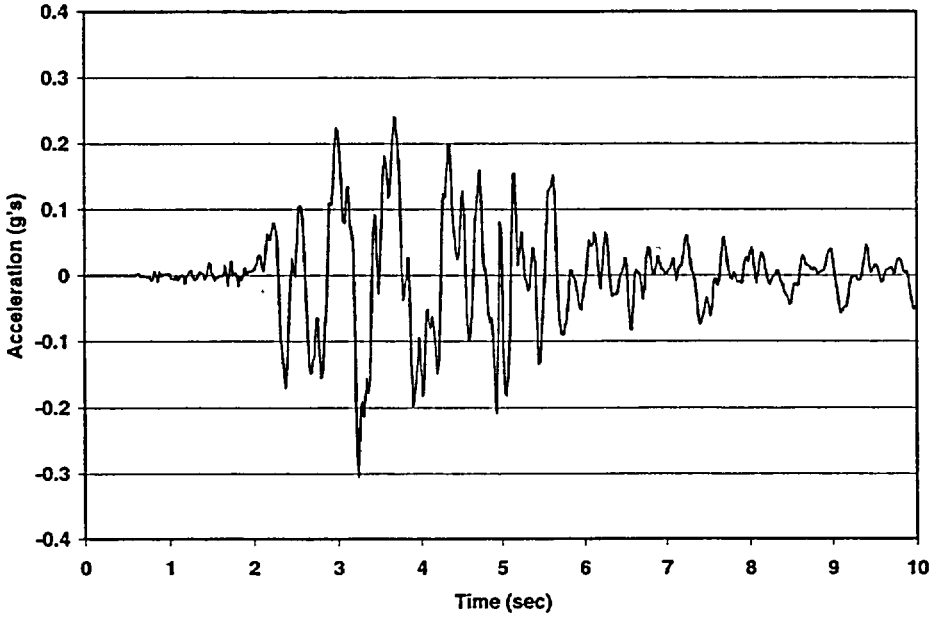

Figure A.85 Time History #29 (Wittier Narrows – 9km) Horizontal - X

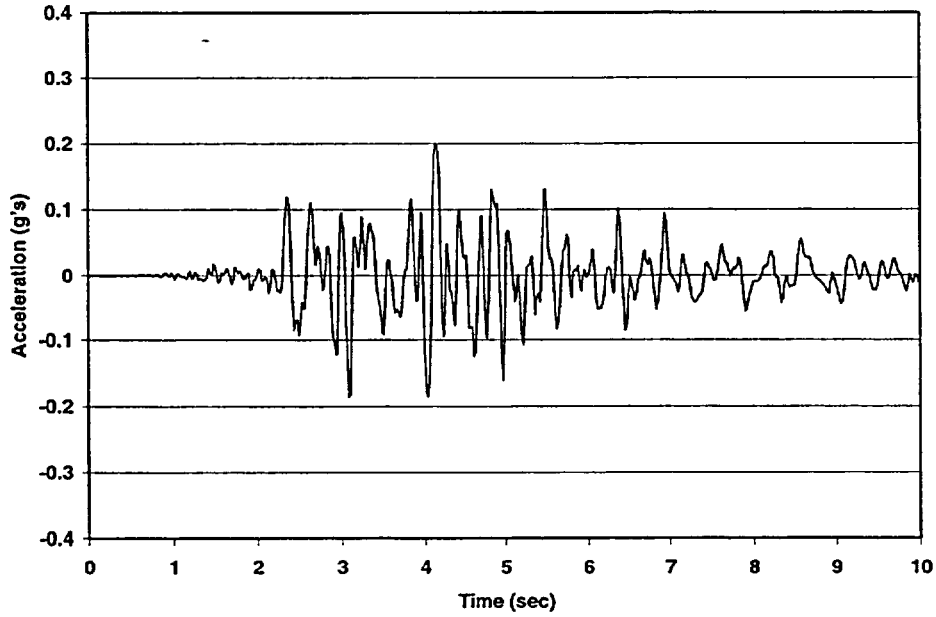

Figure A.86 Time History #29 (Wittier Narrows – 9km) Horizontal - Y

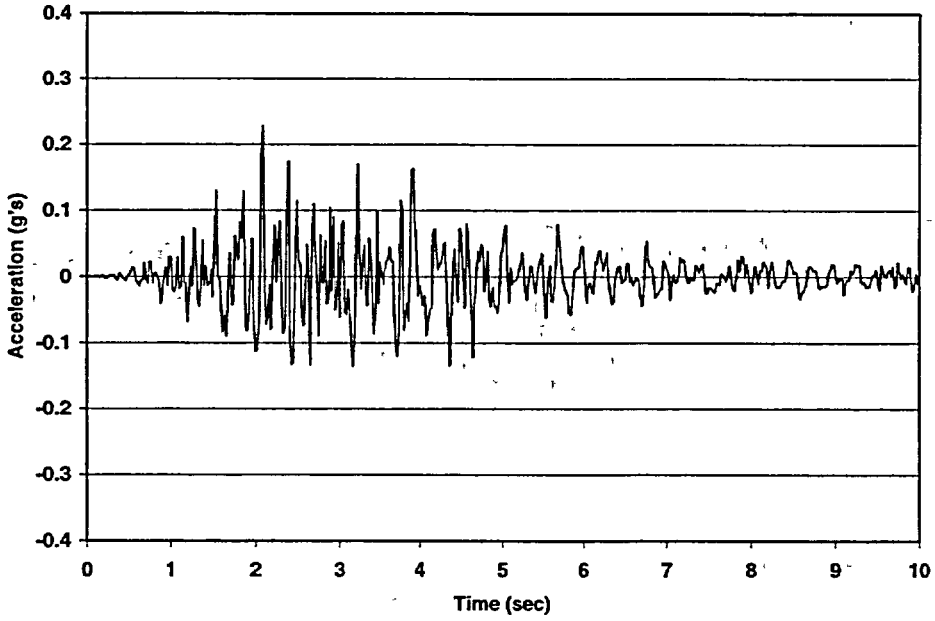

Figure A.87 Time History #29 (Wittier Narrows – 9km) Vertical - Z

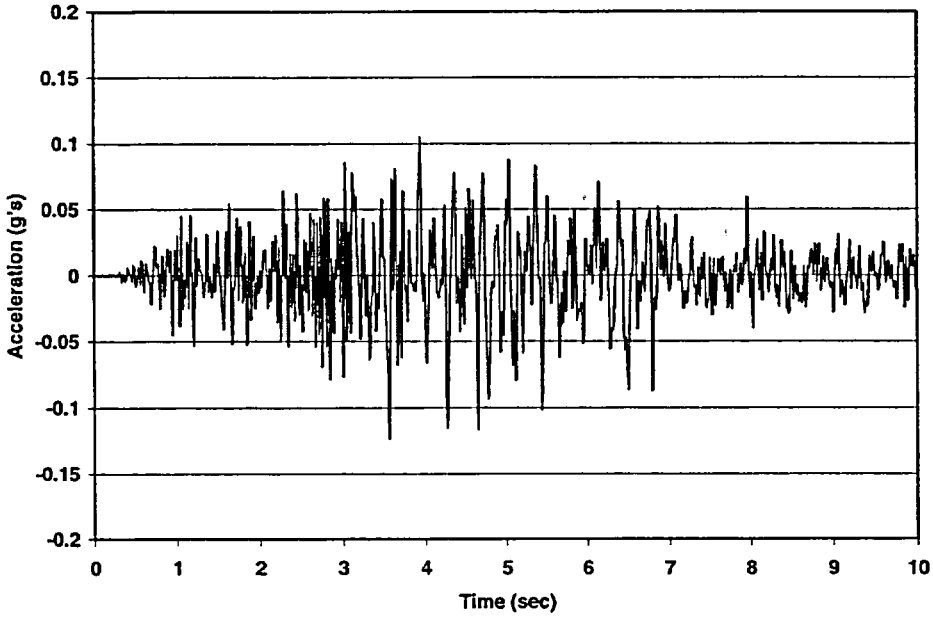

Figure A.88 Time History #30 (Wittier Narrows – 21km) Horizontal - X

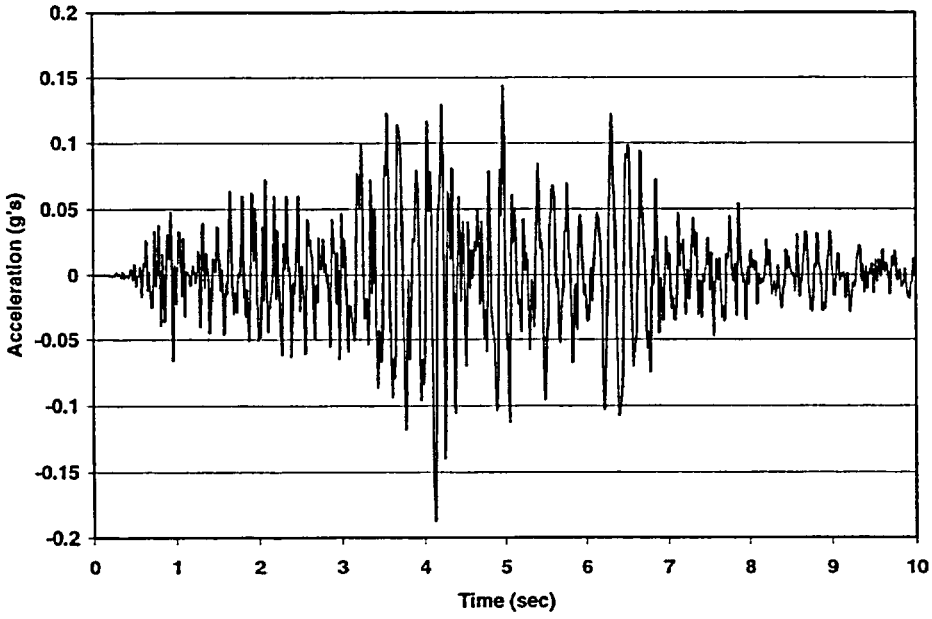

Figure A.89 Time History #30 (Wittier Narrows – 21km) Horizontal - Y

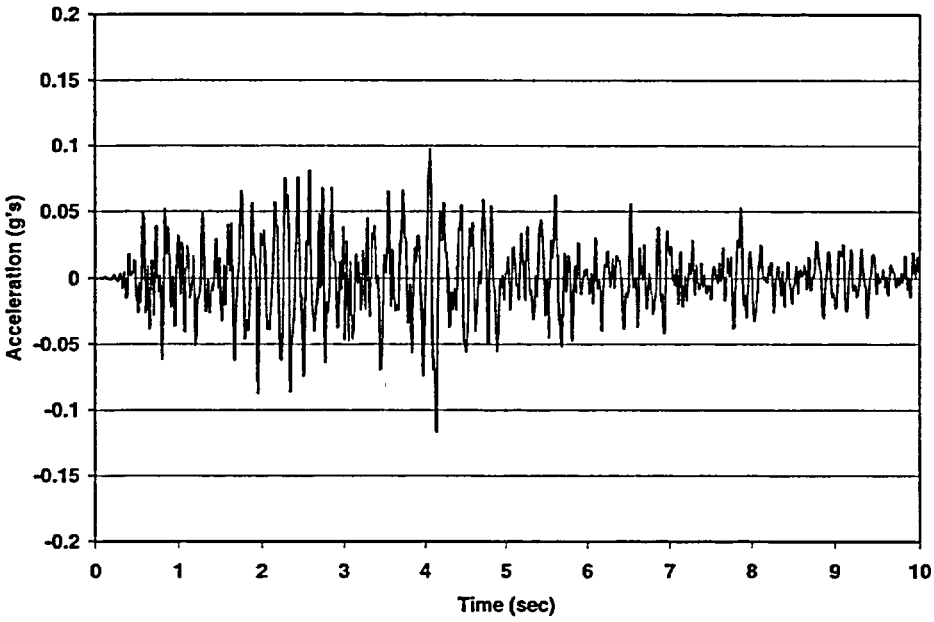

Figure A.90 Time History #30 (Wittier Narrows – 21km) Vertical - Z

Appendix B

Scaled Earthquake Response Spectra

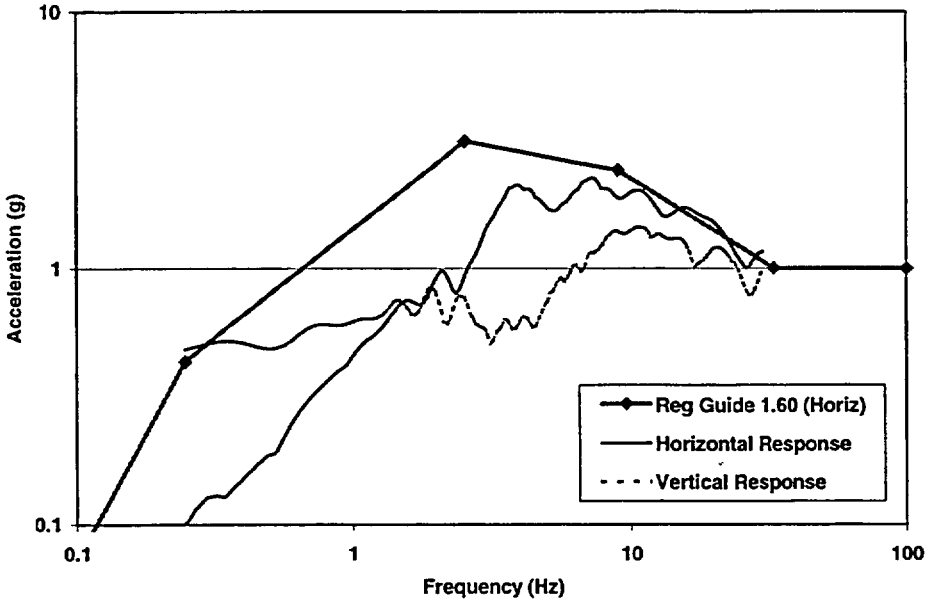

Figure B.1 Scaled Response Spectra – T/H #1 (Cape Mendocino)

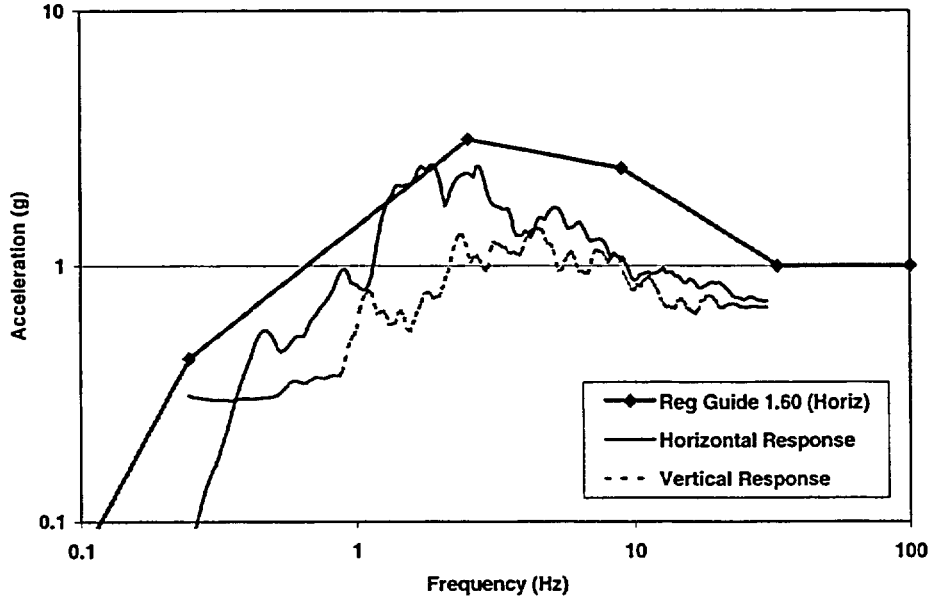

Figure B.2 Scaled Response Spectra – T/H #2 (Chalfant Valley)

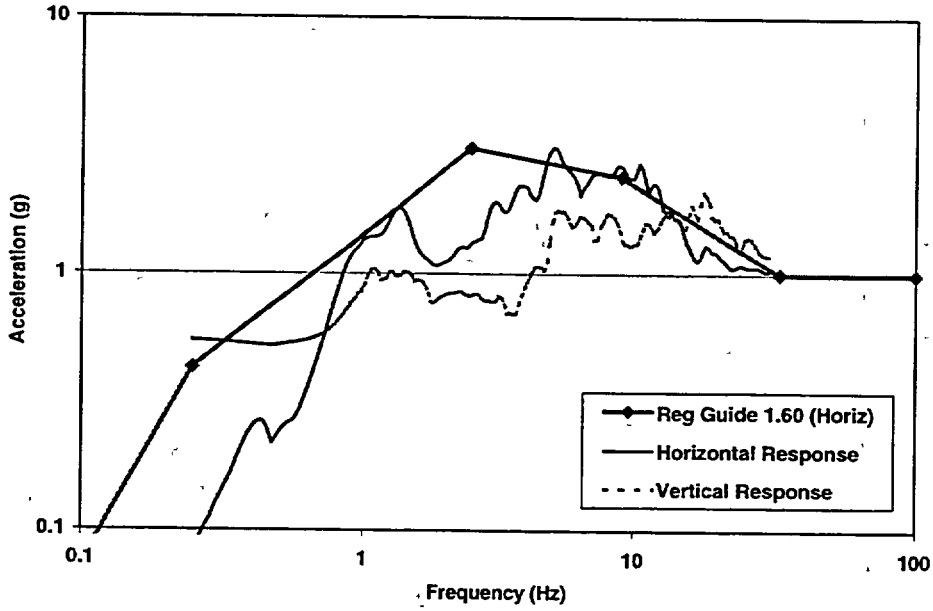

Figure B.3 Scaled Response Spectra – T/H #3 (Colinga – 11km)

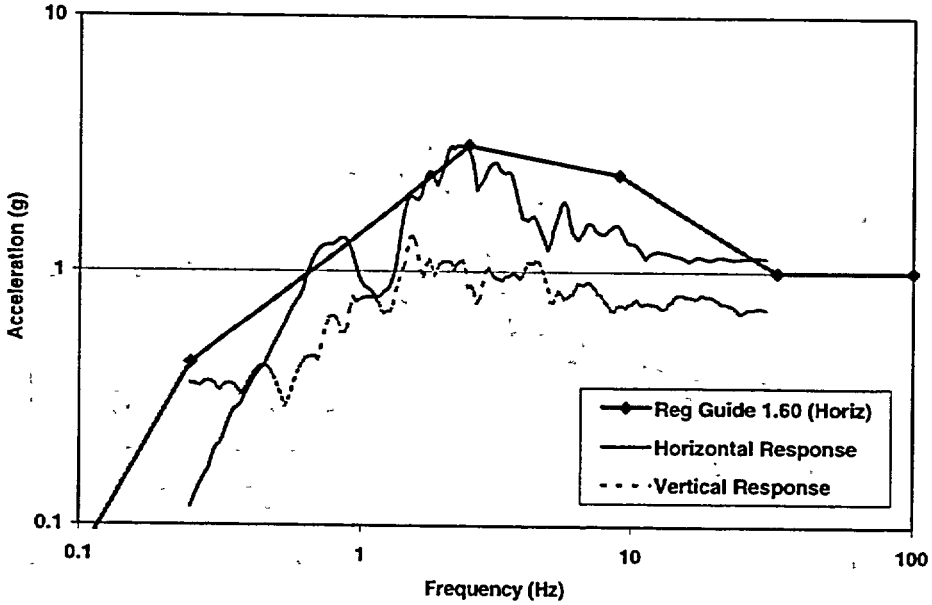

Figure B.4 Scaled Response Spectra – T/H #4 (Coalinga – 34km)

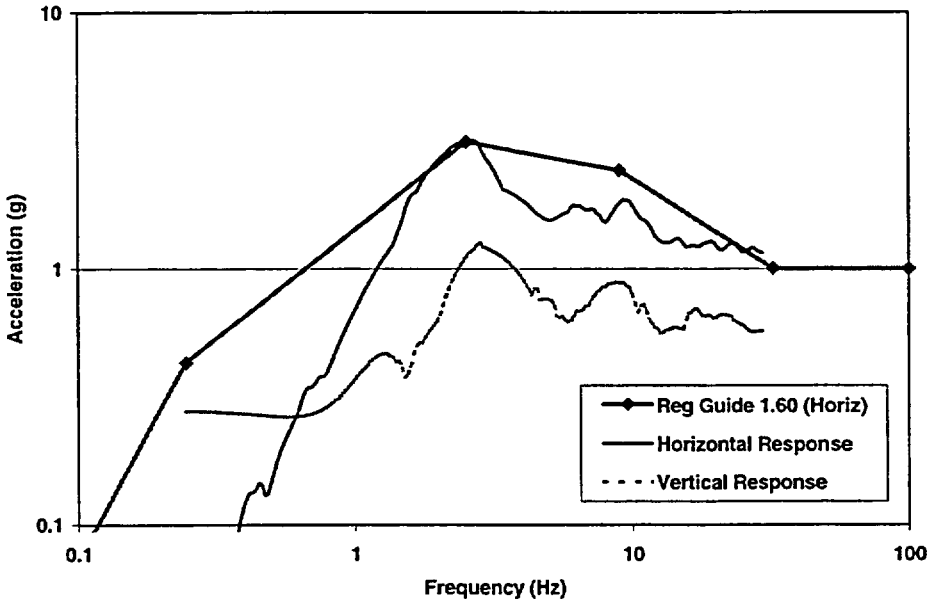

Figure B.5 Scaled Response Spectra – T/H #5 (Coyote Lake)

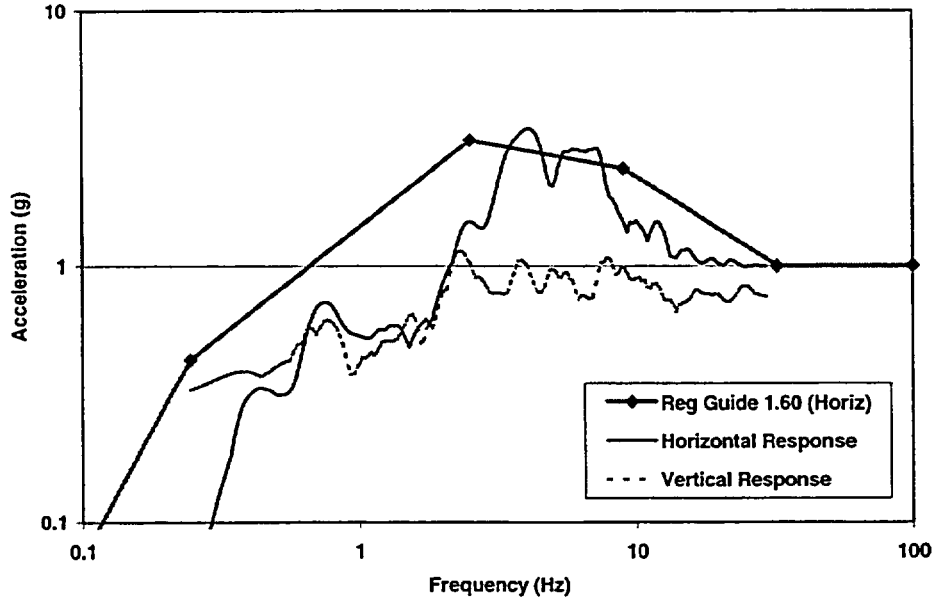

Figure B.6 Scaled Response Spectra – T/H #6 (Friuli, Italy)

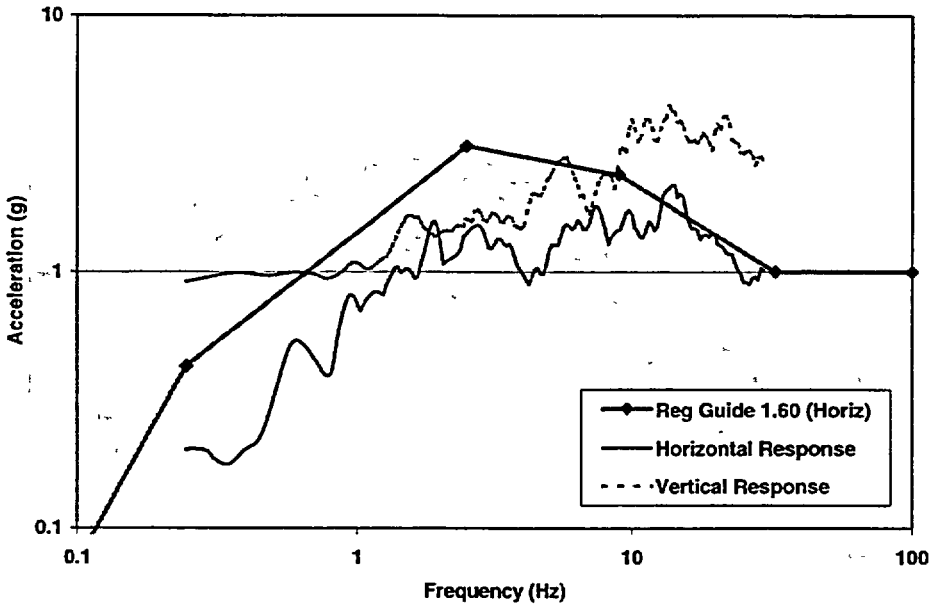

Figure B.7 Scaled Response Spectra – T/H #7 (Gazili, USSR)

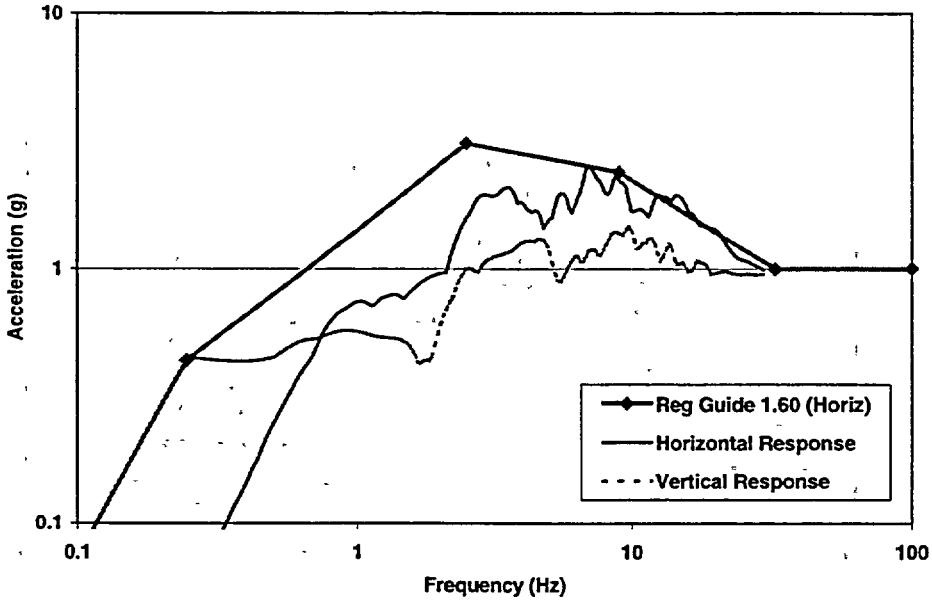

Figure B.8 Scaled Response Spectra – T/H #8 (Helena)

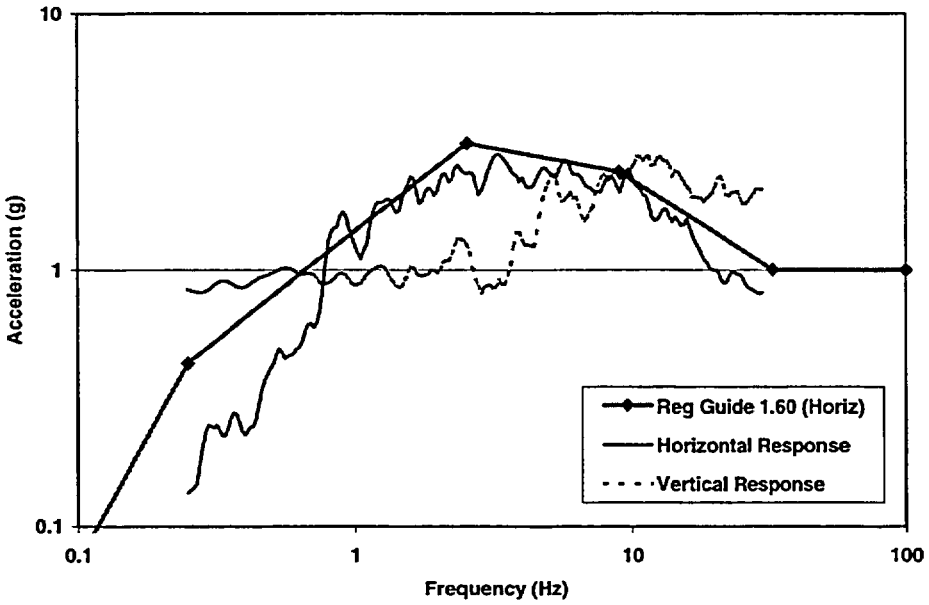

Figure B.9 Scaled Response Spectra – T/H #9 (Imperial Valley)

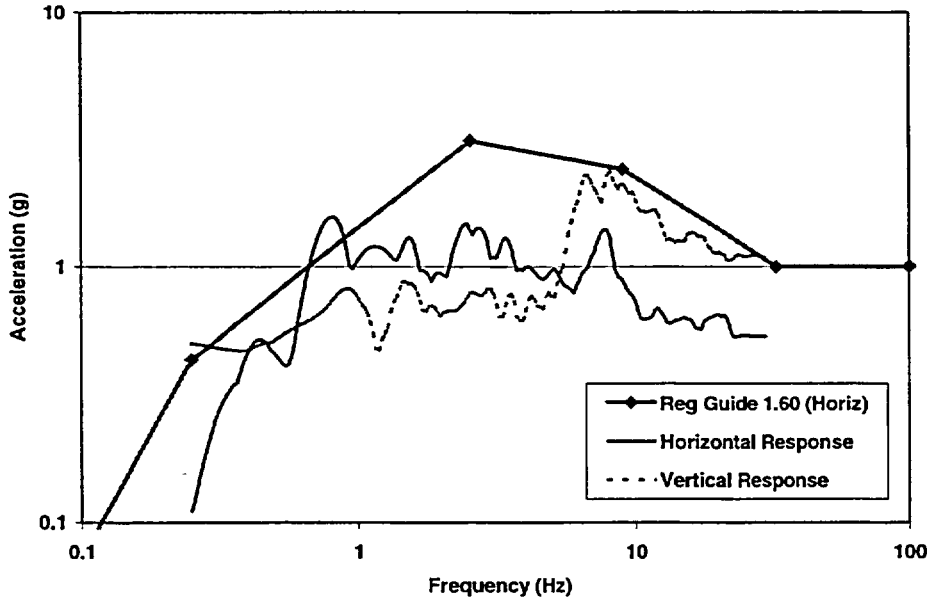

Figure B.10 Scaled Response Spectra – T/H #10 (Kobe, Japan – 0.2km)

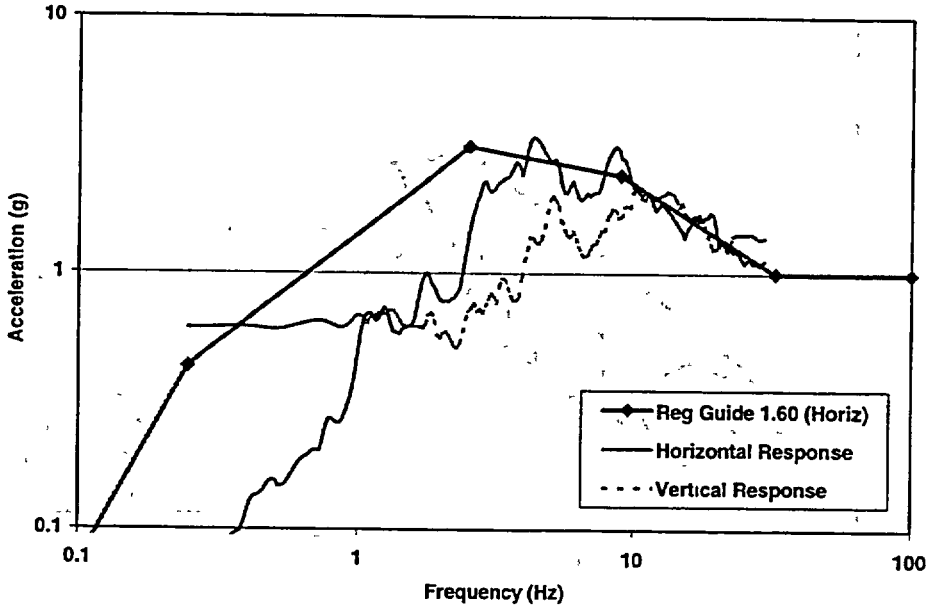

Figure B.11 Scaled Response Spectra – T/H #11 (Kobe, Japan – 49km)

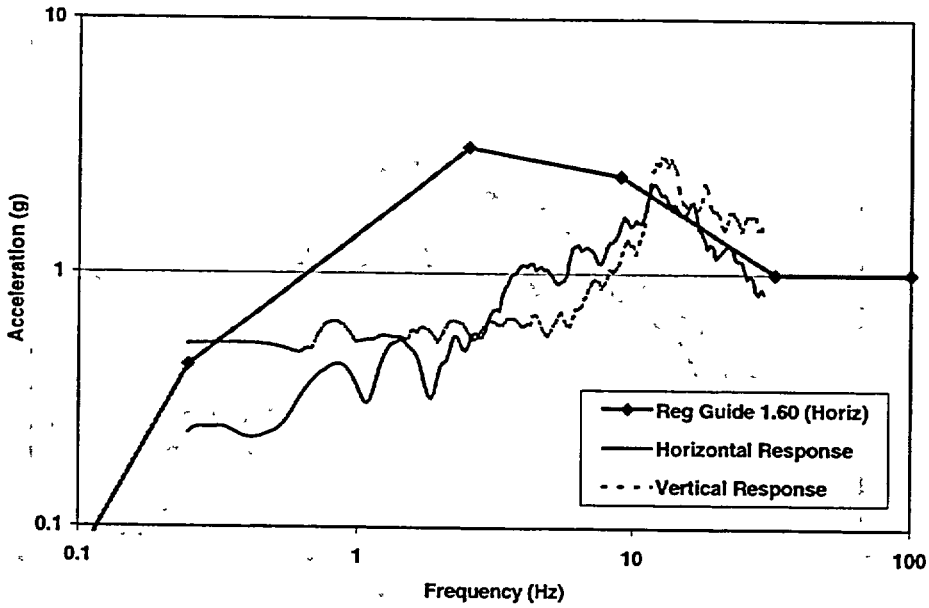

Figure B.12 Scaled Response Spectra – T/H #12 (Landers – 1.1km)

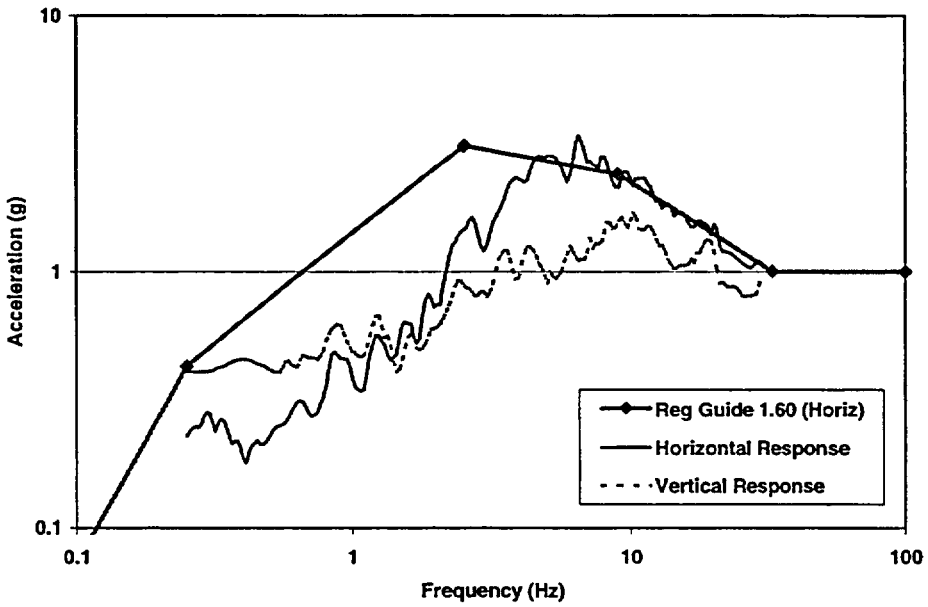

Figure B.13 Scaled Response Spectra – T/H #13 (Landers – 42km)

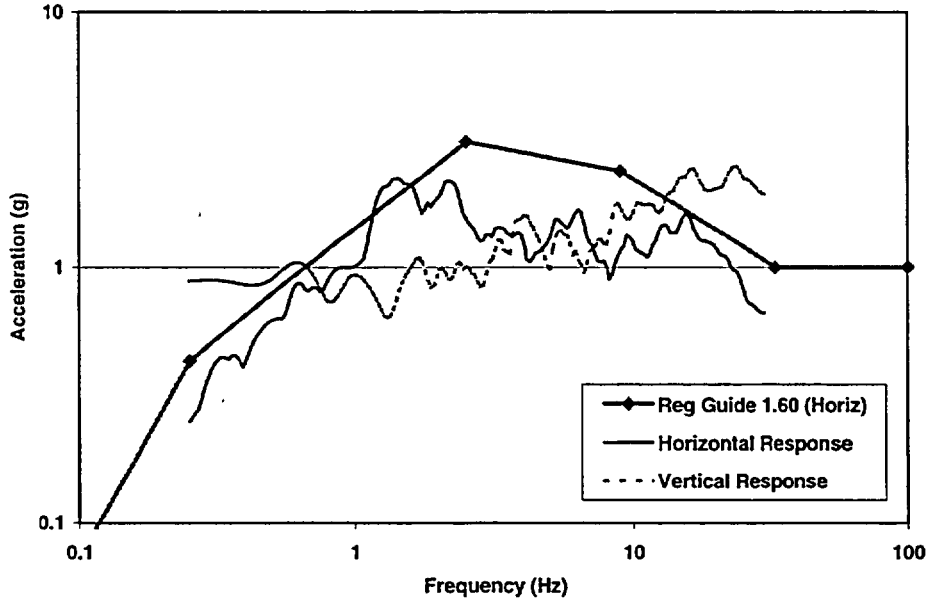

Figure B.14 Scaled Response Spectra – T/H #14 (Loma Prieta – 6km)

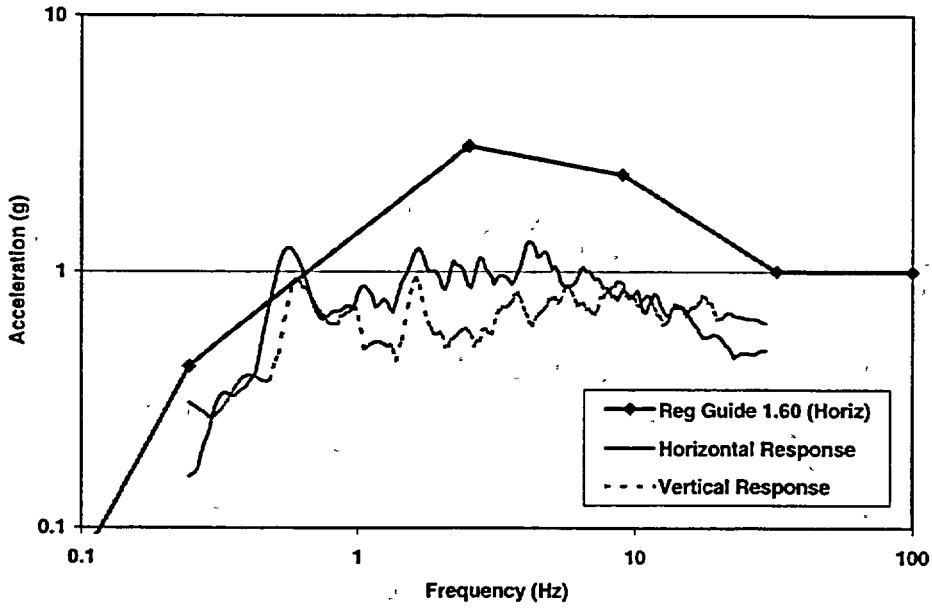

Figure B.15 Scaled Response Spectra – T/H #15 (Loma Prieta – 21km)

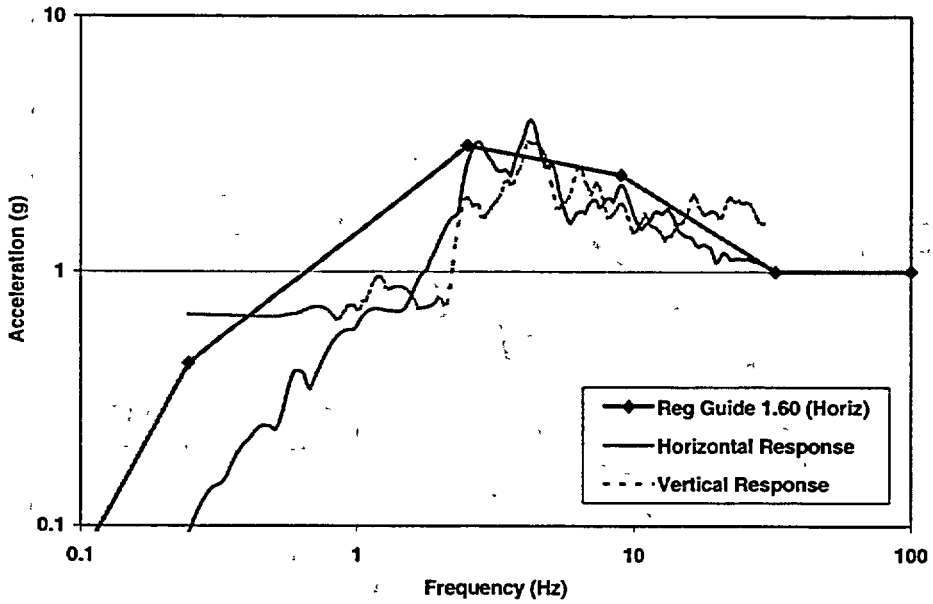

Figure B.16 Scaled Response Spectra – T/H #16 (Mammoth Lakes)

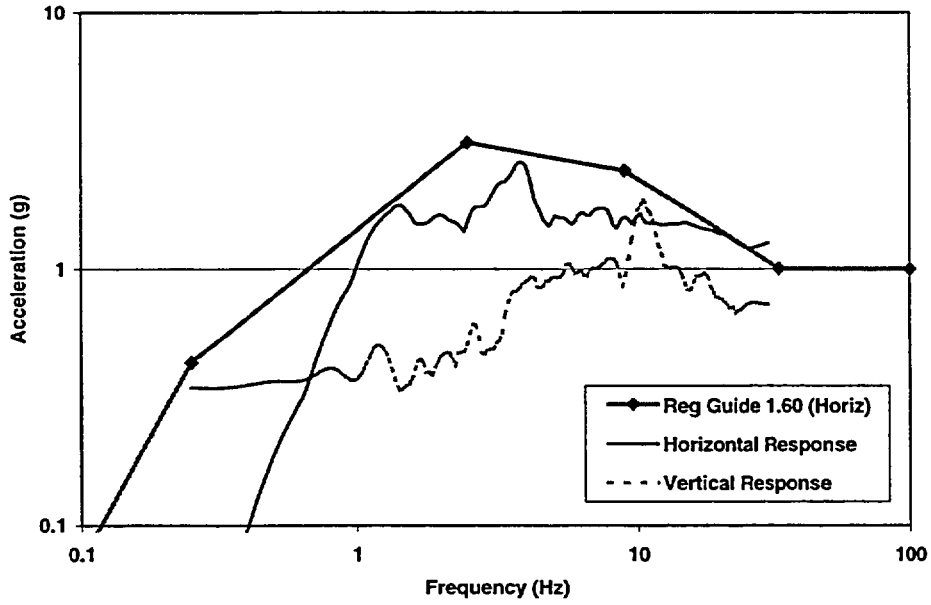

Figure B.17 Scaled Response Spectra – T/H #17 (Morgan Hill – 0.1km)

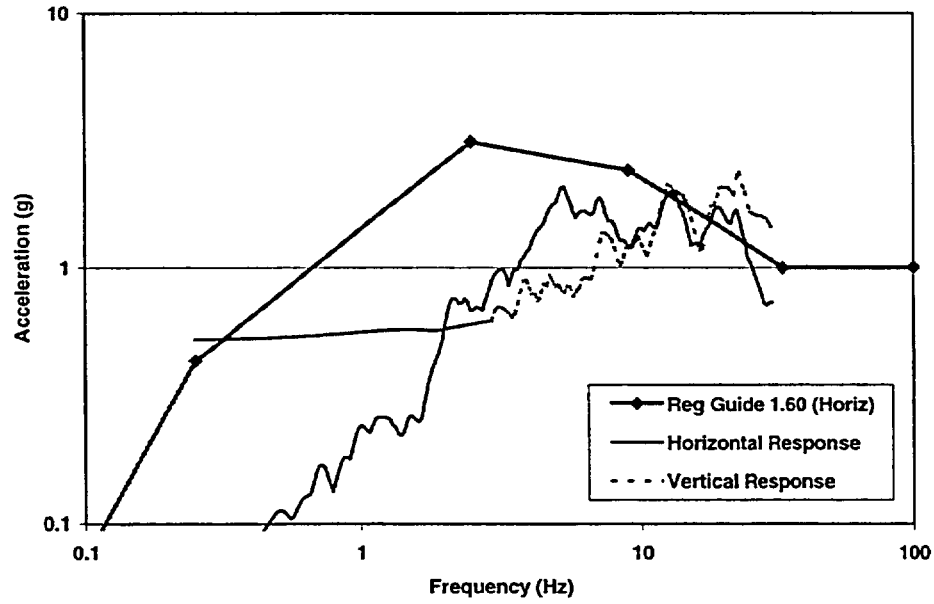

Figure B.18 Scaled Response Spectra – T/H #18 (Morgan Hill – 16km)

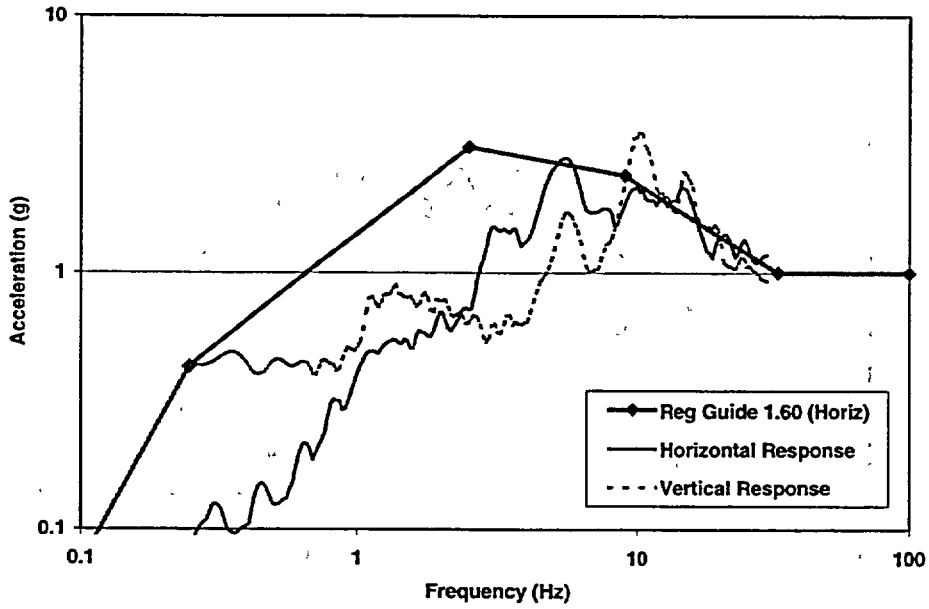

Figure B.19 Scaled Response Spectra – T/H #19 (Nahanni, Canada – 6km)

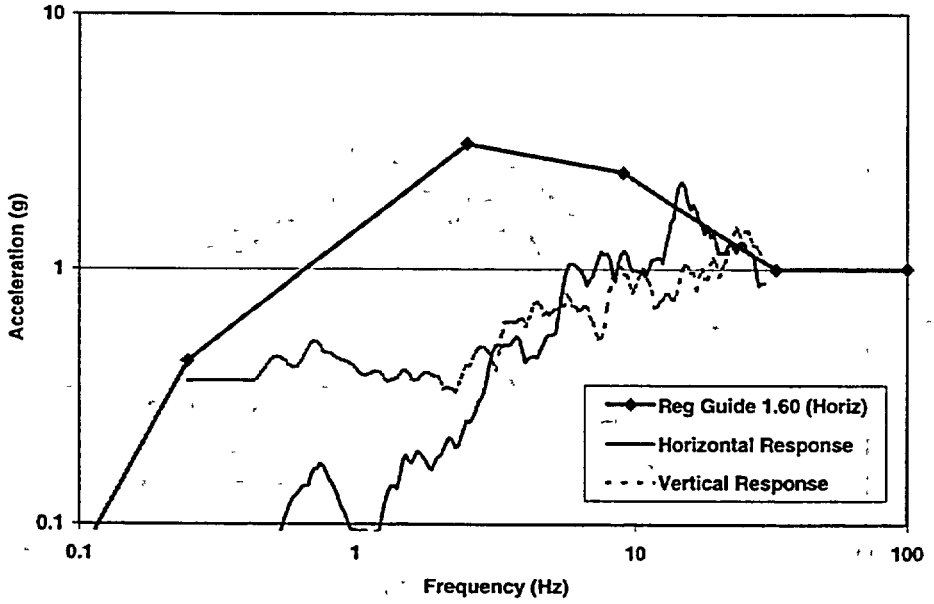

Figure B.20 Scaled Response Spectra – T/H #20 (Nahanni, Canada – 16km)

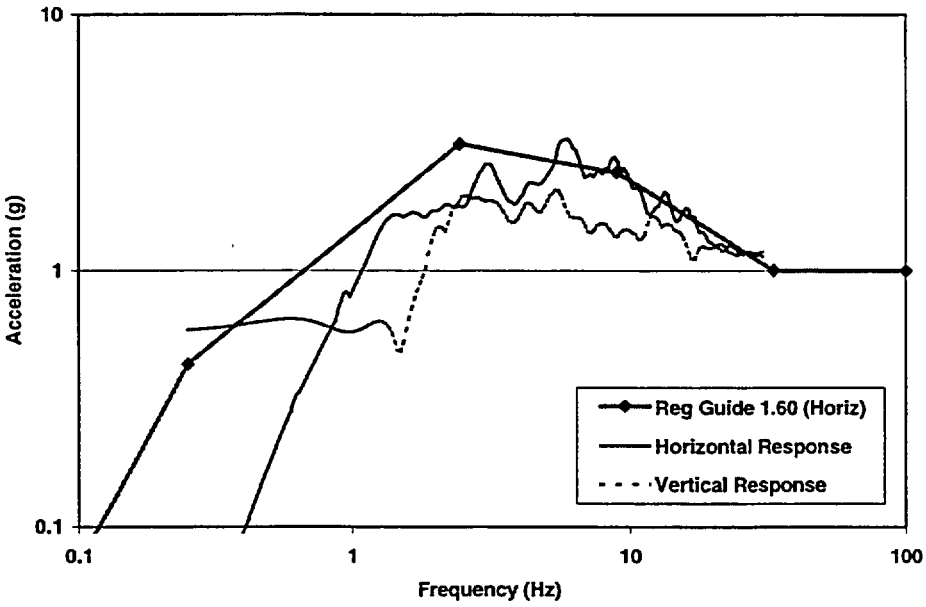

Figure B.21 Scaled Response Spectra – T/H #21 (Northridge – 8km)

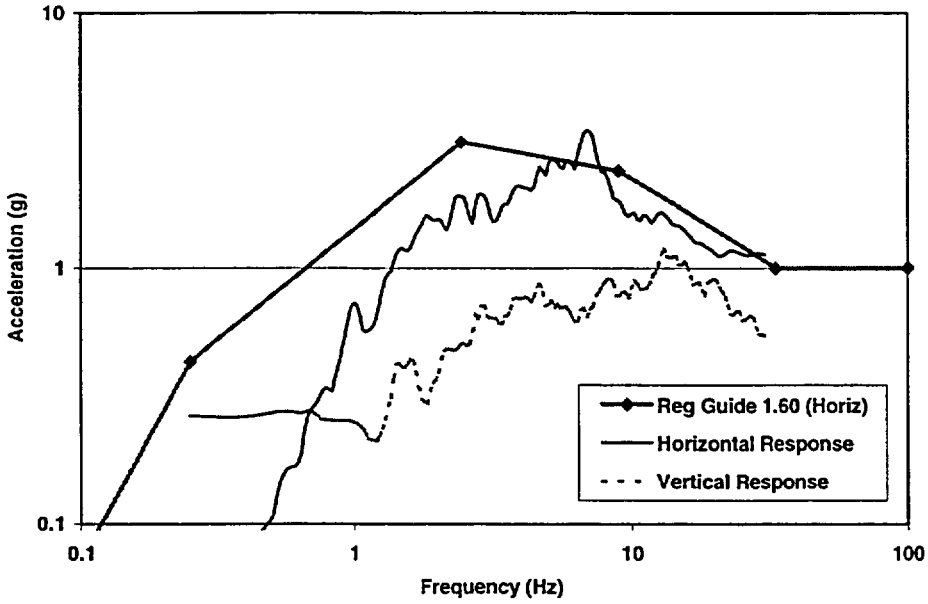

Figure B.22 Scaled Response Spectra – T/H #22 (Northridge – 42km)

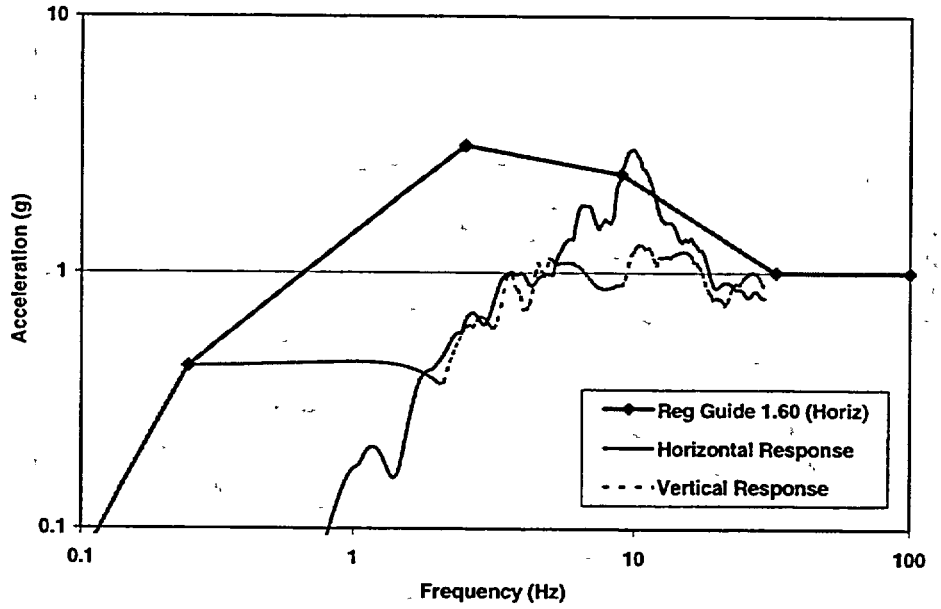

Figure B.23 Scaled Response Spectra – T/H #23 (N. Palm Springs)

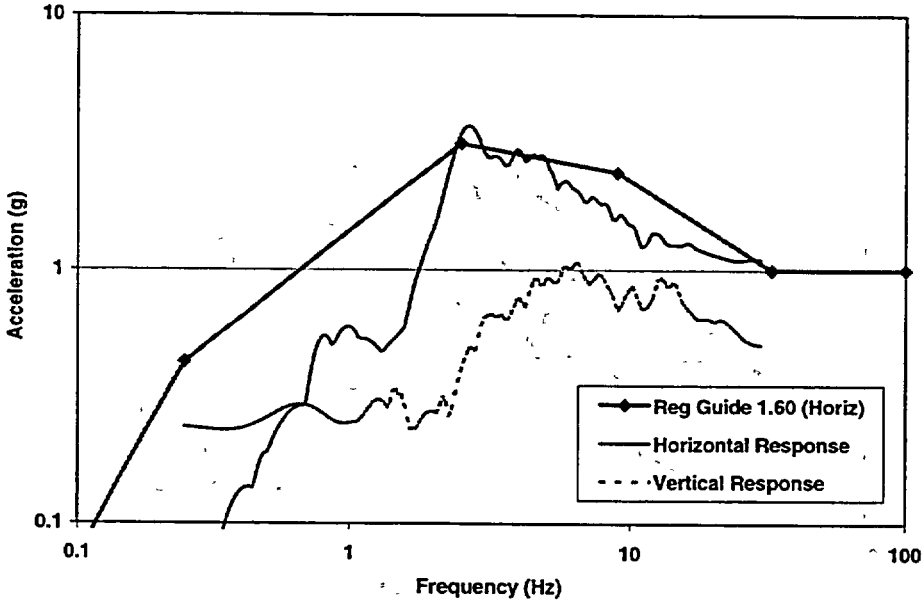

Figure B.24 Scaled Response Spectra – T/H #24 (Parkfield)

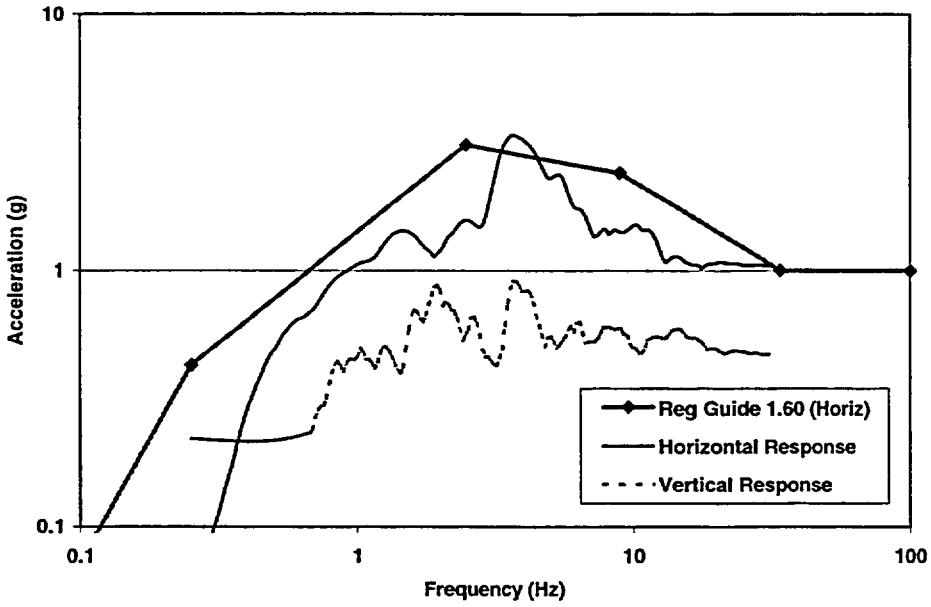

Figure B.25 Scaled Response Spectra – T/H #25 (Santa Barbara)

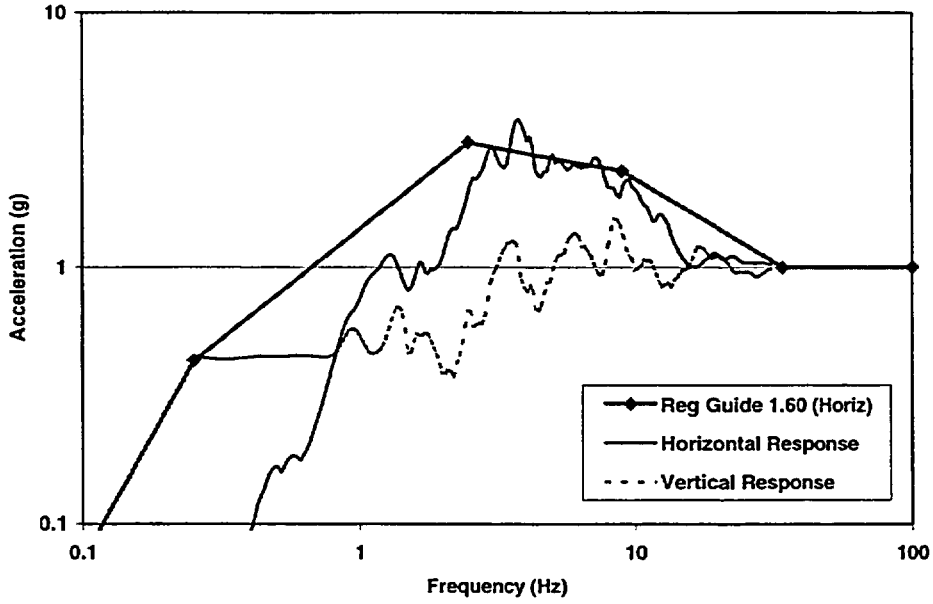

Figure B.26 Scaled Response Spectra – T/H #26 (San Fernando)

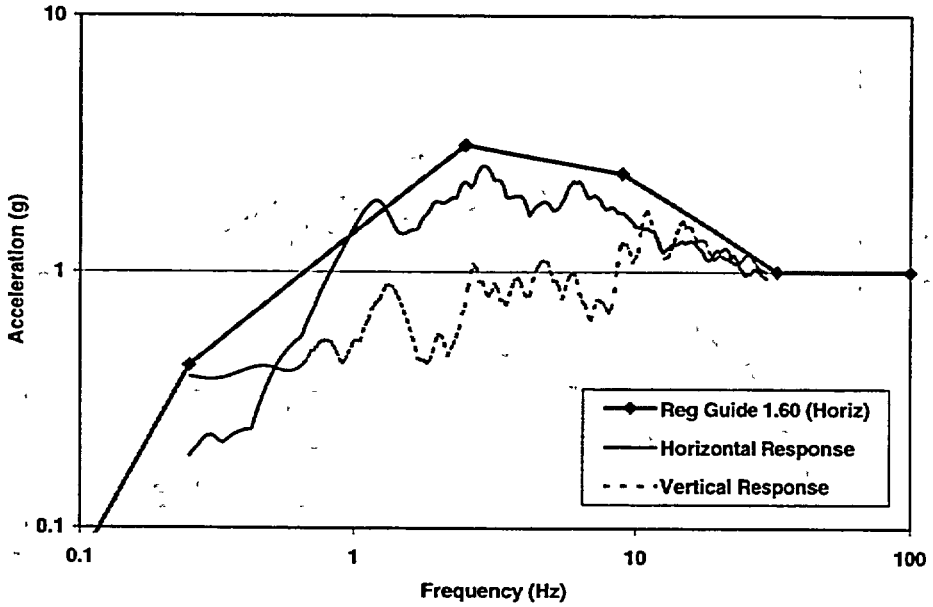

Figure B.27 Scaled Response Spectra – T/H #27 (Spitak, Armenia)

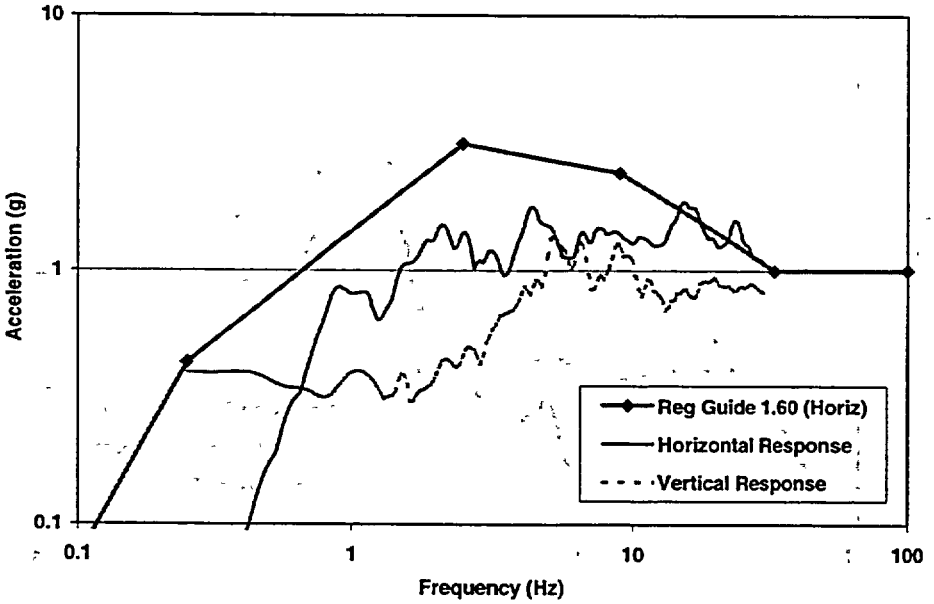

Figure B.28 Scaled Response Spectra – T/H #28 (Victoria, Mexico)

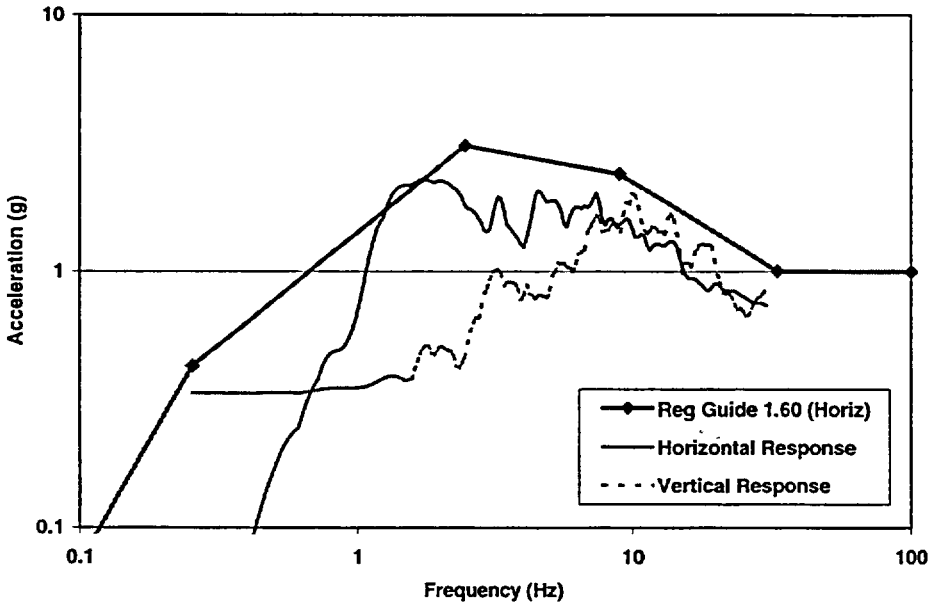

Figure B.29 Scaled Response Spectra – T/H #29 (Whittier Narrows – 9km)

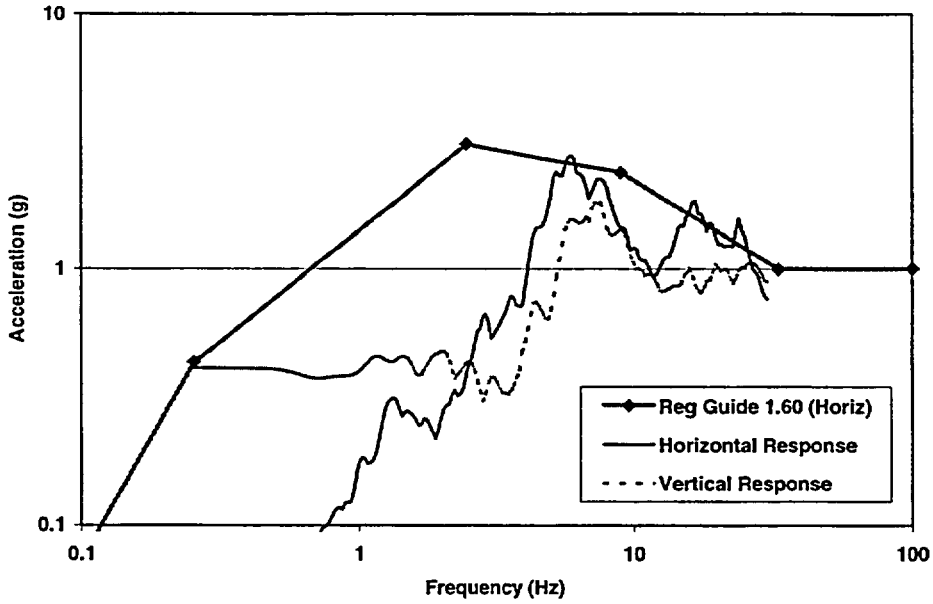

Figure B.30 Scaled Response Spectra – T/H #30 (Whittier Narrows – 21km)

NRC FORM 335 (2-89) NRCM 1102, 3201, 3202

U S NUCLEAR REGULATORY COMMISSION

BIBLIOGRAPHIC DATA SHEET

(See instructions on the reverse)

1. REPORT NUMBER (Assigned by NRC, Add Vol , Supp Rev , and Addendum Numbers, if any)

NUREG/CR- 6783

SAND2002-1996P

2. TITLE AND SUBTITLE

Structural Seismic Fragility Analysis of the Surry Containment

3 DATE REPORT PUBLISHED

MONTH	YEAR
October	2002

4 FIN OR GRANT NUMBER

W6251

5. AUTHOR(S)

Eric W. Klamerus

6 TYPE OF REPORT

Technical

7. PERIOD COVERED *(inclusive Dates)*

8. PERFORMING ORGANIZATION – NAME AND ADDRESS *(If NRC, provide Division, Office or Region, U S. Nuclear Regulatory Commission, and mailing address, if contractor, provide name and mailing address.)*

Sandia National Laboratories
PO Box 5800,
Albuquerque, NM 87185-0744

9. SPONSORING ORGANIZATION – NAME AND ADDRESS *(If NRC, type "Same as above", if contractor, provide NRC Division, Office or Region, U S Nuclear Regulatory Commission, and mailing address)*

Division of Engineering Technology
Office of Nulcear Regulatory Research
US Nuclear Regulatory Commission
Washington, DC 20555-0001

10 SUPPLEMENTARY NOTES

A. J. Murphy, NRC Project Manager

11. ABSTRACT *(200 words or less)*

A detailed finite element model was developed for the Surry Nuclear Power plant containment structure and seismic analyses were performed. Material models that were validated by previous scaled model seismic tests and analyses were used. The Surry model was then subjected to 30 different earthquake time-history accelerations. In addition, Latin Hypercube Sampling was used to vary all the material and modeling parameters of the input to get a realistic distribution for this limited set of runs. Fragilities were generated based on the limiting concrete shear strains In general, the results show the Surry reinforced containment is highly resistant to seismic structural failure when it is modeled on a rigid rock foundation. The most significant variable in the response is the variability in the input earthquakes. Modeling on a rock site, rather than on a soil site, will produce higher concrete stresses and strains than for a less rigid site model, resulting in a conservative estimate of the structural capacity of a reinforced concrete containment. These predictions may be non-conservative for other failure modes (such as pipes breaking), however, because a containment on a soil site would probably see larger displacements than a containment attached to rock.

12 KEY WORDS/DESCRIPTORS *(List words or phrases that will assist researchers in locating the report)*

Earthquake,
Failure Prediction,
Finite Element Analysis,
Fragility Analysis,
Reinforced Concrete Containment Vessel (RCCV),
Seismic,
Surry Containment

13 AVAILABILITY STATEMENT
Unlimited

14 SECURITY CLASSIFICATION

(This Page)
Unclassified

(This Report)
Unclassified

15 NUMBER OF PAGES

16 PRICE

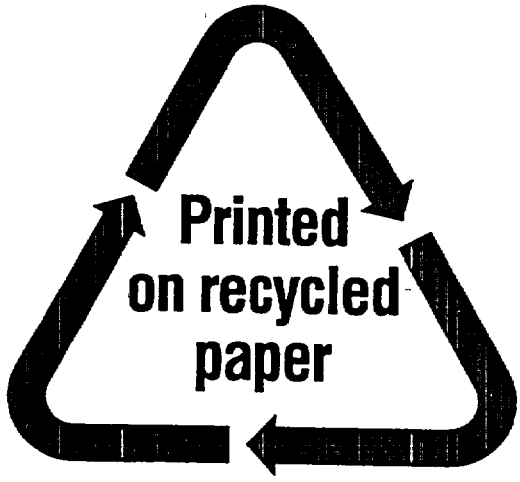

Federal Recycling Program